Winter August 2014

Protein Behavior Directed by Heparin Charge and Chain Length

Burcu Baykal Minsky

PROTEIN BEHAVIOR DIRECTED BY HEPARIN CHARGE AND CHAIN LENGTH

A Dissertation Presented

by

BURCU BAYKAL MINSKY

Submitted to the Graduate School of the

University of Massachusetts Amherst in partial fulfillment

of the requirements for the degree of

DOCTOR OF PHILOSOPHY

May 2014

Chemistry

PROTEIN BEHAVIOR DIRECTED BY HEPARIN CHARGE AND CHAIN LENGTH

A Dissertation Presented

by

BURCU BAYKAL MINSKY

Approved as to style and content by:

_____

Paul L. Dubin, Chair

_____

Igor A. Kaltashov, Co-Chair

_____

Richard W. Vachet, Member

_____

Harry Bermudez, Member

_____

Craig T. Martin, Department Head

Chemistry

DEDICATIONS

To my loving husband and my extended family.

ACKNOWLEDGMENTS

I wish to thank to my parents, my sister, my husband and my parents-in-law for their love and continuous support during my years in graduate school. I have always felt more confident because of their encouragement. I also would like to thank my dear friends Melda, Dila, Irem, Gonca, Hakan, Mahmut, Canan, Zeynep and Sibel for always showing their support, sharing their insights and helping me feel less homesick in the United States.

I highly appreciate the guidance and support from my advisors Prof. Paul Dubin and Prof. Igor Kaltashov throughout my graduate studies. Collaboration with experts in their fields has been an invaluable experience. I want specially thank to Prof. Dubin for his continuous encouragement, and also his patience to improve my writing and presentation skills.

Many thanks go to all the Dubin and Kaltashov group members for being great coworkers in creating a productive and peaceful lab environment. I specially want to thank Dr. Rinat Abzalimov for the fruitful collaboration in my mass spectrometry studies. His guidance in handling mass spectrometry, experimental design and data analysis has been a great asset. I also want to thank Dr. Cedric Bobst for his patience in answering all my questions regarding chromatography techniques and lab equipment handling. Additionally, many thanks go to Daniel Seeman for his support in computational modeling and Bingqian Zheng for being a talented and responsible undergraduate researcher and assisting me with my protein aggregation studies. I also want to thank Dr. Virginie Sjoelund and Adriana Kita for being extremely helpful while I was settling in the lab.

I would like to thank my committee members, Prof. Richard Vachet (UMass, Amherst), Prof. Surita Bhatia (Stony Brook, NY), and Prof. Harry Bermudez (UMass, Amherst) for their useful comments on my studies. I also want to acknowledge Prof. Gerald Manning (Rutgers, NJ), Prof. John Gallagher (Iduron, UK), Prof. David Hoagland (UMass, Amherst), Prof. Adrian Parsegian (UMass, Amherst) and Dr. Steve Eyles (UMass, Amherst) for the stimulating discussions in my studies. I greatly appreciate the generosity of Prof. Gallagher for sending us highly purified heparin oligomer fractions. I also want to acknowledge CSL Behring for providing human plasma α and β-AT samples and GTC Biotherapeutics for recombinant human ATyrn protein samples. I also want express my appreciation to ICE-IGERT for funding my poster presentations at Gordon Glycobiology and Proteoglycan conferences.

ABSTRACT

PROTEIN BEHAVIOUR DIRECTED BY HEPARIN CHARGE AND CHAIN LENGTH

MAY 2014

BURCU BAYKAL MINSKY

Ph.D., UNIVERSITY OF MASSACHUSETTS AMHERST

Directed by: Professor Paul L. Dubin

Glycosaminoglycans (GAGs), highly charged biological polyelectrolytes, are of growing importance as biomaterials and pharmaceutical drugs due to their immense range of physiological functions. They bind to many proteins; however, the degree of structural selectivity in GAG-protein interactions is largely unknown .Our studies have focused on the importance of heparin (a model GAG) charge and chain length in protein binding in order to explore its potential applications in biofunctional tissue scaffold materials, as polysaccharide drugs in anticoagulation, and as inhibitory agents in protein aggregation. We used electrospray ionization mass spectrometry, capillary electrophoresis, size exclusion chromatography, dynamic/static light scattering and electrostatic protein modeling.

Our studies, in the order of presentation in this thesis, showed first that the electrophoretic mobility of Hp oligomers varies inversely with chain length, which is explained by reduced counterion condensation at the chain ends or junctions. This provides an important insight into the biological relevance of sulfation patterns. Second, charge driven interactions among acidic fibroblast growth factor (FGF), tetralysine (K_4) and heparin decamer (dp10) indicated qualitatively that K_4-dp10 complex formation is consistent with binding being driven by the release of condensed counterions, whereas FGF-dp10 binding is driven primarily by screened electrostatics. Third, FGF binding to heparin octamer and decamer chains showed that protein:heparin mixing ratio modulates multiple protein binding equlibria, and highly sulfated chains facilitate the formation of multimeric FGF complexes. Next, the effects of heparin chain length on the complexation between antithrombin (AT) and Factor Xa (FXa) were studied: Shorter heparin oligomer chains induced binary AT·FXa complexes, while longer chains facilitated AT·FXa·dp20 ternary complexes. We used native heparin chains, which represent an extreme case of heterogeneity to investigate binding properties with AT. Using a recently developed mass spectrometry method, limited charge reduction, 1:1, 2:1 and 1:2 (AT:Hp) complexes were detected. Finally, differences between inhibition and reversal of aggregation by heparin were observed for AT and BSA aggregations; inhibition may depend on the stage at which Hp enters the aggregation process, and reversal depends on aggregate size and morphology.

TABLE OF CONTENTS

Page

LIST OF TABLES

Table Page

LIST OF FIGURES

Figure Page

CHAPTER 1

BACKGROUND ON HEPARIN AND HEPARIN -PROTEIN INTERACTIONS

1.1 Glycosaminoglycans (GAGs)

GAGs are negatively charged linear polysaccharides found on cell surfaces, in the extracellular matrix (ECM) and in connective tissue mast cell granules (Figure 1.1). They bind to a multitude of proteins including growth factor/morphogen families and receptors, enzymes, enzyme inhibitors, cytokines, chemokines, cell adhesion molecules and various extracellular matrix components to potentiate cell proliferation, differentiation, adhesion, wound healing, inflammation, embryonic development, homoeostasis, anticoagulation and amyloidogenesis.[1] The GAG family is classified into four groups depending on the saccharide structure, glycosidic bond type and the location of sulfates. These groups are: (1) heparin (Hp)/heparan sulfate (HS), (2) dermatan sulfate (DS)/ chondroitin sulfate (CS), (3) keratan sulfate (KS) and (4) hyaluronic acid (HA). Their structure consists of repeating disaccharide units of a hexuronic acid and a hexosamine, either or both can be decorated with sulfate groups at various positions (excluding hyaluronic acid). GAGs are covalently linked to highly glycosylated core proteins through serine residues to form proteoglycans (PGs).[2] PGs are highly diverse with respect to type of the core protein, size and composition of GAG chains. In the GAG family, HS is expressed in almost all cells,[3] exhibits structural diversity in a tissue-specific manner,[4] and is particularly important in the modulation of critical cellular functions. Heparan sulfates exert their functions by protein binding; however, the way in which polydispersity modulates protein binding is not well understood.

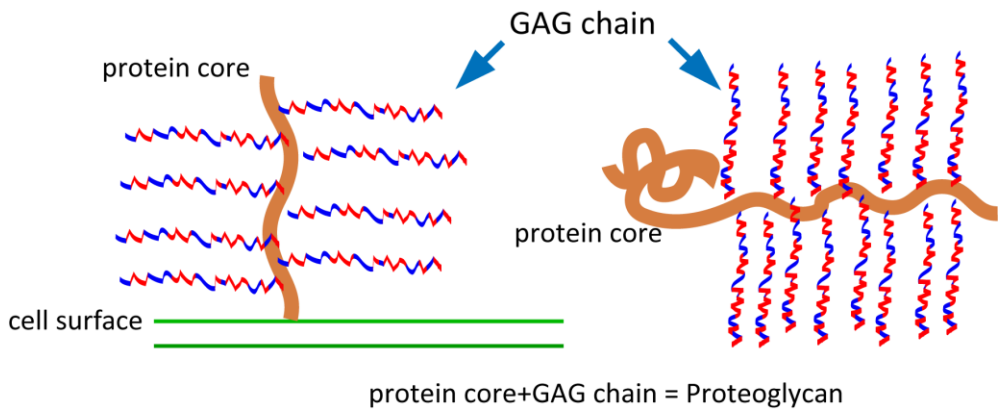

Figure 1.1: Representation of GAGs in the ECM, on the cell surface and in the mast cell granules (Adapted from ref. 3).

1.1.1 Heparan Sulfate and Heparin

The versatility of HS, playing the roles noted above for many growth factors, arises from its structural variability, seemingly random but in fact exquisitely regulated.[5,6] After the synthesis of the polysaccharide backbone, the polymer chain undergoes a series of modifications involving epimerization (transformation of glucosamine unit to L-iduronic acid) and the addition of sulfates to various positions by *N*- and *O*-sulfotransferases (Figure 1.2).

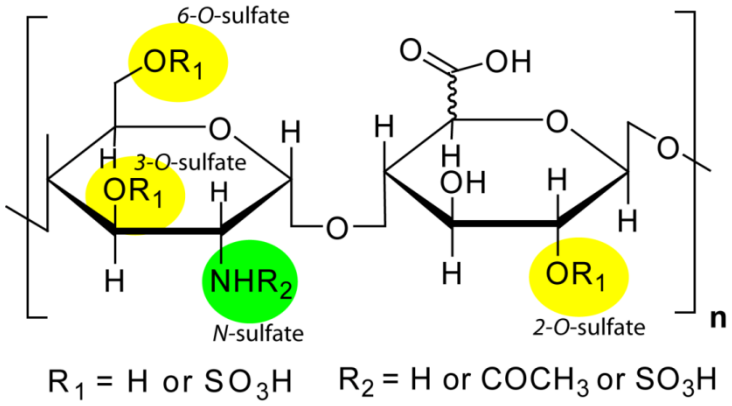

Figure 1.2: Repeating disaccharide unit structure of heparin and heparan sulfate

HS is consequently composed of repeating disaccharide units of *N*-acetylated (GlcNAc)/*N*-sulfated glucosamine (GlcNS) and glucuronic acid (GlcA) or iduronic acid (IdoA).[7] The enzymatic modifications do not occur uniformly across the entire chain during the synthesis; instead, the resultant structure exhibits "domains" of high sulfation, rich in IdoA and *O*-sulfation (NS); non-sulfated but *N*-acetylated (NA) regions; and alternating NS/NA domains.[8] Heparin (Hp) structurally related to HS, but in the mast cell granules, plays a different role by modulating proteins of the coagulation cascade. Hp resembles extended NS domains of HS (Figure 1.3) and contains higher degrees of *N*- and *O*-sulfation.[2]

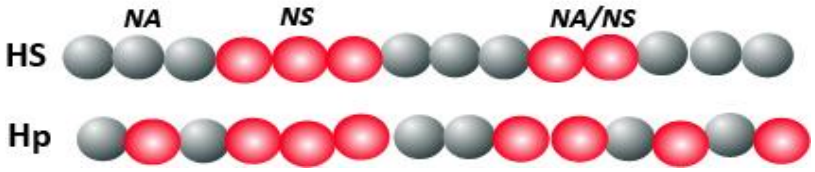

Figure 1.3: Schematic representation of the sulfate distribution on the Hp and HS.

Because these domains are more involved in protein binding events, Hp is commonly used in studies of GAG-protein interactions as a proxy for HS, and their similarity prompted the use of the term "heparinoid." In most studies related to GAG-protein interactions, GAG structure is depicted as rigid, and the dynamic nature of these highly charged polysaccharides in solution have not been given enough attention.[9,10]

1.2 Polyelectrolyte properties of GAGs

An essential feature of nearly all polyelectrolytes in solution is flexibility, stochastic chain dimensions, and characteristic dependences of chain dimensions on MW and ionic strength. GAGs have exceptionally high linear charge density arising from extensive post-translational sulfation. Heparin was first recognized as an anionic polyelectrolyte almost 35 years ago.[11] A variety of physicochemical studies have demonstrated the polyelectrolyte properties of GAGs. For example, Pavlov et al. characterized heparin as a semi-flexible, worm-like chain.[10] Bertini et al. employed high performance-size exclusion chromatography (HP-SEC) with triple array detector to calculate molecular weight and molecular weight distributions of full-length heparin, heparin fractions and dermatan sulfate. Consistent with the worm-like chain model, they found intrinsic viscosity [η] to scale with $MW^{0.84}$. Different GAG's exhibited different

MW-dependence of [η] and the radius of gyration.[12] Guo et al. showed that accurate measurement of MW's of heparin by size exclusion chromatography required salt (1M) to screen electrostatic interactions of heparin with the column packing.[13] These experimentally supported properties of GAGs coincide with the general polyelectrolyte behavior, such as displaying various levels of flexibility in solution depending on their repeat units, having no secondary structure and readily interacting with oppositely charged surfaces.

1.3 GAG-Protein Interactions

While GAGs have tremendous potential in therapeutic applications and regenerative medicine, their structure-function relationships are not well understood due to intra- and inter-chain heterogeneity. This heterogeneity allows them to interact with numerous proteins to potentiate critical cellular functions (Figure 1.4); however, the nature and degree of specificity and selectivity in protein binding (a unique set of GAG sequence arrangements for each protein cognate) is still a matter of debate. The concept of specificity has been associated with precise GAG sequences that interact with proteins via pair-wise interactions. In this perspective, the contributions of sulfate groups at specific locations has been thought to play prominent roles; this model initiated fingerprinting studies to determine key heparin/HS sequences that are involved in protein binding.[14-18] The attempts to unlock signature structural features of GAGs have been partially achieved only for antithrombin,[18,19] but failed in many cases, especially for growth factor/morphogen binding.[20-22] The high charge density, stochastic sulfate groups

distributions , and configuratioal flexibility of GAGs, which could be retained partially at the bound state could lead a definition of "electrostatic epitopes" , as opposed to well defined and unique binding motifs. This lack of consensus on the structural requirements in protein recognition points toward the need for alternative explanations to define the nature of GAG-protein binding.

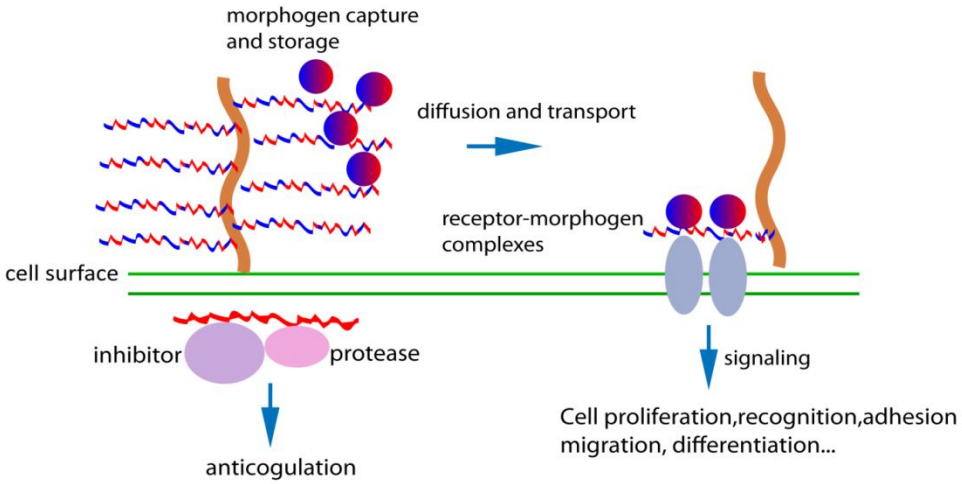

Figure 1.4: Suggested roles of Hp and HS

1.3.1 Conventional models in protein-Hp binding

In protein-ligand interactions, high-affinity invokes the "lock" and key" analogy for protein (host) and (small) ligand (guest). However, applying a similar analogy to protein-GAG systems neglects the inversion of the host-guest relationship. On the other hand, native GAG chains are replaced by low MW analogs in many studies, with the characterization of protein-oligoheparin complexes based on crystallography,[23-25] docking or MD simulations.[26] The Antithrombin-pentasaccharide model (Figure 1.5) epitomizes this perspective, positing a distinctive sequence on the Hp chain that interacts specifically with AT:[27] i.e. a specific pentasaccharide is required to activate AT towards coagulation protease, FXa in the anticoagulation. However, this model failed to take into account the configurational flexibility of Hp, and the enormous diversity of chemical structures, in particular sulfation sequences.

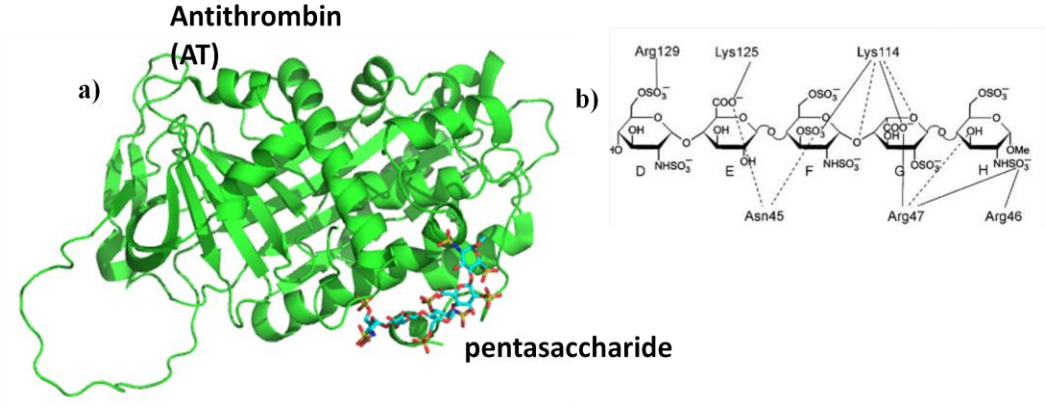

Figure 1.5: a) Crystal structure of AT and pentasaccharide; b) suggested hydrogen bonding (dashed lines) and salt bridges (solid lines) between AT residues and pentasaccharide charged groups.[23]

1.3.2 Alternative models in protein-Hp binding

The pentasaccharide model is increasingly viewed as a "gross approximation", of limited applicability for GAG-protein interactions in general.[9,28,29] Studies of tightly bound MW heparin analogs can be misleading, because enthalpic contributions are overemphasized, while entropic contributions are underestimated.[30] Furthermore, recent Monte Carlo simulations formerly done for a heparin-mimetic binding to BSA,[31] which we now extend to AT (Figure 1.6), point clearly to a dynamic form of binding in which conformational flexibility of the polyelectrolyte is not lost in the bound state (consistent with current ideas of "plasticity" and "promiscuity"). [9,32]

The dynamic nature of GAGs was also considered by Lander et al. who emphasized the contribution of GAG in binding kinetics rather than thermodynamics.[33] He proposed that GAGs act catalytically on the cell surface to capture growth factors and growth factors receptors. In blood coagulation, heparin basically increases the rate of Antithrombin-Thrombin or Antithrombin-Factor Xa interaction. Accordingly, the interaction can be considered in two steps: encounter and reaction. The first is driven by the physics of diffusion for the binding on the same heparin chain of AT and the coagulation protease, with the GAG chain acting as a surface to capture the interacting partners. Similarly, on cell surfaces, HS proteoglycans increase the rate of growth factor and receptor encounters by decreasing the dimensionality from 3-D to 2-D.[33]

Early views of specificity, i.e., the nature of the role of Hp/HS sequence in GF recognition, have been challenged by recent findings of promiscuity of binding between highly sulfated GAG chains and growth factors. Empirically, the correlation of GAG

sulfate density with GF binding appears to exist somewhat independently of precise location of sulfate groups. For example, Catlow et al. showed that the interaction of hepatocyte growth factor/scatter factor (HGF/SF) with HS is dominated by electrostatics and that HS sulfate density affects the selectivity.[34] Krueger et al. found that various FGFs share the same binding domain on HS, with affinity correlated with the level of sulfation.[21] Jastrebova et al. found correlation between overall *O*-sulfation levels and the stability of the FGF-receptor-HS.[35] Zhang et al. showed that the higher degree of sulfation on heparin chains is preferred in interleukin 7 (IL-7) interactions.[36] These findings point to the need for a new concept of GAG-protein specificity that considers charge complementarity between the protein and the related polyanion, i.e. "there is an intermediate specificity based on the gradient of electrostatic interactions that are a function of relative charge densities, in contrast to high conformationally based structure specificity."[37] In addition, arrangements of NS and NA blocks have been shown to provide functional domains for protein binding.[38] For example the interferon-gamma (IFNγ) binding site consists of 24 disaccharide units contains two terminal sulfated domains, each binding to one IFNγ monomer,[39] and separated by a nonsulfated G1cA-rich sequence. Similar binding site exists for platelet factor 4 (PF4),[40] interleukin-8 (Il-8),[41] RANTES[42] and vascular endothelial growth factor (VEGF).[43] Most of these proteins are either multimeric in solution or multimerized upon binding to HS.

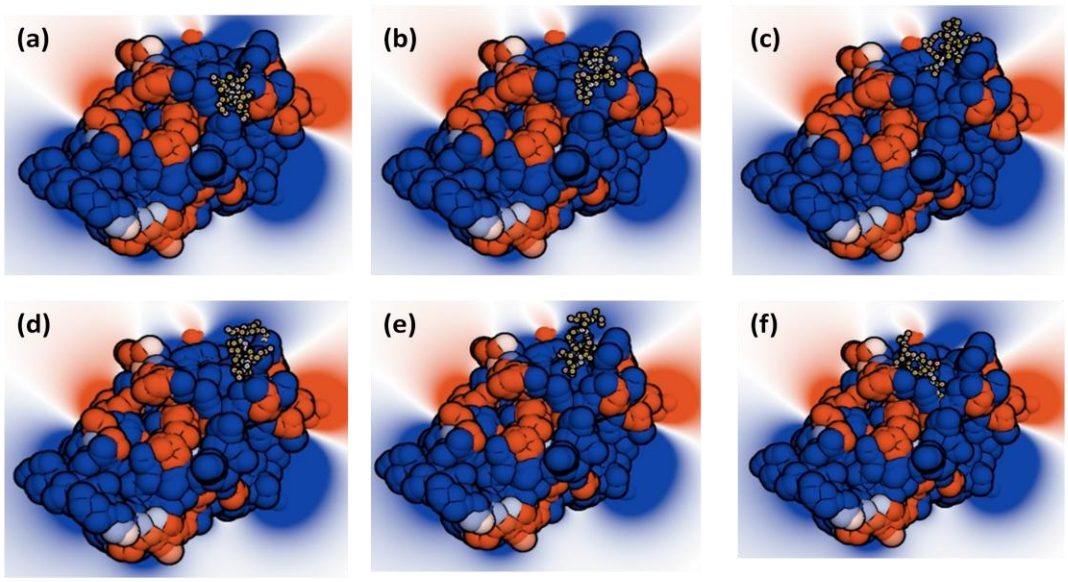

Figure 1.6: Coarse-grained Monte Carlo simulation showing the mobility of bound synthetic polyanion resides on the positive domain of AT, but never stops moving (*I* =10mM, pH=6.8). Red and blue correspond to the negative and positive potentials, respectively and they have been calculated using non-linear Poisson- Boltzmann equation (Courtesy of Daniel Seeman).

1.4 Roles of electrostatics in Hp-Protein binding

Heparin-protein binding affinity arises principally from the electrostatic interactions common to polyelectrolyte-protein systems,[44,45] for which different models have been widely applied. One model inspired by theories for the salt dependence of oligolysine-DNA interactions,[46,47] has been applied to DNA-protein binding. The linear dependence of log K_{obs} (equilibrium association constant) on log I (ionic strength) is consistent with a purely entropic ΔG_{obs}, which arises from the release of DNA counterions (Figure 1.7). However, directly replacing oligolysines with proteins fails to consider the influence of protein charge anisotropy.[48] Nevertheless, extension of this

treatment to Hp-protein binding yields a physically realistic value of Hp structural charge density deduced from measured dlogK_{obs} / dlog I.[49]

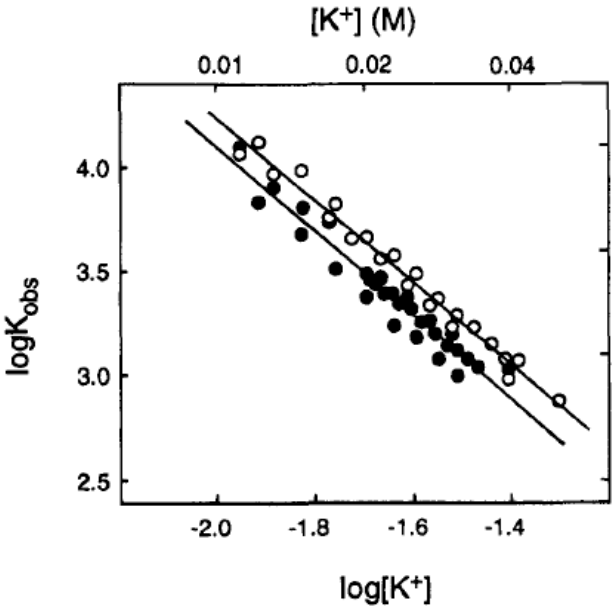

Figure 1.7: The dependence of association equilibrium binding constants Kobs on the salt concentration for KWK-CO2 (●) and RWR-CO2 (○) interactions with heparin (from ref. 49)

On the other hand, many polyelectrolyte-protein systems show clearly different salt dependence more consistent with Debye-Hückel screening.[44,50] This last model takes into account protein charge anisotropy, and effectively accounts for the non-monotonic salt dependence seen when polyelectrolytes (e.g., heparin) bind to proteins with net charge of the same (i.e. negative) sign, through a domain of opposite (i.e. positive) charge, best identified through representation via protein charge calculations.[51] Therefore, it is possible to account for the observed salt dependence of protein-Hp binding by using specific models of heparin binding along with quantitative protein visualization.[28,51] Non-

monotonic ionic strength dependence was observed for AT binding of both full length and low molecular weight heparin. In this system, maximum binding occurs at $5 < I < 30$ mM (Figure 1.8), where the Debye length ($\kappa^{-1} \sim 0.3/\sqrt{I}$) is closer to the protein radius (indication of the combination of short range attractions and long range repulsions).[28]

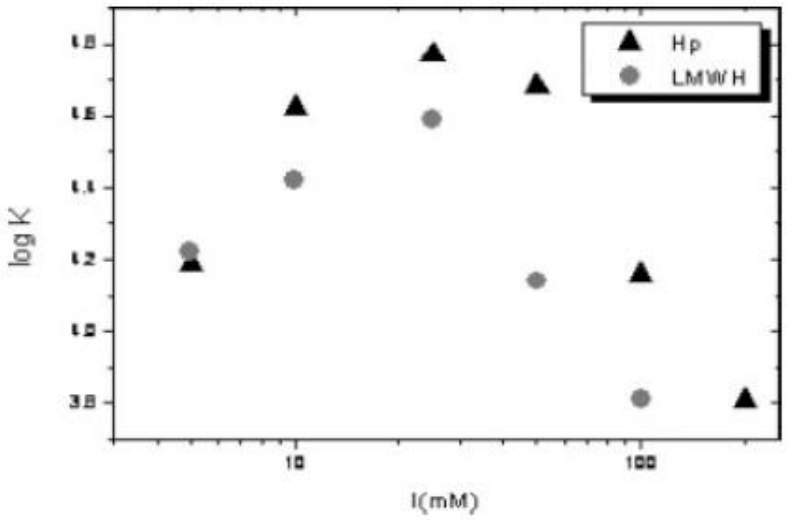

Figure 1.8: Non-monotonic salt dependence of AT binding with Hp and low molecular weight heparin, tinzaparin using frontal analysis continuous capillary electrophoresis (FACCE), from ref. 28.

1.5 Low Molecular Weight Heparins: Therapeutic Significances

The structural complexity of heparin is the major barrier for therapeutic applications of heparin. In order to reduce this complexity, efforts have emerged to generate low molecular weight Hp chains, which are composed of enzymatically or chemically depolymerized native heparin chains (MW 5,000 to 8,000 Da). The commercially available low molecular weight heparin analogs exhibited longer plasma life time than native heparin and have been safely applied in the treatment of anticoagulation and venous thromboembolism.[52] In addition, reduced heterogeneity

facilitates characterization of these Hp analogs and investigation of their protein interactions using various analytical tools. Accordingly, the small molecule Hp surrogates improve the "applicability" of certain experimental technique; however, such oversimplified surrogates of native Hp could deviate from the biologically relevant counterparts (Figure 1.9). Thus, there should be an adequate balance between "engineered" selective Hp chains and the biologically relevant Hp chains that could initiate substantial cellular response.

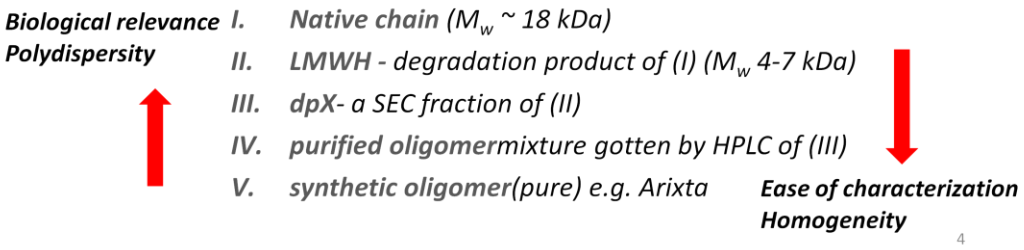

Figure 1.9: Schematic representation of the chain length and biofunctionality relationship of Hp

1.6 Aim and Outline of the Thesis

The purpose of this thesis is to elucidate structure-activity relations in glycosaminoglycan-protein binding. These are not well understood due to the immense polydispersity of heparin (Hp), the model GAG. The effects of GAG overall sulfation, saccharide sequence arrangements and chain length are still controversial. To address these issues, electrospray ionization mass spectrometry, capillary electrophoresis and dynamic light scattering were applied to systems of Hp and its oligomers in combination with either Antithrombin (AT) or Fibroblast Growth Factor (FGF). The effects of heparin

chain length and charge density were investigated in directing protein behavior, i.e., inducing complex formation or modulating higher-order protein assemblies.

The physicochemical properties of native heparin and heparin oligomers were studied using capillary electrophoresis and electrospray mass spectrometry (ESI-MS) as presented in chapter 2. This study indicates an inverse relationship between chain length and electrophoretic mobility of heparin oligomers, which can be explained by a recent theory of polyelectrolyte end effects. Chapter 3 explores mechanistic differences in the binding of a heparin decamer binding to a growth factor vs. an oligopeptide, with consideration of potential applications of heparin oligomers in tissue scaffolds. The effect of heparin oligomer chain length and charge density in FGF-1 binding and the induction of multimeric complexes of FGF-1 are demonstrated in chapter 4. Chapter 5 explores the heparin chain length dependence of FXa binding, focusing on the capabilities of various length Hp oligomers to induce binary and ternary complexes (chapter 5). In addition to Hp oligomers, AT and native heparin complex formation were studied using a recently evolved technique, limited charge reduction with FTICR MS, and these results are presented in chapter 6. Finally, studies that show inhibition and reversal of aggregation of antithrombin and bovine serum albumin by native heparin are presented in Chapter 7.

CHAPTER 2

COUNTERION CONDENSATION ON HEPARIN OLIGOMERS

Minsky, B. B.; Atmuri, A.; Kaltashov, I. A.; Dubin, P. L. Counterion Condensation on Heparin Oligomers. *Biomacromolecules* **2013**, *14*, 1113-1121.

2.1 Abstract

The electropherogram of native heparin shows a broad distribution of mobilities μ which truncates abruptly at a notably high $\mu = 4.7 \times 10^{-4}$ $cm^2V^{-1}s^{-1}$. This highly skewed mobility distribution is also found for the 20-saccharide chain which shows from mass spectrometry a more uniform (symmetrical) with respect to sulfation level. Since a partially degraded heparin exhibits oligomer peaks with $\mu > 5 \times 10^{-4}$ $cm^2V^{-1}s^{-1}$ (appearing to escape the limitation of the mobility value for native heparin), we examined the electrophoretic behavior of chain-length monodisperse heparin oligomers. Their mobilities varied inversely with the logarithm of the contour length *L*, for *L* from 3 to 10 nm and reached an asymptotic limit for *L*> 20 nm. The generality of this effect was indicated by similar behavior for oligomers of poly(styrenesulfonate). A recent theory of polyelectrolyte end effects (Manning, G. S. *Macromolecules* **2008**, *41*, 6217-6227.), in which chain termini exhibit reduced counterion condensation was found to account quantitatively for these results. A qualitative explanation for the anomalously high value of μ of native heparin, 10-20% higher than those seen for synthetic polyelectrolytes of higher linear charge density is suggested on the basis of similar junction effects (Manning, G. S. *Macromolecules* **2008**, *41*, 6217-6227.), which reduce counterion condensation at the interfaces of regions of high and low sulfation. We suggest that these

effects should be considered in models for the biofunctionality of the regulated high and low sulfation (NS/NA) domains of heparan sulfate.

2.2 Introduction

The ability of glycosaminoglycans (GAGs) to biofunctionally bind a multitude of proteins is related in some way to their immense heterogeneity and variable sulfation patterns, but this same heterogeneity poses a problem for virtually all methods of investigation. GAGs are the most highly charged macromolecules in animals, and their affinity for proteins must involve significant electrostatic forces, including even long-range repulsions from the globally negative charge of most "heparin-binding proteins".[9,28] Evidence exists that the negative charge arising from GAG sulfation is modified by counterion condensation, a well-established phenomenon for both natural[53-57] and synthetic[58,59] polyelectrolytes. The biophysical consequences of this are not understood, even though counterion release is likely to play a role in GAG-protein binding.[49] The issue is further complicated by the immense intrinsic heterogeneity of GAGs and the corresponding polydispersity of sulfation patterns, a central problem in efforts to resolve GAG structure-function relations.[30,45] Electrophoretic mobility measurements have provided direct validation of counterion condensation,[58-62] but electropherograms of native heparin are naturally quite complex.[63] Heparin oligomers provide a level of simplification suitable for electrophoresis in conjunction with electrospray ionization mass spectrometry (ESI-MS).

The key to structure-function relations for GAGs clearly involves elucidation of their sulfation patterns;[22,64] regulation of sulfation facilitates their roles in angiogenesis,

cell signaling, proliferation, and blood coagulation.[2,65-67] After elongation, heparin/HS chains are subjected to enzymatic modifications as opposed to being produced by a direct genetic template. The final chains exhibit continuous domains of N-sulfation, N-acetylation and N-sulfation (NS/NA-domains), and unmodified N-acetylation (NS, NA/NS, and NA-domains).[7,68] Epimerization and O-sulfation then preferentially occur in the vicinity of NS domains. Contrary to HS, heparin does not have "domains" of sulfation, but instead extended O-sulfated NS domains**.** In this way, heparin serves as a good model to examine the way in which high charge density is a central feature in the affinity for multiple proteins.

Elucidation of heparin-protein energetics has proceeded by analogy to DNA-protein energetics, which rests on measurements of the ionic strength dependence for DNA-oligolysine interactions[47,69] subsequently extended to DNA-protein binding.[70] Two distinct models have generally been invoked to explain the suppression of polyelectrolyte-protein binding with added salt. The first evolved from counterion condensation theory developed by Manning,[54,55] and extended by Record[69,70] to identify the release of sodium ions from DNA as a driving force for its binding to oligolysines. Conceptually replacing DNA with heparin, Lohman and Mascotti[49] measured the salt-dependent binding constants for heparin with cationic peptides and concluded that a purely entropic ΔG_{obs} arises from the release of heparin counterions. Replacing oligolysines with proteins, however, raises the possibility of the influence of protein charge anisotropy entirely absent in the DNA-oligolysine model.[48] A distinctly different salt effect arises from screening characterized by the Debye-Hückel screening length κ^{-1}, [9,28,51] which takes into account the decay of small ion imbalance near the macroion, an

effect completely distinct from the expulsion of condensed counterions to the bulk solution in the Manning[54,55] and Record[69,70] models.

While experiment suggests that heparin may be subject to counterion condensation, GAGs introduce a level of heterogeneity not encountered with DNA, olioglysines, or proteins. Counterion condensation theory states that the polyelectrolyte effective linear charge density is lower than the structural charge density when the average spacing between charges b is smaller than the Bjerrum length l_b (The latter , l_b, is the distance between two unit charges at which the Coulomb free energy is thermal energy, k_BT). When $\xi = l_b/b > 1$, the ionic distribution around the polyelectrolyte is not stable; therefore monovalent counterions condense to reduce ξ to 1. Evidence for counterion condensation on GAGs arises from several facts: NMR shows that calcium ion binding to heparin does not follow a mass-action law;[71] chondroitin sulfate and keratan sulfate exhibit similar osmotic activities despite the higher sulfation of the former;[72] and the effective charge of heparin from the Donnan distribution is much less than its structural charge.[73] GAG heterogeneity, while recognized, could not be explicitly treated in these studies. Inter- and intra-chain heterogeneity of these GAGs seriously complicates application of the original counterion condensation theory, a challenge which can be greatly simplified with heparin oligomers monodisperse with respect to chain length.

This reduction of polydispersity makes it possible to take advantage of high resolution methods: capillary electrophoresis (CE) and mass spectrometry (MS). CE was used to measure the mobilities of single stranded DNA oligomers of variable charge density at fixed length, or variable degree of polymerization (dp) and at fixed charge.[74]

For heparin oligomers, the resolving power of CE has been mainly directed towards characterization of the structural heterogeneity of oligomers.[75-79] Since MS of GAGs provides a description of the distribution of sulfation levels,[80-83] it can be complementary to CE which provides a description of the distribution of mobilities.[84,85] Of special interest here is the relationship between electrophoretic mobility and sulfation level, since the dependence of mobility on structural charge density has been a central feature in studies validating counterion condensation.[58,63,73,86]

Here we measure mobility distributions for "clinical" heparin, low-MW heparin, and paucidisperse heparin oligomers from hexasaccharide to icosasaccharide (dp6-20), and compare them to distributions of mass and sulfation levels, and distributions of effective sizes, obtained by ESI-MS and SEC, respectively. The mobilities for the most highly sulfated components of the oligomers all show the same inverse length dependence as seen in oligomers of PSS in 2-25 nm regime,[58,84] but contrary to the behavior of oligomers of single-stranded DNA.[74] Our results for the heparin oligomers in the 2-25 nm length regime is in good agreement with a theory for counterion condensation subject to end effects.[87] The results are directly relevant to thermodynamic analyses put forward for the binding of heparin oligomers to proteins, and have implications for the contribution of counterion release to the binding of proteins to heparin chains with regulated patterns of sulfation.

2.3 Experimental

2.3.1 Materials

Heparin hexa, octa, deca and icosasaccharides (dp6, dp8, dp10, dp20) generously donated by Dr John Gallagher from Iduron, were prepared by partial heparin lyase digestion, followed by high resolution gel filtration. Full-length "native" heparin was purchased from Sigma. Low molecular weight heparin, tinzaparin, (5000 Da) provided by LEO Pharma (Ballerup, Denmark), was prepared by enzymatic depolymerization. Native heparin contains longer heparin chains, with average 50-disaccharide units, and tinzaparin includes 2 - 24-mer chains.

2.3.2 Methods

2.3.2.1 Capillary Electrophoresis (CE)

Capillary electrophoresis (CZE) of heparin oligomers was performed using an Agilent instrument equipped with a diode array multiple wavelength detector. The runs were monitored at 200 and 232 nm. An uncoated fused silica capillary with dimensions 50 µm x 33 cm (24.5 cm effective) was used. The voltage applied across the capillary was fixed at 12 kV, and the temperature was maintained at 25.0 °C. The injection of the samples was done in hydrodynamic mode, applying 50 mbar for 3 seconds at the inlet capillary. New columns were rinsed for one hr with 1 N NaOH, followed by one hr with Milli-Q-H2O. Between each run, the capillary was reconditioned for 3 min with 0.1 N NaOH, followed by water and run buffer. The concentrations of heparin oligomers (dp6-dp20) were 1 g/L, native Hp was 5 g/L and tinzaparin were 7 g/L. This difference in

concentration between Hp and Tz has no effect on the results, inasmuch as identical electropherograms are obtained over the range of 1-5 g/L for either heparin or Tz. Heparin oligomers were run in triplicate to verify reproducibility. The run buffer was 10mM sodium phosphate at pH 6.8. The electrophoretic mobility was calculated as:

$$\mu = \frac{v_0 - v_1}{E} = \frac{L_D L_T}{V}\left(\frac{1}{t_m} - \frac{1}{t_s}\right) \qquad \textbf{Eq. 2.1}$$

where v_0 and v_1 (cm s^{-1}) are the electroosmotic velocity (EOF) and solute velocity, respectively; E is the strength of the applied electric field (V cm^{-1}); L_D is the effective length of the capillary, and L_T is the total length of the capillary (cm); V is the applied voltage; and t_m and t_s are the migration times of the reference marker (mesityl oxide) and the sample, respectively.

2.3.2.2 Mass Spectrometry (MS)

Stock solutions (2 g/L) of dp6, dp8, dp10 and dp20 in water, were diluted to 10 µM with 10mM NH_4Ac. Mass spectra for dp6-10 were obtained using a QStar-XL hybrid quadrupole-time-of-flight MS equipped with a nano-ESI-source (AB Sciex, Toronto, Canada). Sulfate group loss was minimized by applying mild desolvation parameters (Declustering potential (DP): 40, Focusing Potential (FP): 150, DP2: 15). The representation of the assigned peaks follows the Roepstorff-Henriksen nomenclature,[80] (X,Y,Z), where X = degree of polymerization, Y = number of sulfate groups and Z = number of acetyl groups. All MS analysis for dp6-10 were carried out in the positive ion mode; therefore NH_3 adduct formation was observed depending on the level of sulfation. The extent of NH_3 adduct formation was determined using the correlation between charge

state and the number of adducts provided by Abzalimov et al. for heparin hexamer.[88] The mass measurement of dp20 sample was carried out with a Bruker's SolariX fourier transform ion cyclotron resonance mass spectrometer (FT-ICR MS) equipped with a 7-T magnet (Bruker Daltonics, Billerica,MA) using internal calibration at a 100 000 mass resolution.

2.3.2.3 Size Exclusion Chromatography (SEC)

The hydrodynamic size distribution of native heparin and tinzaparin were determined on a TOSOH SW2000 size exclusion column equipped with UV detector at 232 nm with an injection volume of 20 μL using 150mM pH 6.9 NH_4Ac, as mobile phase. The SEC column had V_0 = 2.3 mL (by DNA injection), and V_t = 5.4 mL (by acetone injection). The calibration curve (log R_h vs V_e) for the TOSOH SW2000 column was constructed using protein standards of thyroglobin (R_h = 7.9 nm), antithombin (R_h = 3.9 nm), bovine serum albumin (R_h = 3.5 nm), ovalbumin (R_h = 3.0 nm), β-lactoglobulin (R_h = 2.6 nm), carbonic anhydrase (R_h = 2.3 nm), ribonuclease A (R_H= 1.8 nm), and cytochrome C (R_h = 1.6 nm). The universal log R_H vs V_e curve[89] was converted to the heparin calibration curve (log M_w vs V_e) by using an R_H-M_w relationship for heparin based on measurements for various heparin M_w fractions[10] and diffusion coefficients ($D_T = 6\pi\eta R_H/k_BT$) in reference 10.

2.4 Results

Several important features appear in Figure 2.1A, which shows superimposed electropherograms of native heparin and Tinzaparin. (1) The electropherogram of native

heparin was abruptly truncated at $\mu = 4.7 \times 10^{-4}$ cm^2 V^{-1} s^{-1} in a manner uncorrelated with the shape of the molecular size (SEC) distribution in Figure 2.1B. This result is consistent with limitations due to diminution of effective charge by counterion condensation for polyelectrolytes with $\xi > 1$.[55] However, the limiting mobility is remarkably high: a search of the literature[58,63,84,90] produces only one report of a mobility[91] as high as our result for μ_L^{∞} of heparin. (2) Mobilities of the oligomers (dp $\leq$ 20) are even larger than the limiting value for native heparin. The SEC chromatograms show the expected level of overlap of molecular size distributions in that roughly 1/3 of the mass of heparin is within the MW range of Tinzaparin. Nevertheless, nearly 70 % of the species in Tz display larger values of mobility than any native heparin components, i.e. $\mu > 4.7 \times 10^{-4}$ cm^2 V^{-1} s^{-1}.

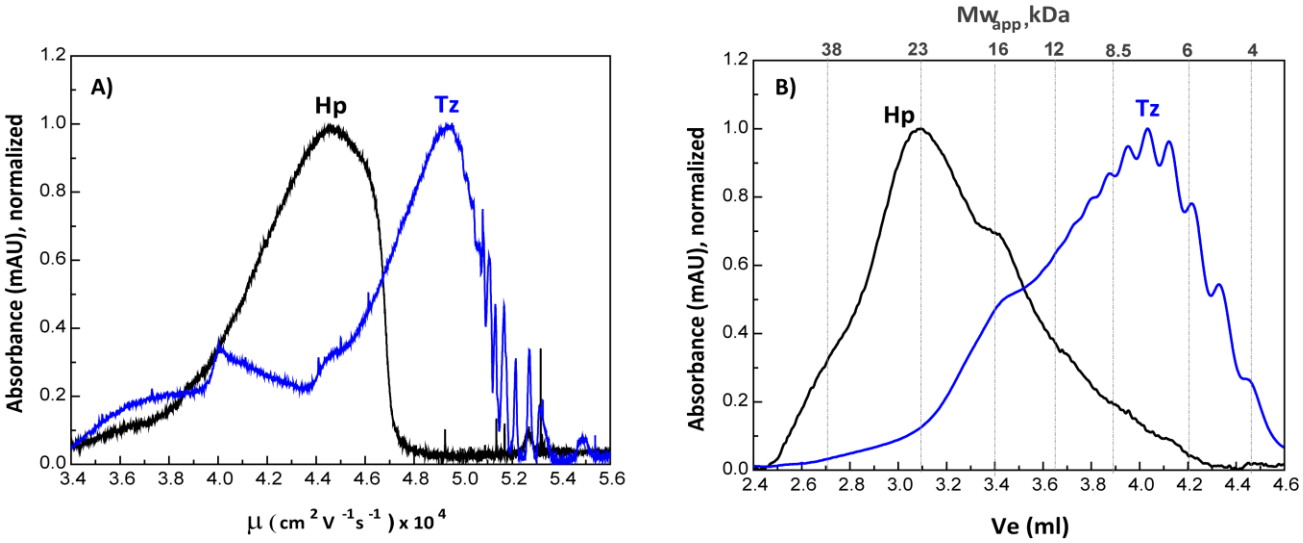

Figure 2.1: Comparison of native heparin (black) and low-MW heparin (Tinzaparin, Tz) (blue). (A) Electropherograms obtained at 10 mM phosphate buffer at pH 6.8 (detection at 200nm). (B) Size exclusion chromatograms of native heparin and tinzaparin on TOSOH SW2000 column in 150 mM Ammonium acetate, pH 6.9 (detection at 232 nm).

The appearance of well-resolved species at one end of the distribution of mobilities, and also at one end of the distribution of sizes prompted us to consider a hypothetical correlation between small size and high mobility for Tz species (*vide infra*). While a similar correlation was noted for olgiomers of PSS[58,84] and acrylic acid,[92] no physicochemical explanation for such common behavior of linear PE oligomers has been offered**.** The striking observations are thus (1) the high mobilites for native heparin, nevertheless abruptly truncated at $\mu = 4.7 \times 10^{-4}$ cm^2 V^{-1} s^{-1}; and (2) the even higher mobility of Tz oligomers, as if they were not subject to counterion condensation. We will show later that different structural features within heparin lead to these two effects.

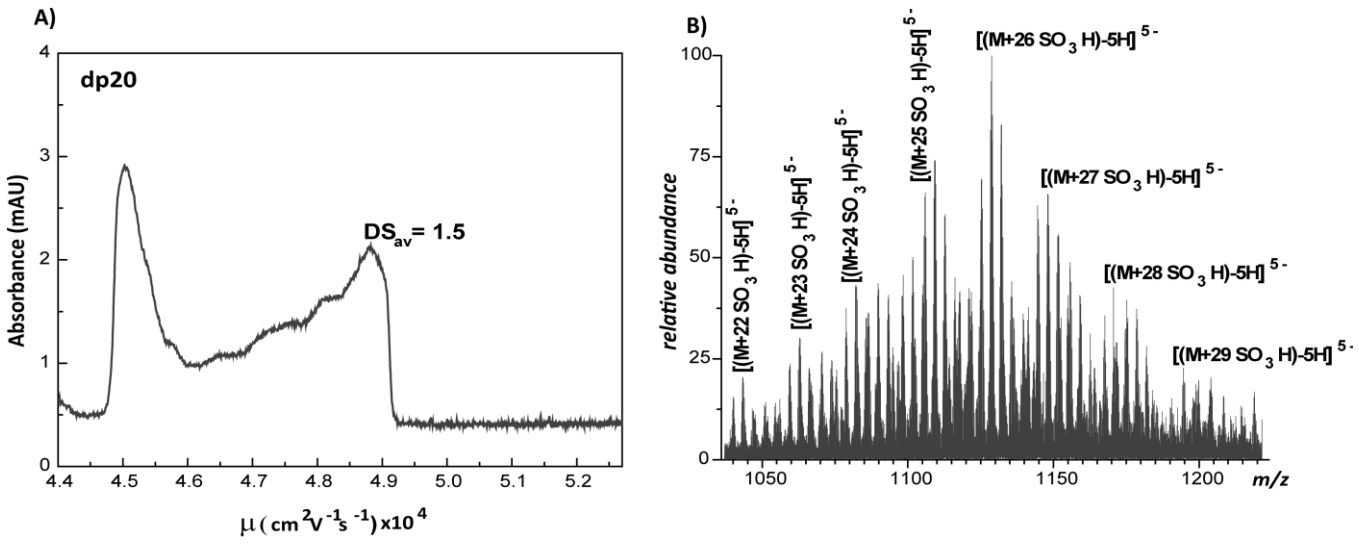

Figure 2.2: Qualitative comparison of the shapes of distributions from capillary electrophoresis and mass spectrometry for dp 20. A) The electropherogram of heparin dp20 (1 g/l) in 10 mM phosphate buffer, pH 6.8. B) Mass spectrum of dp20 obtained at -5 charge states using FT-ICR MS (buffer: 50:50 MeOH: H_2O with 10 mM ammonium acetate)

The electropherogram and mass spectrum of dp 20 in Figures 2.2A and 2.2B make it possible to compare mobility and mass distributions. Mass distributions could be recognized as distributions of sulfation levels: all signals correspond to dp20 chains having in common the components shown in Figure 2.3 with R_1 and R_2 groups designating variations due to post-polymerization enzymatic modification. Mass spectrum showed the number of SO_3H in dp20 ranges from 22 to 29. While the distribution of mobilities is truncated at $\mu = 4.9 \times 10^{-4}$ $cm^2 V^{-1} s^{-1}$ in CE, the distribution of sulfation is somewhat symmetrical in MS; therefore we can suggest that the most highly sulfated oligomers (1.5 sulfates per saccharide on average) eluting at the leading edge of the electropherogram. It was obvious that the truncation of the mobility for dp20 arises from the same effect demonstrated for heparin in Figure 2.1A.

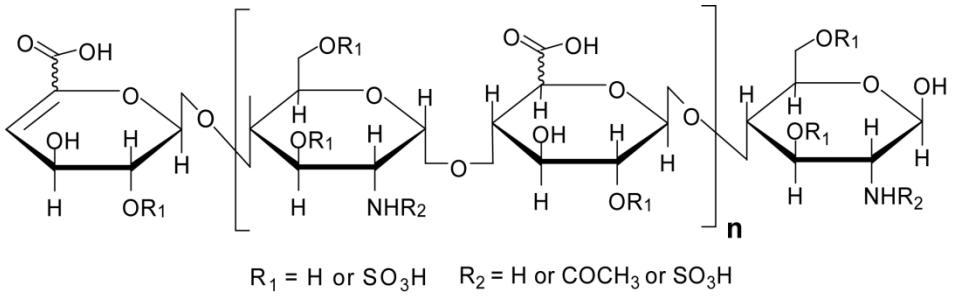

Figure 2.3: Representation of heparin structure

The behavior of the oligomeric components seen in Figure 2.1A was explored using size-fractionated oligoheparins that are monodisperse with respect to chain length (dp). The breadth of the electropherogram for dp 20 in Figure 2.2A is attributable to sulfation, variable with respect to sequence arrangement and degree (sulfates per saccharide repeat unit, DS). A leading edge for dp20 in Figure 2.2 at $\mu = 4.9 \times 10^{-4}$ cm^2

V^{-1} s^{-1} is seen as well for dp 6,8 and 10 in Figure 2.4; the mass spectra for these, while insensitive to sequence arrangement, show that these leading edges can be assigned to the highest average sulfation level, DS = 1.5. For this reason, we use the leading edge mobility μ_{max} to establish chain length dependence, i.e. at constant DS = 1.5. Figure 2.4A shows the dramatic effect of chain length on mobility, as anticipated from Figure 2.1A, focusing on the DS = 1.5 components. Table 2.1 summarizes molecular weight, contour length *L* and μ_{max} for heparin and also incorporates comparable results for oligomers of sodium poly(styrenesulfonate) (to be discussed below).

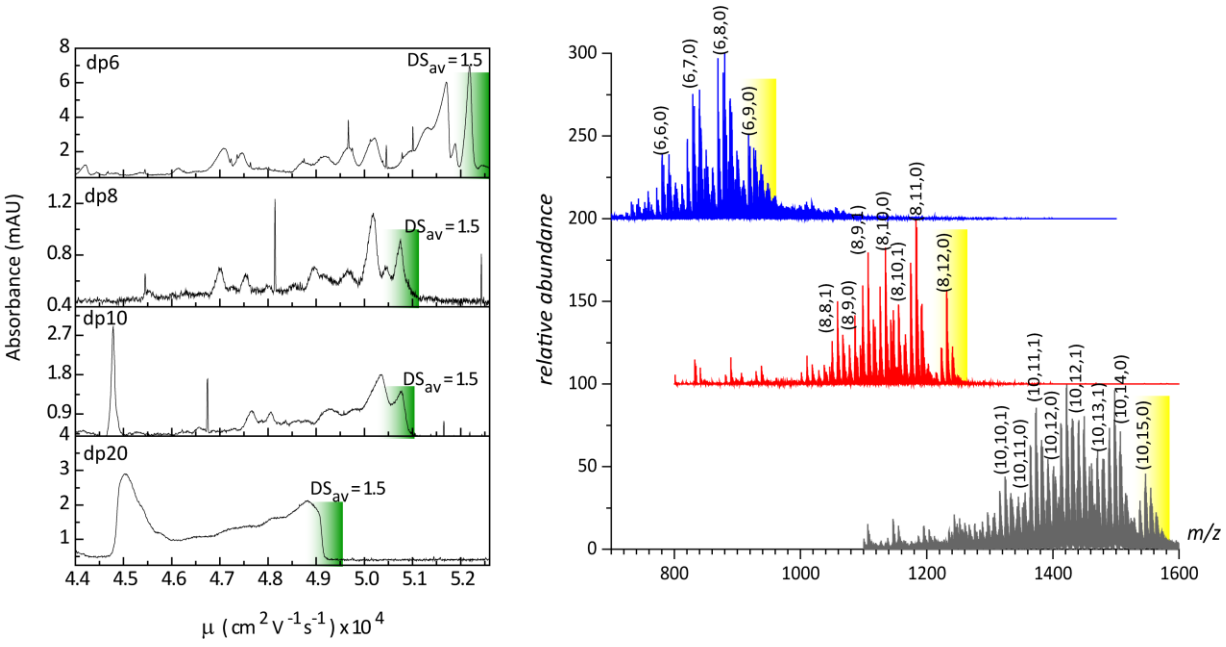

Figure 2.4: A) The electropherograms of heparin oligomers (1 g/L) at 10 mM phosphate buffer, pH 6.8 B) Individual mass spectrum of heparin oligomers (dp6, dp8, dp10) at +2 charge states (Buffer: 10 mM ammonium acetate, pH 6.8). (X, Y, Z) represents degrees of polymerization, number of sulfate groups and number of acetyl groups, respectively.

Table 2.1: Mobility versus contour length for heparin oligomers and NaPSS

Heparin			NaPSS[d]			
	L^a (nm)	μ_{max} (10mM)	M_w, x10 $^{-3}$ g/mol	L^c (nm)	μ_{max} (40mM)	μ_{max} (10mM)
dp4	2 [b]	5.3[b]	1.6	2.4	4.72	5.3±0.3
dp6	3	5.2	5.4	8	4.48	5.1±0.3
dp8	4	5.1	12	18	4.25	4.7±0.3
dp10	5	5.1	35.2	52	4.20	4.26
dp20	10	4.9	70	104	4.28	4.26
native	24	4.7	88	131	4.22	4.26
	44	4.7	250	372	4.20	4.26
	65	4.7	500	744	4.20	4.26

a: Disaccharide length 1nm[10]
b: From tinzaparin electrophoregram.
c: NaPSS repeat unit contour length 0.25 nm
d: Data for 4 0mM is taken from reference 85. The data for 10 mM is calculated using values in reference 58 and 84. Contour lengths calculated as M_w/m_0 , where m_0 is the residue mass corrected for degree of sulfonation.

2.5 Discussion

Data from Table 2.1 for dp6-20, presented in Figure 2.5 show that μ_{max} varies inversely with log L, converging on μ_L^∞ for native heparin (dotted line). The mobility of dp20 coincides with the electrophoretic front of native heparin (Figure 2.1A), because counterion condensation in both cases determines the maximum possible mobility. In order to establish the generality of this effect, we plot in the inset of Figure 2.5 similar data for oligomers of sodium poly(styrenesulfonate) (PSS), both as the values given in reference 85 at 40 mM salt, as well as values extrapolated to 10 mM salt using the salt-dependences in references 58 and 84. With either data set, PSS mobility decreases with increasing chain length, reaching μ_L^∞ ~ 25 nm, very close to the behavior for heparin, although μ_L^∞ shows a significant 10% diminution relative to heparin. Overall, Figure 2.5

suggests a fundamental relationship between contour length and mobility independent of structural detail. We note that the monotonic behavior of μ_L seen in Figure 2.5 does not persist for PE oligomers below L = 2 nm.[58,84] Such small molecules, not subject to counterion condensation, and with complex frictional properties, should not be viewed as members of the apparently homologous series of heparin dp6-20 and their behavior is beyond the scope of the present study.

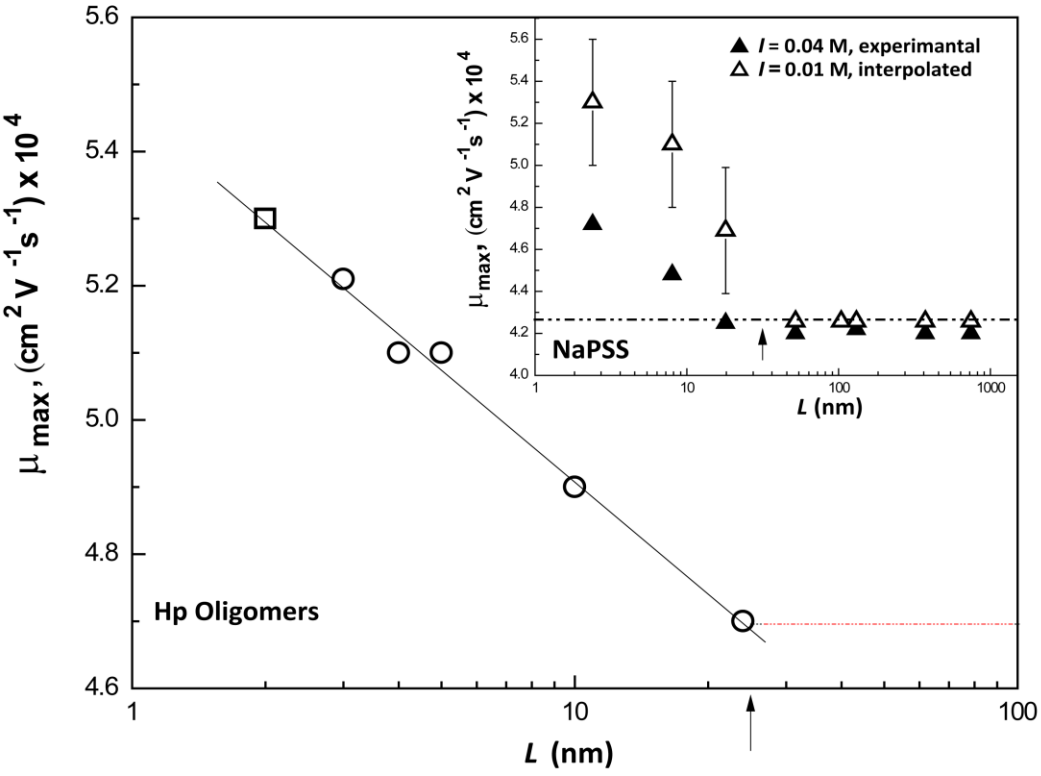

Figure 2.5: Leading edge mobility μ_{max} versus contour length for heparin oligomers (dp4-dp20) of DS = 1.5, and limiting value for native heparin (red dotted line). The open square is used to indicate that the mobility of dp4 was taken from the tinzaparin electropherogram (Figure 2.1A). Inset: Mobility vs. contour length for poly(styrenesulfonate) (PSS) measured at 40 mM, from ref 85, and the calculated mobilities for 10 mM, using the experimental PSS mobility data for various ionic strengths from refs 58 and 84. Arrows indicate the contour length at which the limiting mobility is reached.

We calculate from structure that the mean dimensionless structural linear charge densities ξ for Hp (2.84) and 80 % sulfonated NaPSS, (2.25) are essentially independent of chain length, so that explanation of the *L*-dependence of Figure 2.5 must be sought elsewhere. While relationships between friction coefficient and chain length have been proposed,[93] it is difficult to understand why that effect would truncate at a common length for different polyelectrolytes. For this reason, we turn to the *L*- dependence of the *effective* value of ξ, i.e. the charge density after counterion condensation.

Explanation of these observations appears in a recent treatment of end effects on ξ_{eff} for oligopolyelectrolytes.[87] In brief, the electrostatic potential arising from a sequence of neighboring polyelectrolyte units responsible for counterion condensation must be diminished at the sequence termini, e.g. at chain ends. The increasing fraction of terminal sulfate groups with decreasing dp is then responsible for the reduced counterion condensation. This is equivalent to a monotonic increase in ξ_{eff} for shorter chains and accounts for the remarkably high mobilities noted for dp 4-10 in Figures 2.1A and 2.5.

The equilibrium value of the effective charge fraction *f(s)* for any segment along the length of a polyelectrolyte oligomer with univalent counterions is given by;[87]

$$f(s) = \frac{1}{2\xi}\left(1 - \frac{\ln(\kappa b)}{\ln(s/b)}\right) \qquad \textbf{Eq. 2.2}$$

where κ is the inverse of the Debye screening length, *s* the distance from the end, *b* the axial spacing between neighboring charged groups, and ξ the dimensionless charge density parameter:

$$\xi = \frac{e^2}{4\pi\varepsilon k_B T b} = \frac{l_b}{b} \qquad \textbf{Eq. 2.3}$$

Here, e is the electron charge, ε the permittivity of the solvent, k_B the Boltzmann constant, and l_b the Bjerrum length. In order to calculate the effective charge fraction for heparin oligomers, each disaccharide is assumed to have the same average number of charges, 4 per disaccharide (three sulfates and one carboxylate, viewed identically because the carboxylate is fully ionized at pH 6.8). With a length of 1 nm per disaccharide, b = 0.25 nm and ξ = 2.84. Figure 2.6 shows the way in which heparin structure is represented in a form consistent with Eq 2.2

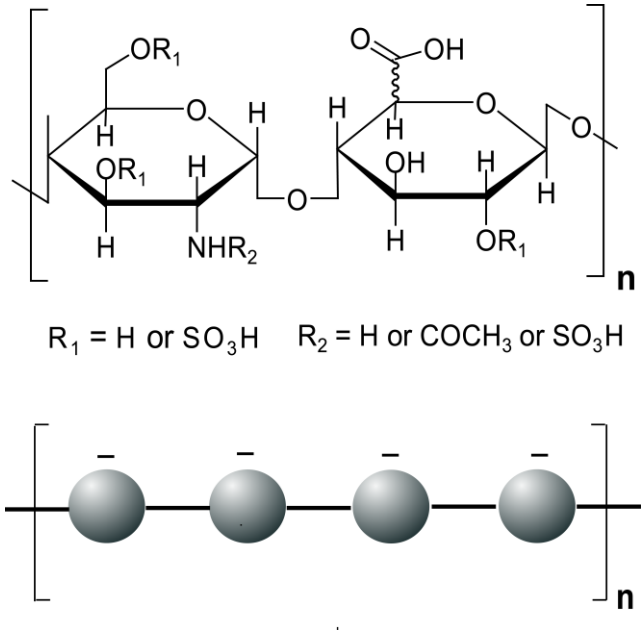

Figure 2.6: Representations of an average heparin structure. Above: molecular structure of the heparin disaccharide unit. Below: representation adopted for implementation of Eq.2.2: each disaccharide is represented by four segments with one charge apiece. Actual disaccharide length is 1 nm,[10] average distance between charges *b* (segment length) is 0.25 nm.

These resultant values of *f(s)* are averaged over the values of *s* for each oligomer chain to give the mean effective charge fraction f_{av} in Table 2.2. The effective charge

fraction was calculated at each charge sites and summed over the entire length of the oligomer, which gives the total effective charge of the oligomer. This effective charge is then divided by the total number of charge sites to get average *f(s)*. For small oligomers (dp8 and below) f_{av}/L decreases rapidly with L because condensation effects propagate only $0.2\kappa^{-1}$ (~0.5 nm) from the ends. The minimum value for f_{av} (full condensation) approached asymptotically at high L is 0.3. The lower mobilities of NaPSS relative to Hp in Figure 2.5 (about 10% less) can now be understood as a consequence of its lower effective charge density f_{av}/b. These lower effective charge densities arise from its structural charge density $1/b$ which is 26% lower than that of Hp. This result, $\mu_{Hp}/\mu_{PSS} \sim 1.1$ is observed even in the limits at high MW. Interpolating the results of Cottet et al.,[84] for the ionic strength dependence of high-MW (88% sulfonated) PSS mobility to I = 10 mM leads to an identical result of $\mu_{Hp}^{\infty}/\mu_{PSS}^{\infty}$ = 4.7/4.2. Most importantly, Table 2.2 clearly shows the dramatic increase in the mean segment effective charge with decreasing chain length as was seen in Figure 2.5.

Table 2.2: Calculated effective charges and charge fractions of heparin oligomers and NaPSS at I = 10 mM

Heparin				NaPSS			
***L*(nm)**	**Total $Q_{structural}$**	**Total $Q_{effective}$**	f_{av}	***L* (nm)**	**Total $Q_{structural}$**	**Total $Q_{effective}$**	f_{av}
2	8	6.8	0.85	2.4	8	7.2	0.91
3	12	8.7	0.72	8	25	15.4	0.62
4	16	10.3	0.64	18	57	27.9	0.49
5	20	11.8	0.59	52	167	66.3	0.40
10	40	18.7	0.47	104	333	120.4	0.36
24	96	35.6	0.37	131	419	147.7	0.35
44	176	58.1	0.33	372	1190	383.6	0.32
				744	2381	735.8	0.31

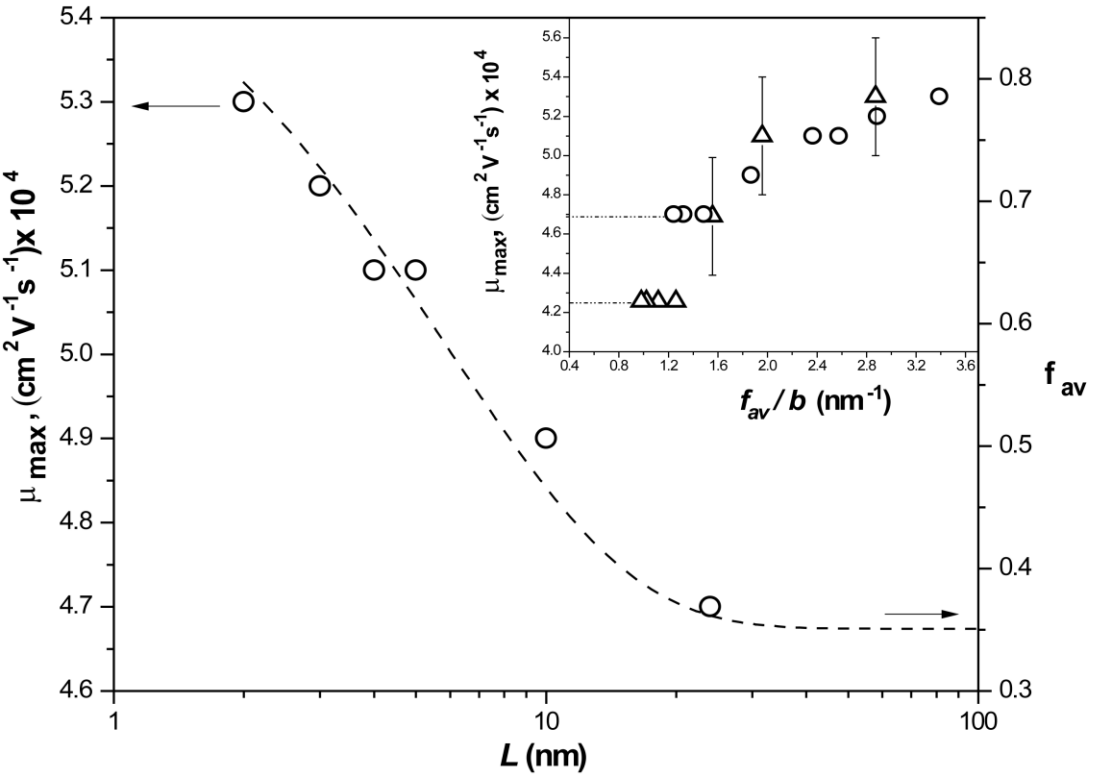

Figure 2.7: Contour length dependence of the leading-edge mobilities for heparin oligomers (dp4, dp6, dp8, dp10, dp20 and native heparin limiting value) compared to theoretical average effective charge (dashed line). Positions of the two vertical axes are arbitrary. Inset: Dependence of mobility on theoretical effective charge per segment length for Hp (○) and NaPSS (Δ).

Figure 2.7 shows that the contour length dependence of measured mobilities from Figure 2.5 closely resembles the contour length dependence of f_{av} calculated from Eq. 2.2 (dashed line). This result reflects the interdependence of μ and f_{av}, which is shown in the inset, although the arbitrary nature of the two ordinate axes limits the interpretation of the apparent congruence of experiment and theory. Further evidence for a fundamental basis for this relationship comes from the nearly congruent data for heparin and PSS, at least in the region of intermediate chain length. The difference between these two

polyelectrolytes with respect to limiting mobilities will be discussed below. Regardless of this difference, μ_L^{∞} = 4.7 x10^{-4} cm^2 V^{-1} s^{-1} -- for heparin at large L -- is a condensation barrier: chains in excess of L = 20 nm are subject in principle to full condensation. This barrier is the basis for the truncated electropherogram of native heparin in Figure 2.1A, and for the leading edge of the electropherogram for dp20 in Figure 2.2A. With further decrease in L, components of lower degrees of sulfation escape this barrier, leading to the more complex electropherograms in Figure 2.4A. The different levels of sulfation for dp6-10 are relatively few in number: the complexity of those electropherograms largely reflects different sequence arrangements[94] that are not distinguishable in the mass spectra, see Figure 2.2B.

While the end effect explains the dependence of mobility on L for heparin oligomers, it is necessary to consider the difference in structural charge densities for heparin and PSS in order to compare those polyelectrolytes. Data for PSS and heparin are normalized in the inset of Figure 2.7 by multiplying f_{av} by the mean structural linear charge density, $1/b_{av}$. The congruence of results for heparin and PSS in the inset for $5<L<20$ nm strongly suggests that the *effective* linear charge density f_{av}/b is the main determinant of mobility in the region of intermediate chain lengths.

The convergence of μ as a function of (f_{av}/b) for heparin and PSS in the inset of Figure 2.7 does not extend to full-length chains inasmuch as the limiting values for heparin and PSS at $L>25$ nm (low f_{av}/b here) are 4.7 and 4.2, respectively. This might reflect differences between heparin and PSS in the value of the friction coefficient per segment (F). Inverse dependence on L is seen both for the effective charge per heparin charge site obtained from Eq 2.2, and for the friction per PSS segment obtained from

simulations.[93,95] However, the variation of the latter in the relevant range of L is small[93] compared to the variation of f_{av}. Consequently, $\mu \sim f_{av}/F$ should increase with L, opposite to our results in Figure 2.7. Thus, the lower mobility for PSS vs heparin at L>25 nm cannot be due to a difference in monomer friction coefficients. These simulations for PSS also show that the value of L_μ^∞ at which the charge per monomer becomes constant is larger than the value of L at which F becomes constant,[93] i.e. the charge effect propagates further from the chain ends than the friction effect.

The value of μ_L^∞ = 4.7 x10^{-4} cm^2 V^{-1} s^{-1} for heparin is not only larger than for PSS, and even exceeds values (μ< 4.2[63,90]) reported for other polyelectrolytes at this ionic strength. To explain the anomalously high values for PSS and especially heparin, we consider a common feature of both polyelectrolytes, their non-uniform linear charge sequences. Here, PSS was prepared by sulfonation of low MWD polystyrene which results in charge distribution of sulfonation sequence. Similar to the variety of sulfation sequences in heparin, this could lead to intrachain sequences of low charge, especially at large L. Reduction of condensation for a charged segment at a junction with a neutral sequence[87] is a natural extension of the diminution of condensation on chain ends. For heparan sulfate HS, a near cousin of heparin, such low- and high-sulfation domains (NA and shorter NS domains) are understood to be somehow related to the remarkable breadth of growth factors whose activities are modulated by HS.[22,38,96-100] NS segments at NA/NS interfaces are thus subject to reductions in counterion condensation. Such junction effects are expected to be minimal for PSS oligomers, the likelihood of a charged segment having an uncharged neighbor being only 20%, and the congruence of PSS with intermediate length heparin oligomers in the inset of Figure 2.7 suggests that they are not

significant for heparin either. However, it does seem likely that junction effects could be responsible for the remarkably high electrophoretic mobility of native heparin compared to e.g. synthetic polyelectrolytes with higher structural charge densities.[59]

The application of this model to native heparin is beyond the scope of the present work, but it is of interest to note that the more biologically functional HS is known to have sequences of high and low sulfation (NS and NA domains) whose arrangement appears to be strictly regulated.[5,101] While the precise role of NS and NA domains in growth factor binding is the subject of debate,[2,20,22] it is worth pointing out that the dimensions of the positive "heparin-binding domain" identified on the typically net-negative heparin-binding proteins is similar to the dimensions of the NS domains of heparin sulfate.[38] These domains comprising 2-8 heavily sulfated saccharides, are characteristically bracketed by NA domains.[97] Thus, junction effects could preserve the high effective charge density of NS domains by inhibiting counterion condensation. On the other hand, it has been proposed that heparin-protein binding is analogous to DNA-oligolysine interactions, in the sense of being driven by the entropy of expelled counterions,[49,70] in which case an increase in the effective charge of the protein-binding domain on HS could amplify the binding constant. At this point, it can only be suggested that examination of NA/NS domains take into account to relationship between sulfation patterns and counterion density.

2.6 Conclusions

The truncated electropherogram for native heparin, highly skewed in comparison to either distributions of molecular size or degrees of sulfation, is best explained by a

limiting effective charged density arising from counterion condensation. For a partially cleaved heparin, some oligomers "escape" this counterion condensation limit, in agreement with the mobilities μ obtained from well-defined heparin oligomers, which show inversed dependence of mobility on chain length *L*. The μ vs *L* relationship is remarkably similar for oligomers of both heparin and the partially sulfonated PSS; heparin however exhibits ~10% larger limiting mobility value ($\mu_{Hp}^{\infty}/\mu_{PSS}^{\infty}$ = 4.7/4.2). A theoretical treatment for polyelectrolyte end effects shows the reduced counterion condensation, i.e. larger effective charges (f_{av}) for short chains, accounting for the inverse relationship between μ and *L* for both heparin and PSS. In addition to the end segments, junctions separating regions of different charge densities could lead to diminishing counterion condensation,[87] and this effect could be more pronounced for heparin due to its higher degree of heterogeneity.

ACKNOWLEDGEMENTS

This work was supported by grants from the National Science Foundation CHE-0750389 (to I.K.), CHE-0619039 (to P.D.) for Burcu Baykal Minsky and CBET-0853551 for Anand Atmuri. We would like to acknowledge John T. Gallagher (Iduron, UK) and Gerald S. Manning (Rutgers, NJ) for stimulating discussions.

CHAPTER 3

A HEPARIN DECAMER BRIDGES A GROWTH FACTOR AND AN OLIGOLYSINE BY DIFFERENT CHARGE-DRIVEN INTERACTIONS

Minsky, B. B.; Nguyen, T. V.; Peyton, S. R.; Kaltashov, I. A.; Dubin, P. L. Heparin decamer bridges a growth factor and an oligolysine by different charge-driven interactions. *Biomacromolecules* **2013**, *14*, 4091-4098.

3.1 Abstract

Full-length heparin is widely used in tissue engineering applications due its multiple protein-binding sites that allow it to retain growth factor affinity while associating with oligopeptide components of the tissue scaffold. However, the extent to which oligopeptide coupling interferes with cognate protein binding is difficult to predict. In order to investigate such simultaneous interactions, we examined a well-defined ternary system comprised of acidic fibroblast growth factor (FGF), tetralysine (K_4), with a heparin decamer (dp10) acting as a non-covalent coupler. Electrospray ionization mass spectrometry was used to assess binding affinities and complex stoichiometries as a function of ionic strength for dp10-K_4 and FGF-dp10. The ionic strength dependence of K_4-dp10 formation is qualitatively consistent with binding driven by the release of condensed counterions previously suggested for native heparin with divalent oliogpeptides (Mascotti, D. P.; Lohman, T. M. *Biochemistry* **1995**, *34*, 2908-2915). On the other hand, FGF binding displays more complex ionic strength dependence, with higher salt resistance. Remarkably, dp10 that can bind two FGF molecules can only bind one tetralysine. The limited binding of K_4 to dp10 suggests that the tetralysine might not block growth factor binding, and the 1:1:1 ternary complex is indeed observed. The

analysis of mass distribution of the bound dp10 chains in FGF·dp10, FGF_2·dp10 and FGF·dp10·K_4 complexes indicated that higher degrees of dp10 sulfation promote the formation of FGF_2·dp10 and FGF·dp10·K_4. Thus, the selectivity of appropriately chosen short heparin chains could be used to modulate growth factor sequestration and release in a way not feasible with heterogeneous native heparin. In support of this, human hepatocellular carcinoma cells (HEP3Bs) treated with FGF-dp10-K_4 were found to exhibit biological activity similar to cells treated with FGF.

3.2 Introduction

Glycosaminoglycans (GAGs) such as heparin (Hp) are incorporated into tissue engineering scaffolds with the intention of mimicking their ability in the extracellular matrix (ECM) to sequester and release numerous growth factors (GFs).[7,33,68,99] Effective assembly strategies accomplish this through specific and non-specific association of GAGs with matrix components such as peptides. Model ternary systems can facilitate *in vitro* investigation of simultaneous complex formation among glycosaminoglycans, growth factors and scaffold elements, revealing how non-covalent e.g. electrostatic, interactions can be utilized. Combination of growth factors with peptide and GAG components of reduced heterogeneity is currently necessary in order to analyze these ternary systems with powerful characterization techniques such as electrospray ionization mass spectrometry (ESI-MS).

GF-binding heparinoids have been coupled to scaffold polymers in order to achieve modulated release of the protein either with or without heparin. The covalent attachment of heparin to scaffolds has been pursued through many strategies[102-109] which

may obstruct GF binding sites or introduce toxic cross-linking agents.[110] This is avoided by means of oligopeptide scaffold components that bind heparin non-covalently.[108,110-113] The scaffold structure and Hp-oligopeptide affinity determine the release rate of Hp-GF.[110,111] The strength of the heparin-GF bond determines both the rate of GF release and whether it is released along with bound Hp. It is therefore important to consider whether differences in the nature of two interactions allow them to be independently modulated by either ionic strength or heparin microstructure.

The model used here for the binding of oliogpeptides to heparin originates from the counterion condensation theory of Manning,[54,55] initially developed to describe the binding of oligolysines to DNA.[47,70] In the oligolysine-DNA case, the driving force is the entropy of the release of DNA counterions (Na^+) from the condensed layer. This leads to a particular form of the ionic strength dependence of the binding constant: - log $K_{obs} \sim n$ log I, where K_{obs} is equilibrium association constant, I is ionic strength and n is ligand charge. Lohman and Mascotti[49] applied this concept to oligopeptide/heparin binding (conceptually replacing DNA with heparin) and measured the salt dependence of the binding constants. Finding linearity of log K_{obs} vs. log I for heparin and cationic oligopeptides, they concluded that the measured ΔG_{obs} was purely entropic. This observation, along with recent direct measurement of counterion condensation by heparin,[114] provides strong evidence for the release of condensed counterion during the binding of cationic ligands to heparin. However, further extension of the Manning-Record model in which the oligopeptide has been replaced by a protein[17,115,116] has since been questioned on the basis of fundamental uncertainty regarding the expanded role of long-range interactions.[48]

While non-covalent coupling of growth factors to Hp is recognized as a valuable approach for the development of bio-functional tissue surrogates, questions arise about "electrostatic" heparin-oligolysine binding vs "specific" Hp-GF interactions. The former has been widely accepted as non-specific, but the precise nature of the latter has remained controversial. Models based on the definition of Hp-GF as a cognate system emphasize "specific", i.e. short-range forces comprising hydrophobic and pair-wise interactions (H-bonding and salt bridges).[117-120] These are thought to impose on heparin precise structural and/or conformational requirements for protein recognition. However, there is increasing evidence that strong binding occurs between globally negative heparin-binding proteins and polyanions,[45] especially when polyanion charge distributions are arranged in a way that minimizes long-range repulsion while optimizing short range attractions with locally positive protein domains.[31,51,121] This can result in a level of selectivity that does not arise from short-range interactions such as hydrogen-bonding or "ion-pair" formation.[9,45] Supporting this perspective, recent findings indicate that various FGFs share the same GF-binding sites on HS,[16,21] where binding affinity is correlated with the extent of sulfation.[21] Catlow et al. showed that the interaction of hepatocyte growth factor/scatter factor with HS is dominated by electrostatics inasmuch as sulfate density as opposed to the presence of particular types of sulfation affects the selectivity.[34] Thus the interactions considered here could be intrinsically promiscuous[20,35] and dominated by columbic forces. There is also growing evidence that these interactions can be highly selective.[122,123]

When Hp-GF interactions are viewed in the context of the vast array of polyelectrolyte-protein interactions,[44] the role of ionic strength is to diminish long-range

electrostatic interactions between Hp and complementary protein positive "patches,"[44] an effect typically parameterized by the Debye-Hückel screening length κ^{-1}.[9,28,51,124] The possible role of long-range interactions also leads directly to consideration of long-range repulsion between Hp and the negatively charged domains of many of its morophogen cognates,[125] an additional issue when the oligocationic "ligand" in the Record-Manning model is envisioned as part of a protein that may be larger than its heparinoid "host".

The differences in the effects of both Hp microstructure and ionic strength on the two types of interactions could make it possible to control the relative strengths of Hp-GF and Hp-oligopeptide interactions either by using appropriate heparin fractions, or by adjusting salt concentration. Hp microstructure, difficult to define for the immensely heterogeneous native heparin, can be better identified using GF-specific oligoheparins. The length of such oligoheparins must be sufficient to allow for non-covalent binding to both scaffold oligopeptide units and growth factors. Competition between oligopeptide and GF for the heparin chains could then be modulated if the two types of binding are driven by different mechanisms, e.g. counterion release for the former and the screened electrostatics for the latter. These differences could make it possible to tune the two interactions so that binding of oligopeptide and GF could take place simultaneously. In theory, end effects on counterion condensation by heparin oligomers[87] suggest that the central saccharide units, rich in condensed counterions,[114] could provide unique sites for Record-Manning type oligolysine binding, leaving the distal heparin units available for screened GF binding, i.e. suppressed at length scales larger than the Debye length, κ^{-1} (nm) $\approx$ 0.3 $I^{-1/2}$ in 1:1 electrolyte.

The model system studied in this work allows for in vitro investigation of simultaneous complex formation among low MW GAGs, GFs and scaffold peptide elements. The mechanism of ternary and binary complex formation involving these species could contribute to molecular level understanding of the assembly of scaffolds and their ultimate behavior in cell culture. A specific hypothesis to be tested is that the GF binding sites within a given chain have unique sulfate charge densities. Elucidation of protein "recognition sites" on heparin has been pursued by crystallography, typically involving assumptions about certain pair-wise interactions not directly related to sulfate charge densities.[23,126]

In this work, ESI-MS is applied to determine the stoichiometry and ionic strength dependences for a ternary model system comprising FGF-1, a heparin decamer (dp10) and tetralysine (K_4). ESI-MS of native state proteins has recently evolved as a very important tool to detect their non-covalent complexes, revealing compositional details of the ligand-protein complexes.[88,127,128] Increased sensitivity, low sample requirements and applicability to transient complexes have improved the importance of native ESI-MS. We examined the effects of ionic strength on the FGF-1-dp10 and K4-dp10 interactions, and found the latter but not the former to be analogous to the well-known oligolysine-oligonucleotide electrostatic model.[48,70] Furthermore, our results indicated that the ability of the components of dp10 to engage in the ternary complex or bind multiple growth factors depends on their sulfation levels.

3.3 Experimental

3.3.1 Materials

Heparin decasaccharide (dp10), prepared by high-resolution gel filtration of partial heparin lyase digestion of high quality heparin, was generously donated by Prof. John Gallagher from Iduron (Manchester, UK). Acidic fibroblast growth factor (includes His to Gly 93 mutation to increase stability,[129] pI = 7.8) was provided by Prof. Robert Linhardt (RPI, Troy, NY). Tetralysine (K4) was purchased from Sigma.

3.3.2 Methods.

3.3.2.1 Mass Spectrometry

All experiments were performed with a QStar-XL hybrid quadrupole-time-of-flight MS equipped with a nano-ESI-source (AB Sciex, Toronto, Canada). The measurements were performed using closed (2 μm id) glass nanospray capillaries (New Objective, Woburn, MA). FGF-dp10 binding experiments were acquired using following settings of ion optics in the ESI interface: DP: 100, FP: 265, DP2: 15. K4 and dp10 binding experiments were performed utilizing mild ion desolvation conditions (DP: 40, FP: 150, DP2: 15). FGF-1 was buffer exchanged using Amicon (10kDa cut off) with 100 mM NH4CH3CO2, and the protein concentration was verified by UV-VIS using molar absorptivity of 17545 M^{-1} cm^{-1}. FGF, dp10 and K4 were diluted from the stock solutions to the final concentrations (2 μM, 3 μM and 10 μM, respectively) in the desired ammonium acetate concentrations. ESI-MS was used to determine stoichiometries of FGF-1-dp10 complexes, and m/z values of the protein and the complexes were assigned

with BioAnalyst v1.1.5 (MDS Sciex/Applied Biosystems, Toronto, Canada). The mass distribution of the protein-bound heparinoid molecules were calculated using the following formula:

$$\left(\left(\frac{m}{z}\right)\cdot z - mH\right) - nM_{FGF} \qquad \textbf{Eq.3.1}$$

where *n* represents total number bound FGF-1 molecules, *m* is the total protons attached and M_{FGF} is the mass of a single FGF molecule. Since all analyses were performed in the positive ion mode, it is expected that each ionic species will also contain 4-5 cations (NH^{4+}). Shaded boxes are used in Figure 3.3 and 3.5 to indicate the mass ranges for heparinoid species with different extent of sulfation (the overlap is due to the uncertainty in the number of cationizing agents attached to each polyanionic chain).

3.3.2.2 Computational

DelPhi V. 4r1.1,[130,131] which applies non-linear Poisson-Boltzmann equation to generate the potential surface of the protein, was used to model the electrostatic potential around FGF-1 (PDB id: 1K5U) and heparin decamer (Solution NMR: 1HPN). The structures were taken from the protein data bank (http://www.rcsb.org/). The charges of amino acids on the protein were determined using the spherical-smeared charged model put forward by Tanford.[132]

3.3.2.3 Cell Culture and Proliferation Assays

All cell culture supplies were purchased from Life Technologies, Carlsbad, CA, unless otherwise noted. Human hepatocellular carcinoma cells (HEP3Bs, American Type

Culture Collection, Manassas, VA) were cultured in modified Eagle's medium (MEM) supplemented with 10% Fetal Bovine Serum (FBS) and 1% penicillin-streptomycin (P/S) at 37 oC and 5% CO2. To quantify cell growth in response to growth factors and growth factor complexes, HEP3Bs were seeded at 10,000 cells/well in 96-well plates (Corning, Tewksbury, MA), in standard growth medium. After 24h, the medium was replaced with the serum-free medium containing 1% P/S and either fibroblast growth factor (FGF) or FGF.dp10.K4, ranging from 0 to 50 ng/mL. We used the CellTiter 96 AQueous One Solution Cell Proliferation Assay (Promega, Madison, WI) to measure cell proliferation at 24 h and 72 h. After 3 h of incubation, the absorbance was read at 490 nm with a BioTek ELx800 microplate reader (BioTek, Winooski, VT).

3.3.2.4 Statistical Analysis

One-way ANOVAs were performed with using Prism v5.04 (GraphPad Software, La Jolla, CA), the Tukey post-test was used to determine significance of pairwise differences. Data are reported as mean ± standard error with N = 3. $P \leq 0.05$ is denoted with *, ≤ 0.01 with **, and ≤ 0.001 with **

3.4 Results and discussion

3.4.1 K4 binding to dp 10

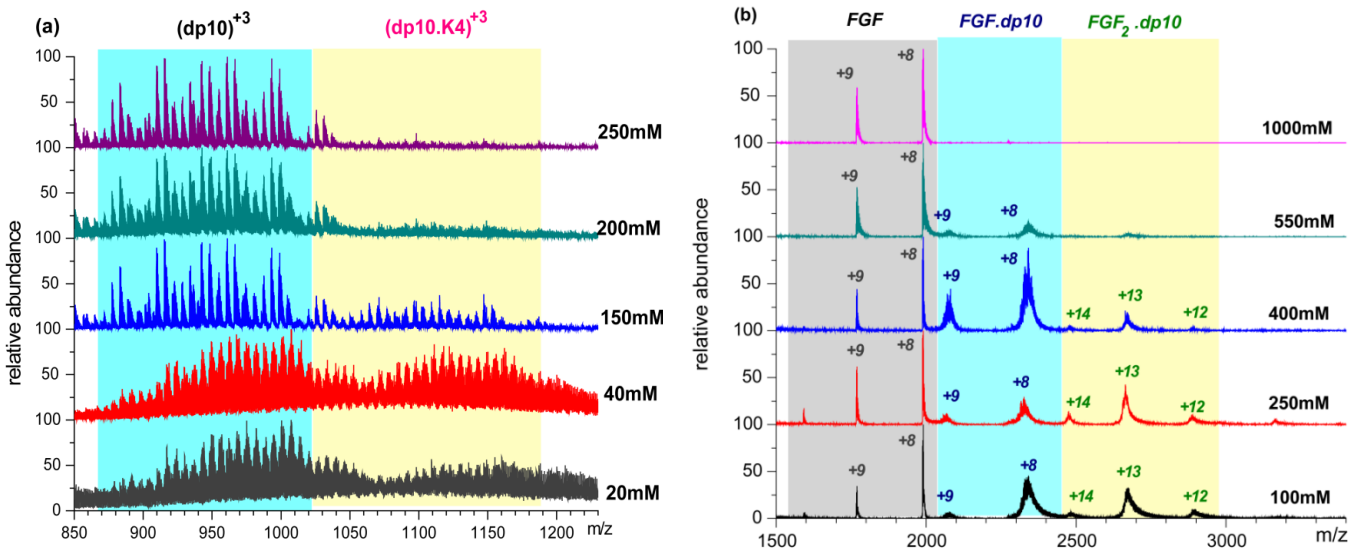

Figure 3.1: (a) ESI mass spectra of dp10 (3 µM) and K_4 (10 µM) in pH 6.8 ammonium acetate at varying ionic strengths. Not shown: free K_4 (m/z = 531, z = +1). (b) ESI mass spectra of FGF-1 (2 µM) and dp10 (3 µM) in 100, 250, 400, 550 and 1000 mM ammonium acetate. The shaded columns represent (a) dp10 and dp10·K_4; (b) FGF, FGF·dp10 and FGF_2·dp10.

Figure 3.1 shows the effect of ionic strength on the binding of dp10 at pH 6.8 to K_4 (a) and to FGF (b). Even though K_4 is in molar excess (10:3 K_4:dp10), K_4 forms only a 1:1 complex with dp10. This is in contrast to the ability of dp10 to bind *at least* two FGF molecules. Furthermore, the contour length of dp10 (5 nm) is significantly larger than that of K_4 (~ 2 nm). It appears that the binding energy for the second K_4 is diminished, i.e. binding is apparently anticooperative. Arguments based on variations in local

sulfation would not explain why there are *no* dp10 chains that bind two oligolysines. We therefore explore the earlier studies of oligolysines and heparin, which supported the model put forward by Manning and Record.[46] As noted above, these studies showed that the driving force for oligocation binding to polyanion (e.g. DNA) is the entropy of the release of the polyanion's counterions from its condensed layer. A more recent theoretical result by Manning for oligo-polyelectrolytes is the diminution of condensation at and near chain ends,[87] subsequently verified by Minsky et al. for heparin oligomers.[114] Representation of the heparin disaccharide structure (Figure 2.6, above) neglecting positional variations of sulfation leads to visualization of the chain as treated in the condensation model (Figure 2.6, below), with the condensed counterion layer depleted at chain ends. If those ions are involved in the oligolysine binding process, the strongest K_4 binding site would comprise chain units far from the ends of dp10, i.e. saccharides 3-8 (contour length ~3 nm). The remaining distal regions are incompetent binders with respect to both length (1 nm) and condensed counterions. To further examine the applicability of this model, we examine whether the strong binding suppression with an increase from 40 to 150 mM ionic strength in Figure 3.1(a) is consistent with the condensed counterion model.

In order to compare dp10-K_4 results to those in the highly influential Mascotti and Lohmann paper,[47,49] it was necessary to extrapolate from the binding constants, $K_{obs,}$ which were obtained in refs. 30 and 32 for native heparin with a +2 oligolysine (n =2). While their study[49] only covered a narrow range $12 < I < 30$ mM, they obtained $K_{obs} \sim I^{-2}$ in agreement with theory in which the number of released counterions is equal to the ligand charge ($-(d\log K_{obs} / d\log I) = n$),[46] subsequently supported by Manning et al.[48]

With n = 4, K_{obs} is expected to exhibit I^{-4} dependence for K_4. Thus, the dramatic suppression of binding seen in Figure 1(a) for the ca. 4-fold increase in I from 40 to 150 mM is entirely consistent with the 200-fold ((ca. 40/150)$^{-4}$) decrease in K_{obs} as predicted by theory, suggesting that the binding of K_4 to dp10 is driven by the release of condensed counterions. The remarkably different I dependence in Figure 3.1(b) shows that a different mechanism must drive the binding of FGF to dp10 at 400 mM; binding based on the displacement of condensed counterions is not possible when the bulk ionic strength exceeds 380 mM, the local concentration of condensed counterions for heparin.[48]

3.4.2 FGF binding to dp10

In order to compare binding strengths for FGF-dp10 vs K_4-dp10, the former was also investigated using salt concentration as a surrogate for binding affinity. Figure 3.1 (b) shows the formation, in pH 6.8 ammonium acetate, of 1:1 and 2:1 complexes of FGF-dp10 at I = 100, 250, 400 mM. If we use the salt resistance of complex formation as a measure of binding affinity, we find that the FGF-dp10 1:1 complex is more stable than the K_4-dp10 complex (see Figure 3.1), and also the FGF-dp10 2:1 complex. However, even the FGF-dp10 1:1 complex is fully suppressed at I > 550mM, indicating the role of screened electrostatics. Although the pH used is only moderately lower that the pI, the charge distribution is anisotropic leading to a discernible positive domain (Figure 3.2).

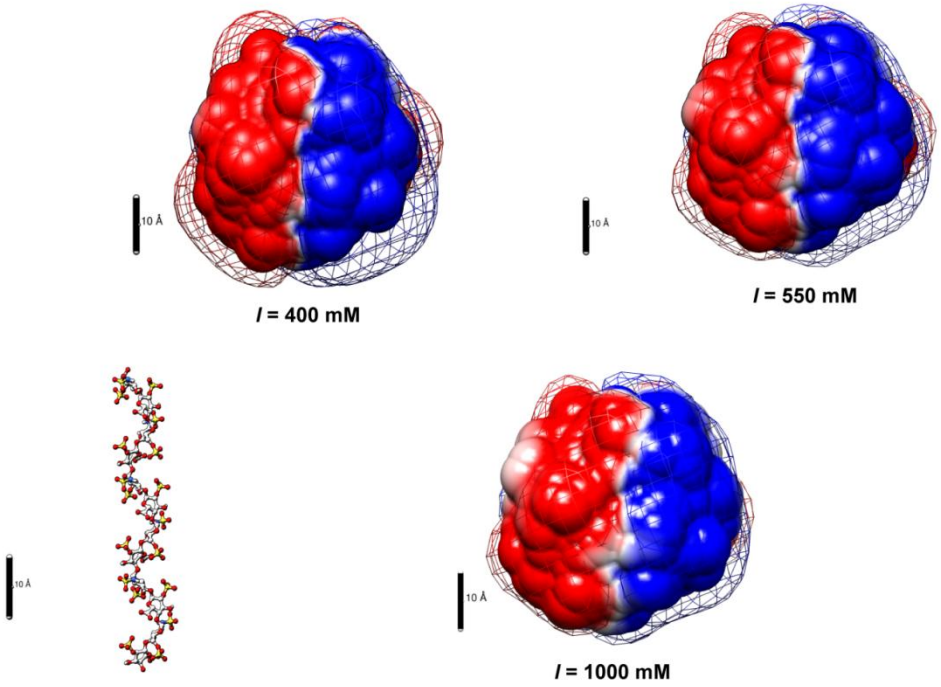

Figure 3.2: FGF-1 (PDB id: 1K5U) electrostatic images for pH 7.0 and *I* = 400 mM, 550 mM and 1000 mM. 5 Å surfaces (magnitude of charge shown by color intensity, blue positive, red negative), and equipotential surfaces (grids) +0.2 kT/e and -0.2 kT/e. The heparin decamer (Solution NMR id: 1HPN) is drawn to scale to help visualize its ability to reside within the FGF positive domain (sulfate groups are shown in yellow). The pH differences between Figure 3.1 (b) and the DelPhi calculations have no significant effect on the aminoacid charges

Calculations of screened electrostatics by DelPhi have been recognized as a quantitative tool for elucidating the electrostatic binding energy of both protein-polyelectrolyte[50] and protein-protein interactions,[133] and comparisons with experimental results are facilitated by the display of electrostatic potential contours. The potential contours represented as grids in the DelPhi images arise from the conjoint sum of all possible pair-wise coulomb forces that are subjected to the moderating influence of the ionic strength. This screening results from the asymmetric distribution of small ions as

parameterized by the Debye screening length ($\kappa^{-1} \sim I^{-1/2}$) , the distance at which the electrical potential due to the protein surface charges decays to 1/*e* of the protein's surface potential. This approach, which needs to be clearly differentiated from the behavior of condensed counterions, explains the maximum in binding when $\kappa^{-1} \approx$ protein radius seen for binding at pH > pI for polyanions,[51] including heparin.[28]

This approach here is embodied in the DelPhi images of Figure 3.2 for FGF at pH 7.0 and 400-1000 mM salt. The protein itself is represented at 5Å from Van der Waals surface to account for retention of heparin and FGF solvation, and the potential contour grids are presented at $\psi = 0.2\ kT/e$. As shown in Figure 3.2 for I = 400 mM, the volume between the 5Å surface and the contour grid is sufficient to accommodate at least -5 heparin charges (1.5-2 disaccharide units, ~2-3 nm dp10 segments), a dimension consistent with the FGF-binding site size on heparin.[134] The consequent electrostatic binding energy then is on the order of 1 *kT*, which represents the onset of the binding. [50] The diminution of this volume seen with increasing salt portrays screening; therefore the number of dp10 charges bound is reduced at 550 mM and abolished at 1000 mM as seen in Figure 3.1(b). The predominant role of screened electrostatics does not necessarily negate release of some bound counterions, but the number of these is debatable.[48]

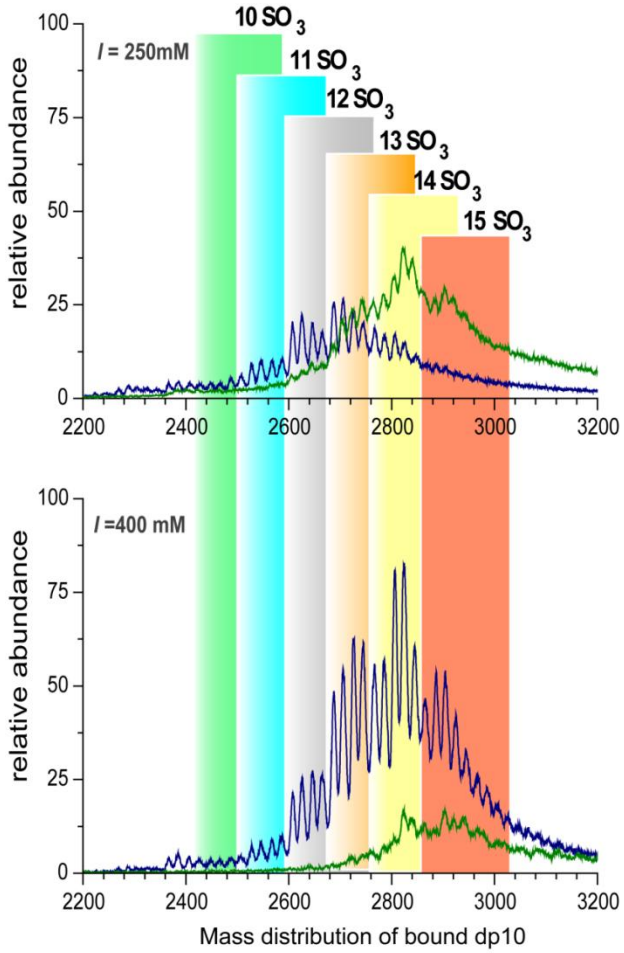

Figure 3.3: Mass distribution of protein-bound dp10 molecules in FGF·dp10 (blue trace) and FGF_2.dp10 (green trace) determined at ionic strengths of 250 and 400 mM.

The stability of the ternary complex requires not only that K_4 not compete with FGF, but also that the stronger binding of FGF to dp10 does not lead to its occupying all potential K_4-binding sites. As noted in Figure 3.1, dp10 can bind either one or two FGF molecules; the ratio of FGF_2·dp10 to FGF·dp10 decreases with salt concentration *I*, most notably near *I* = 400 mM. This corresponds to a Debye length (κ^{-1} = 0.4 nm) suggesting that screening repulsions at that length scale could weaken the binding. To further explore the difference between the first and second binding events, we consider the

sulfation of dp10 molecule found in FGF_2·dp10 vs. those found in FGF·dp10. Figure 3.3 shows, in the absence of K_4, the mass spectra of FGF-dp10 complexes plotted on the adjusted mass scale where the mass of the protein component was subtracted from 2:1 and 1:1 complexes at 250 and 400 mM, and represents in blue and green the collection of dp10 molecules found respectively in FGF.dp10 and in FGF_2·dp10. Given the presence of free FGF at all conditions, it might appear if one were to neglect the different sulfation patterns that the binding of FGF is anticooperative at high salt. A more reasonable explanation can be sought in differences in dp10 sulfation for the first and second binding sites, presumably higher for the high-affinity first site. The phase transition-like behavior of polyelectrolytes adsorption on oppositely charged surfaces can be extended to binding to oppositely charged colloids[135,136] and oppositely charged proteins.[137] Critical conditions for binding are then expressed by Eq. 3.2:

$$\sigma_c \xi \sim \kappa^b \qquad \textbf{Eq.3.2}$$

where σ_c is the effective charge density of the protein positive patch, ξ is the polyelectrolyte structural linear charge density, *b* is an empirical scaling parameter and κ (nm) $\approx 0.3\ I^{-1/2}$. According to eq 3.2, the critical ionic strength (above which no binding occurs) is described by $\kappa_c \sim \xi^{1/b}$. If the high-affinity first binding site is more highly sulfated, i.e. $\xi^I > \xi^{II}$, then $\kappa_c^I > \kappa_c^{II}$ so binding at site I may persist when binding to site II is suppressed. Focusing on the results for the 1:1 complexes alone (blue trace in Figure 3), the increase in dp10 sulfation with ionic strength is consistent with eq 3.2. Typical values of *b* range from 0.5 to 3, a much smaller ionic strength dependence than the I^{-4} dependence of condensed counterion release, as noted in the comparison of Figures 3.1(a) and (b).

3.4.3 Ternary complex formation

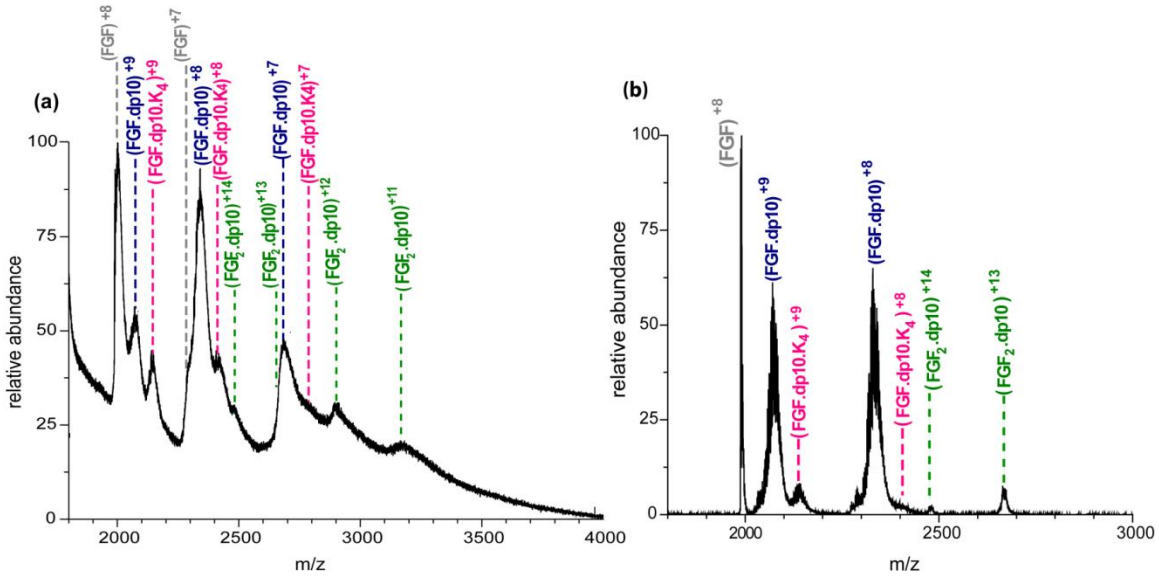

Figure 3.4: ESI mass spectra of mixtures of FGF (2 µM), dp10 (3 µM), K_4 (10 µM) in 20 mM pH 6.8 (a) and 100 mM pH 5.5 (b). FGF present as: FGF·dp10·K4; FGF·dp10; FGF_2·dp10; and free FGF.

Figures 3.4 (a) and (b) show the ESI mass spectra for a ternary mixture of FGF, dp10 and K_4 of 2:3:10(µM) stoichiometry at 20 and 100 mM ionic strengths, respectively. The signal from dp10.K_4 is not shown in Figure 3.4(a) due to excess noise, but K_4 does appear in the 1:1:1 FGF·dp10·K_4 (ternary) complex. The 5:1 excess of K_4 does not impede FGF binding, either because K_4 occupies an oligoheparin site distinct from that of FGF, or because dp10-K_4 binding is intrinsically weaker. The ternary complex is less abundant at 100 mM (Figure 3.4(b)) most likely because high salt weakens the dp10-K_4 interaction (vide supra).

FGF·dp10 and FGF_2·dp10 are observed, the former is more abundant than the latter. The restriction of K_4 binding to 1 per chain, despite its small size, can be explained on the basis of the release of condensed counterions (vide supra), which are more

abundant in the middle of dp10. On the contrary, if FGF binding were governed by screened electrostatics, the larger effective charge due to less counterion condensation at these terminal saccharides could account for facile binding of 2 FGF molecules per chain.

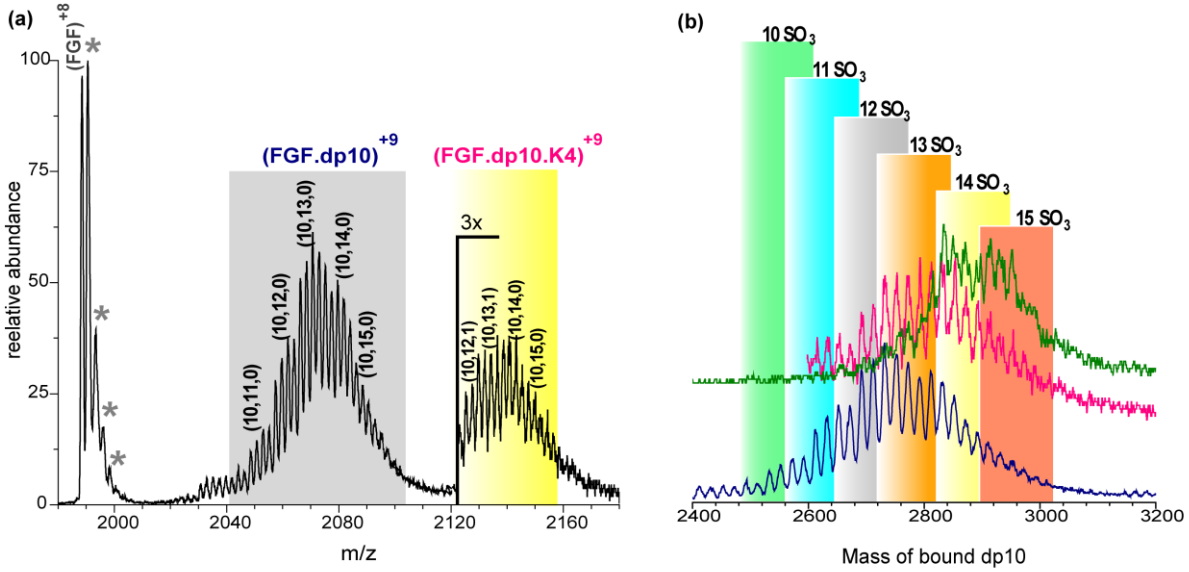

Figure 3.5: The assignment of sulfation levels of dp10 for the FGF·dp10·K4, FGF·dp10 and FGF_2·dp10 complexes presented in Figure 4 (b). (a) Expansion of the m/z regions of FGF·dp10.K4 and FGF·dp10 complexes (nomenclature by Roepstorff and Henriksen[138] for bound dp10). NH_4^+ adducts on the unbound FGF are shown with asterisks (*). The m/z region of FGF·dp10·K4 is amplified 3 times for clarity. b) Mass distribution of bound dp10 in FGF·dp10 (blue trace) FGF·dp10·K_4 (pink trace) and FGF_2·dp10 (green trace).

Expansion of the spectral region that comprises FGF·dp10 and ternary complex shown in Figure 3.4 reveal the levels of sulfation of the bound dp10 chains (Figure 3.5 (a) and (b)). The sulfation density in the ternary complex, slightly higher than that seen in FGF·dp10, suggesting that dp10 chains with low sulfation (< S12) only bind to a single FGF, while those with higher sulfation (> S12) can bind K_4 along with FGF. The strong

suppression of K_4 binding at high salt noted above is responsible for the observation of an increase in FGF·dp10 at the expense of the FGF·dp10·K_4 ternary complex at high salt.

The extended spectral range at 100 mM salt to include FGF_2·dp10 is shown in Figure 3.5 (b). Here, the masses of FGF, K_4 and 2FGF are subtracted from the calculated mass distribution of the complexes in order to compare the sulfation levels of the relevant host dp10 chains. Within the limitations of ESI-MS resolution, i.e., the overlapping distributions due to the uncertainty in the number of cationizing agents attached to each polyanionic chain, the higher mean levels of sulfation (S14 and S15) of dp10 within FGF_2·dp10 compared to those within FGF·dp10 complexes (S10-14) were observed, and chains that contain S12-15 appear to bind both FGF and K_4. While chains of low sulfation may bind only one FGF, highly sulfated FGF·dp10 chains appear to be subject to competition between K_4 and FGF for the second binding site. Comparison of the highly sulfated (15S) dp10 species in Figure 3.5 (b) suggests that FGF preferentially occupies this site. Since K_4 binding depends on the condensed layer of counterions, the opposing effects of sulfation density and end effects may explain the absence of a clear effect of the former.

Binding to dp10 by K_4 and FGF differ in several ways. The salt dependence of K_4·dp10 complexation is consistent with binding driven by the release of condensed counterions; on the other hand, FGF binding to dp10 exhibits higher salt resistance and more complex ionic strength dependence consistent with screened electrostatics. While FGF_2·dp10 complexes are formed over a wide range of ionic strength, dp10 can only bind one K_4. Estimates of the size of the FGF-binding site on heparin suggest ca. two disaccharides, similar to the mean protein hydrodynamic radius i.e. 2 nm, consistent with

the maximum number of proteins that can bind to native Hp.[134] K_4 (≈ 2 nm contour length) can then be easily accommodated near the center of dp10 with a distal region of higher effective charge density accessible for FGF. FGF binding is facilitated by high dp10 sulfation, whereas the effect of sulfation levels on K_4 binding can be obscured by the conjoint influence of end effects on the concentration of dp10 condensed counterions.

These observations pointed out that control of *I* and overall sulfation levels of heprarinoids could be used to manipulate the balance between matrix component- and growth factor affinity in tissue engineering. The selection of the conditions could be used to influence the rates of morphogen release and also the presence or absence of heparin accompanying the free growth factor.

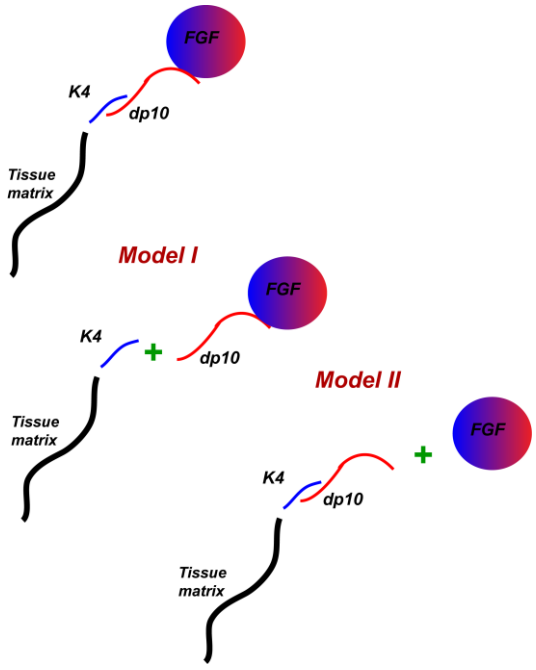

Figure 3.6: Models of FGF release

The stability of the FGF·dp10 versus K_4·dp10 complexes at selected conditions will determine which bond will break first in the tissue scaffolds to release FGF, and as a result of this breakage, FGF will be released with or without heparinoid. The use of low ionic strength (< 40mM) during the assembly process should enhance ternary complex formation and higher ionic strength of the environment could lead to the dissociation of the dp10- K_4 bond first; then GF would be released in the heparinoid-bound form during the dissociation process (Figure 3.6). In addition to addition of salt, increasing the degrees of sulfation definitely promotes capturing a large number of growth factors and the formation of ternary complexes. Therefore, heparin chains with higher degrees of sulfation could be used to deliver high concentration of GFs in the tissue environments.

3.4.4 Biological activity of FGF vs FGF·dp10·K_4

We investigated whether the complexation of FGF to dp10 and K4 would alter its bioactivity when compared to FGF alone (Figure 3.7). HEP3Bs were stimulated with FGF or FGF complex across concentrations ranging from 0 to 50 ng/mL. We found that binding of dp10 and K4 to FGF does not significantly alter its activity at any of the tested concentrations. As expected, HEP3B proliferation at 24h increased by approximately 10% with FGF and FGF complex as compared with the control. After 72 h, cell proliferation is maximized, and neither treatment showed any significant difference in proliferation across the concentrations tested here.

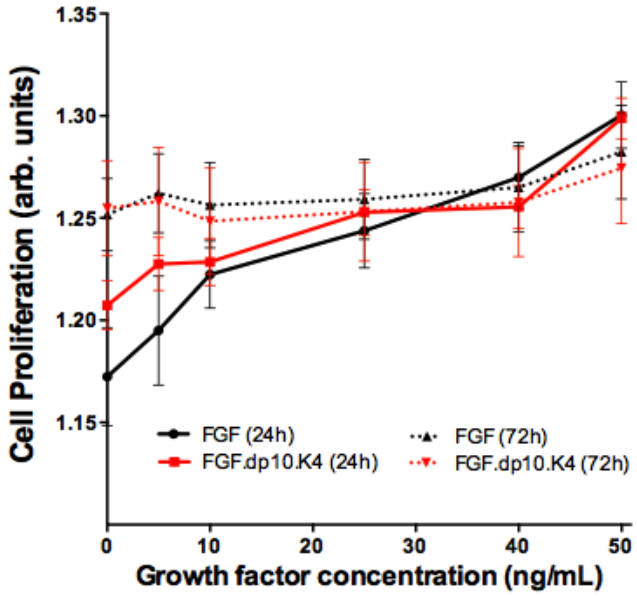

Figure 3.7: FGF·dp10·K_4 mixture retains biological activity of FGF·HEP3Bs were treated with either FGF (black) or FGF·dp10·K_4 (red), and cell proliferation was quantified at 24 (solid) and 72 hours (dashed). No statistical differences were noted when comparing cell proliferation with FGF and the FGF·dp10·K_4, at any time point. Proliferation increases with FGF concentration at 24 hours, and is maximized at all concentrations at 72 hours. In both formats, FGF of 50 ng/mL is statistically higher than the no growth factor condition at 24 hours.

3.5 Conclusions

A heparin decamer (dp10) in the presence of tetralysine (K_4) can bind either one or two molecules of acidic fibroblast growth factor (FGF), or FGF and K_4, but cannot bind two molecules of K_4. Using electrospray mass spectrometry (ESI-MS) to investigate the ionic strength effect on the formation of these complexes, we concluded that the formation of K_4-dp10 is driven by the release of condensed counterions. We have previously shown that the concentration of condensed counterions on dp10 is strongly reduced near its chain termini, and therefore propose that K_4 binding is constrained to the central region of dp10. The markedly different ionic strength dependence of FGF binding suggests a different mechanism (based on screened electrostatics), which removes this

constraint, so that the growth factor can bind along with K_4 ("ternary complex") or along with a second FGF. ESI-MS characterization of bound dp10 chains in various complexes indicates that FGF binding is enhanced by heparin sulfation, while K_4 binding is relatively indifferent to it due to competing effects. Cell culture studies indicated that complexation of FGF in the form FGF-dp10-K_4 does not significantly change its biological activity. These observations suggest the application of shorter heparin chains as a route to growth factor sequestration and release in tissues matrices could be more effective than the use of heterogeneous native heparin chains.

ACKNOWLEDGEMENTS

This work was supported by grants from the National Science Foundation CHE-0750389 (to I.K.), CHE-0619039 (to P.D.) for Burcu Baykal Minsky. S.R.P. and T.V.N. were partially supported by a Barry and Afsaneh Siadat Career Development Award. We would like to thank Robert J. Linhardt (RPI, Troy,NY) for providing FGF-1.

CHAPTER 4

STRUCTURAL DETERMINANTS OF ELECTROSTATIC INTERACTIONS BETWEEN PROTEINS AND POLYANIONS: AN ESI-MS STUDY OF FIBROBLAST GROWTH FACTOR BINDING TO HEPARIN OLIGOMERS

Minsky, B. B.; Dubin, P. L.; Kaltashov, I. A.

4.1 Abstract

The interactions between fibroblast growth factors (FGFs) and their receptors (FGFRs) are facilitated by heparan sulfate (HS) and heparin (Hp). The molecular basis of this modulation is highly complex due to the structural heterogeneity of HS/Hp, with regard to both chain length and sulfation. In this work, we employed electrospray ionization mass spectrometry (ESI-MS) to investigate the association of acidic fibroblast growth factor (FGF-1) with relatively homogeneous heparins octamer (dp8) and decamer (dp10). FGF-1 forms 1:1, 2:1 and 3:1 (FGF:heparinoid) complexes with dp8/dp10, and the fraction of bound protein is highly dependent on FGF:heparinoid bulk stoichiometry. The multimeric complexes were preferentially formed on the highly sulfated Hp oligomers. When solution stoichiometry led to only 1:1 complex, the sulfate distribution of FGF-bound oligomers was skewed from low to high in the complex. These results showed how interactions between FGF-1 and Hp oligomers are influenced by the heparin oligomer charge density and bulk mixing ratio, and also demonstrate the power of ESI-MS as a tool to study multiple binding equilibria between proteins and highly complex polyanions.

4.2 Introduction

Glyscosaminoglycans (GAGs), such as heparan sulfate (HS) and heparin (Hp), are engaged in a wide spectrum of physiological effects including embryogenesis, immune response, cell proliferation, differentiation and angiogenesis. All of these are related to the ability of GAGs to potentiate the activity of numerous signaling proteins, accomplished largely by mediating the interactions of these growth factors and their cell surface receptors. The main challenge in characterizing GAG-protein binding arises from the immensely polydisperse GAG structure due to apparently stochastic post-translational sulfation patterns. While this polydispersity correlates with promiscuity in protein binding, the details of the relationship between the sulfation and protein affinity remain elusive. The fact that GAGs are the most highly charged macromolecules in animals suggests that electrostatic forces play significant roles in their protein affinity, but such long-range interactions are typically relegated to supportive roles in protein recognition. The development of structure-property relations, which would remove a major barrier to the development of potential biomedical applications of GAG's, is thus coupled to the need to understand how sulfation patterns determine binding of their physiological partners. While many approaches focus on the presence or absence of a particular glycoside or glycoside substituent, electrospray ionization mass spectrometry (ESI-MS), focusing on the characterization of individual molecules, can provide unique insights into the structural distinctions between high and low affinity GAG molecules.

Efforts to characterize HS/Hp interactions with growth factors (GF) have until recently focused on the contribution of certain sulfation features, such as 6-*O*- sulfation for FGF-10, 2-*O* sulfation for FGF-2, or both for FGF-4 and FGF-7.[117,118] The underlying

assumption is that the protein-heparinoid interaction is driven by pair-matching of basic residues on the protein and sulfates on heparin, the fact that heparin was clearly and credibly identified 30 years ago as a polyelectrolyte[11] notwithstanding. In most studies, the importance of more global "charge complementarities" between the protein and the polyelectrolyte-like heparinoid had been ignored,[17,44] thus failing to consider the heterogeneity and highly dynamic nature of the Hp/HS chains,[10] and the well-defined positive domains of the many globally negative heparin-binding proteins.[139] There is increasing evidence that strong binding occurs between globally negative proteins (such as antithrombin) and polyanions (such as heparin) when polyanion charge distributions are arranged in a way that minimizes long-range repulsion while optimizing short range attractions with locally positive protein domains. This can result in a level of selectivity that does not arise from short-range interactions such as hydrogen-bonding or "ion-pair" formation.[31,51,121] Supporting this perspective, several groups suggested that GAG-GF interactions might be intrinsically non-specific. Catlow et al. showed that the interaction of hepatocyte growth factor/scatter factor with HS is dominated by electrostatics.[34] Krueger et al. indicated that various FGFs share the same binding domain on HS, where binding affinity is correlated with the extent of sulfation.[21] Jastrebova et al. extended these studies to FGF-2 and its receptors, and revealed that ternary complex formation was related to overall chain sulfation.[20,35] These studies strongly suggest that non-specific electrostatic interactions can play a role in recognition.[45]

For various signaling proteins, certain sequences in GAG structure may either interact with protein multimers or promote multimerization.[38] In this way, FGF-HS binding in the distal region of cell surfaces generates FGF dimers along HS

chains.[134,140,141] Evidence, both in vivo and vitro, suggests that these dimers are the biologically preferred architecture for inducing receptor activation.[142] The crystal structure of FGF-2 with a heparin decamer (dp10) revealed the existence of a homodimer, or "*cis*-dimer"[143], in contrast to the "*trans*-dimer" formed for FGF-1 with a 4-5 monosaccharide sequence sandwiched between the two proteins.[144] Other oligoheparins larger than heptasaccharides can lead to biologically active FGF-1 dimers[145]. *In vitro* light scattering studies of full-length Hp have shown that it accommodate 14-15 FGF-1 molecules.[134]

Sulfation sequence arrangements are clearly determinants of the intra-polysaccharide organization of bound proteins, but the techniques mentioned above only reflect the average behavior of intrinsically heterogeneous heparin oligomers. On the other hand, the unmatched resolution of mass spectrometry provides insight into the behavior of single molecules, clearly correlating sulfation level and protein-oligoheparin stoichiometry. Native electrospray ionization mass spectrometry (ESI-MS) is thus an important tool in the detection of non-covalent protein-ligand complexes,[146] revealing compositional details of macromolecular complexes that involve nucleic acid and heaprin.[88,127,128] Increased sensitivity, low sample requirements and ability to detect dynamic and transient complexes have contributed to the importance in this field. Therefore, we applied native ESI-MS to probe interactions of FGF-1 and short heparinoids, focusing on the influences of heparin chain length, extent of sulfation and solution concentration on the induction of multimeric complexes of FGF-1. Analysis of the number of sulfate groups on the Hp chains involved in complex formation revealed the basis of FGF-1 selectivity of Hp chains.

4.3 Experimental

4.3.1 Materials

Acidic fibroblast growth factor (includes His to Gly 93 mutation to increase stability,[129] pI = 7.8) was provided by Prof. Robert Linhardt (RPI, Troy, NY). Octa and decasaccharides (dp8 and dp10), prepared by partial heparin lysis, followed by high-resolution gel filtration, were generously donated by Dr. John Gallagher from Iduron (Manchester, UK).

4.3.2 Methods

4.3.2.1 Electrospray Ionization Mass Spectrometry (ESI-MS)

All experiments were performed with a QStar-XL hybrid quadrupole-time-of-flight MS with a nano-ESI-source (AB Sciex, Toronto, Canada). The measurements were performed using both closed and pre-opened (1-2 μm id) glass nanospray capillaries (New Objective, Woburn, MA). ESI-MS was used to determine stoichiometries of FGF-1-dp8/dp10 complexes and monitor depletion of dp8/dp10. Growth Factor concentration was kept constant during each experiment (0.08 g/L, ca. 5 μM) and dp8/dp10 concentration was adjusted to 1, 2.5, 5, 10 and 25 μM at 100 mM $NH_4CH_3CO_2$ at pH 6.8. FGF-1 was buffer exchanged using Amicon (10 kDa cut off) with 100 mM $NH_4CH_3CO_2$, and the concentration was verified by UV-VIS using molar absorptivity of 17545 $M^{-1}cm^{-1}$. Dp8 and dp10 were diluted from 2 mg/mL stock solutions. Binding experiments were acquired using following settings of ion optics in the ESI interface: DP, 100; FP, 265; DP2, 15 and dp8/dp10 depletion experiments are acquired under mild ionization

conditions (DP, 40; FP, 150; DP2, 15),where DP is the declustering potential and FP is focusing potential. The mass distribution of the protein-bound heparinoid molecules were calculated using the Eq. 4.1.

$$\left(\left(\frac{m}{z}\right)\cdot z - mH\right) - nM_{FGF} \qquad \textbf{Eq.4.1}$$

where *n* represents total number bound FGF-1 molecules, *m* is the total protons attached and M_{FGF} is the mass of a single FGF molecule.

4.3.2.2 DelPhi Calculations

DelPhi V. 4r1.1,[130,131] which applies non-linear Poisson-Boltzmann equation to generate the potential surface of the protein, was used to model the electrostatic potential around FGF-1 (PDB id: 1K5U) at the experimental conditions as described (pH 7.0, I = 100 mM). The structures were taken from the protein data bank (http://www.rcsb.org/). The charges of amino acids on the protein were determined using Tanford's spherical-smeared charged model.[132]

4.3.2.3 Monte-Carlo Simulations

The MC technique with the Metropolis algorithm[147] was used for generating equilibrium states. The MC technique ensures that the system eventually reaches thermal equilibrium for the oligomer-protein complex. Heparin was presented by a decamer of 6 units of acrylamidopropylsulfonate and 4 units of acylamide; this AMPS-AAm oligomer has the same chain length and net charge as the well-known heparin pentasaccharide.[19] The temperature chosen for the simulations was T = 300 K. The charges on the various

residues were those appropriate to FGF-1 at pH 7.0 and protein was modeled as partially coarse-grained.

4.4 Results and Discussion

4.4.1 Heparin facilitates formation of FGF-1 multimeric complexes

The ESI mass spectrum of FGF-1 (5 μM) in the absence of heparin oligomers showed no evidence of dimers or higher-order multimers (Figure 4.1). However, in the presence of dp8 or dp10, at concentrations ranging from 1.25 to 25 μM corresponding to [FGF] / [Hp] ratio r = 4, 2, 1 and 0.2, formation of 1:1, 2:1 and 3:1 (FGF:heparin) complexes were observed (Figure 4.1a and 4.1b). When FGF was in excess relative to heparin, 3:1, 2:1 and 1:1 complexes were detected, but the 3:1 complex formation was most prominent in the presence of dp10 (Figure 4.1b). On the contrary, the 1:1 complex was detected as the most populated ionic species in the case of the excess heparinoid (at r = 0.2).

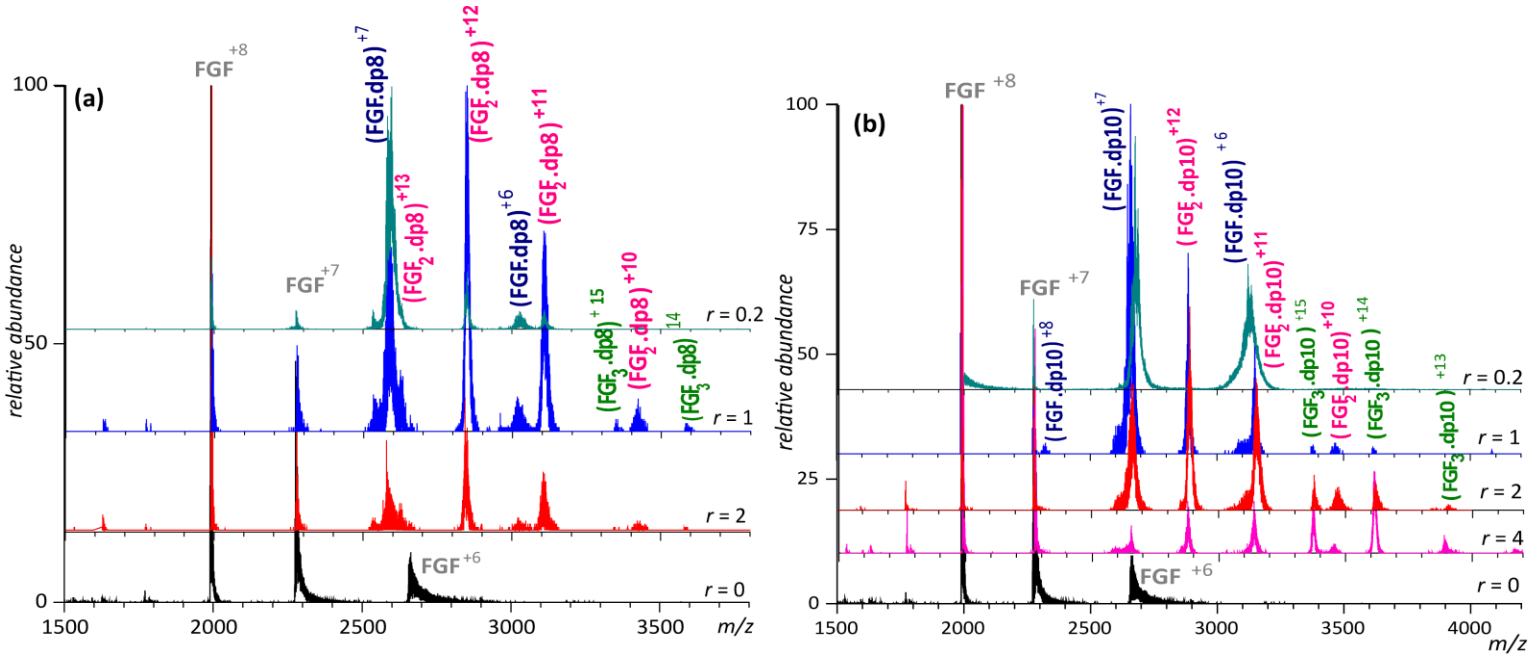

Figure 4.1: ESI mass spectra of FGF-1/heparinoid complexes at 100 mM $NH_4CH_3CO_2$, pH 6.8 *(a)* r ([FGF-1] / [dp8]) = 2, 1, 0.2 and 0. *(b)* r ([FGF] / [dp10]) = 4, 1, 0.2 and 0. The charge state distributions of free protein, 1:1, 2:1 and 3:1 complexes are presented gray, blue, pink and green labels, respectively.

The dependence of complex stoichiometry on the mixing ratio suggests a multiple binding equilibrium with heparin as the host molecule. For excess heparin, the presence of free protein indicates either that affinity is low, or that high affinity sites are fully occupied. These results, however, do not reveal how such high and low affinity sites are distributed among the heparin chains.

The formation of 3:1 complex, particularly favorable at high *r* (excess protein), brings up the need to explain how the heparin oligomer chain can accommodate three FGF molecules. The DelPhi image of FGF-1 (Figure 4.2), showing the 0.5kT/e electrostatic potential contours, indicates a dominant positive patch at pH 7.0, *I* = 100

mM. Even though the exact location of the bound Hp chain cannot be determined, it can be assumed that highly negative heparin would avoid the negative domains of the protein. Such predominant electrostatic effects make the classical "lock and key" interaction unlikely. The immediate vicinity of the positive domain can be viewed as creating a strong attraction basin for polyanions without forcing them into highly defined and thus entropically disfavored conformations. This dynamic behavior notwithstanding, the FGF-binding site size on heparin of 4 contiguous units (~2 nm) as determined from dynamic and static light scattering studies,[134] would seem to indicate that dp10 (contour length 5 nm) could not realistically bind three FGF-1's with hydrodynamic diameters of 4 nm, particularly in a *cis* complex. However, heparin, a semi-flexible chain,[10] can exhibit local conformations in solution[148] to facilitate FGF-1 binding from multiple directions , i.e., formation of a *trans* complex (as in Figure 4.2b and c).

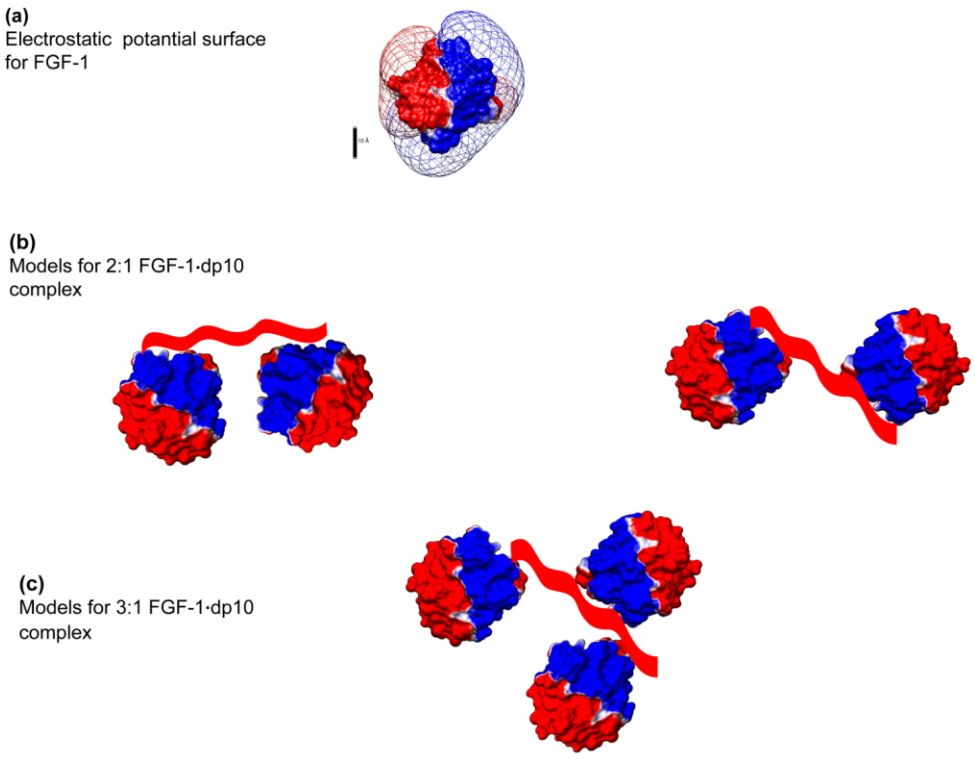

Figure 4.2: (a) Electrostatic potential contours (-0.5 kT/e (red) and 0.5 kT/e (blue)) generated around FGF-1 (PDB id: 1K5U) at 100 mM pH 7.0. Possible models for the structural arrangements of the (b) 2:1 and (c) 3:1 complexes are presented.

Additional evidence for the arrangements of the 3:1 complexes can be deduced from Monte Carlo simulations of the FGF-bound Hp-mimetic oligomer chain. Simulation snapshots shown in Figure 4.3, indicate that only a small part of the polyanion interacts with the protein at any instant. From this point of view, three FGF may be "bridged" by dp10, in the sense that they are highly co-localized with transient interactions with the oligoheparin overcoming intrinsic inter-protein repulsions.

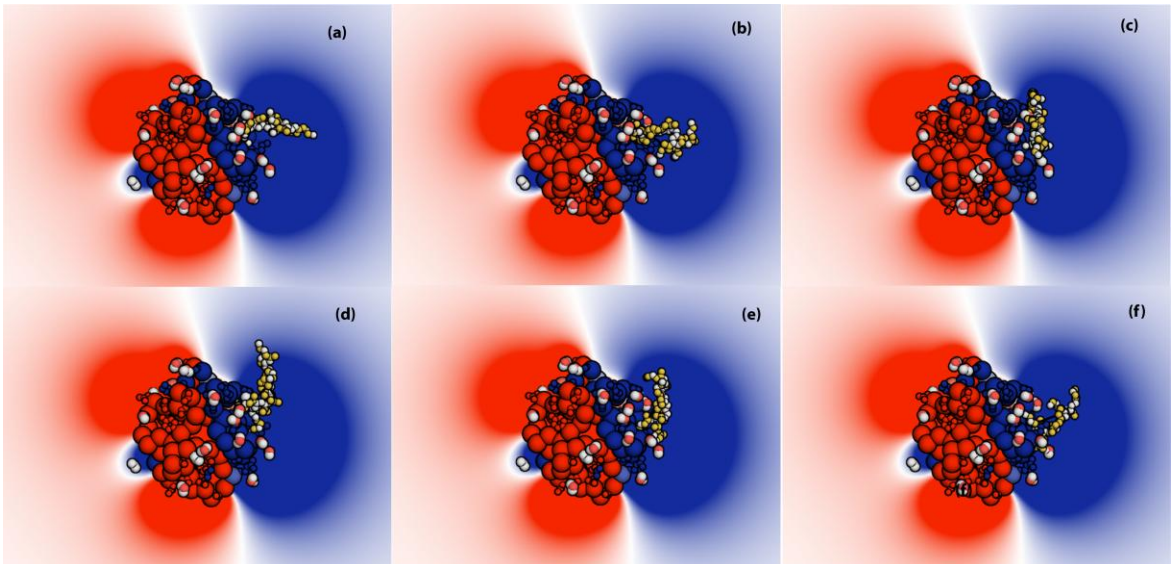

Figure 4.3: The MC snapshots of FGF and charged decamer residing at the FGF binding site at pH 7.0 and *I* =10 mM. FGF is represented with the electrostatic potentials at 0.5 kT/e, red and blue correspond to negative and positive protein potentials via solutions of the nonlinear Poisson-Boltzmann equation. The frames shown (a) through (f) are 25K MC steps apart and they are in the range of 225K to 350K MC steps (Courtesy of Daniel Seeman).

4.4.2 Higher sulfated chains promote formation of multimeric complexes of FGF-1

Heparin structure is immensely heterogeneous due to the seemingly random placement of sulfate groups (Figure 4.4). Dp8 and dp10 fragments exhibit structural polydispersity with respect to both total levels of sulfation and their distribution across the polysaccharide backbone.

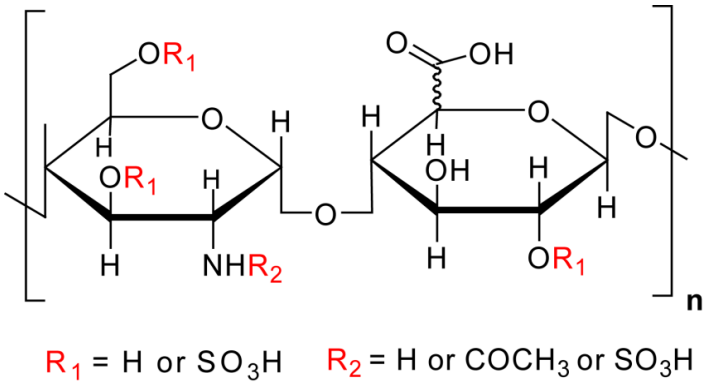

Figure 4.4: Repeating disaccharide unit of heparin oligomers. The possible locations for sulfate substitutions are shown in red. (n is equal to 4 and 5 for dp8 and dp10, respectively.)

Observation of different stoichiometric complexes with dp8 and dp10 indicated existence of multiple biding sites with various levels of affinity for FGF-1. In order to identify the structural features, i.e. degrees of sulfation of the dp8 and dp10 binders, the mass distribution of bound dp8/dp10 was determined. Mass to charge ratio for the most abundant peak of a protein/heparinoid complex (+7 for 1:1, +12 for 2:1 and +14 for 3:1) was converted to neutral mass using Eq. 4.1, and the mass distribution of the bound dp8 and dp10 are presented in Figure 4.5 and 4.6. Since all analyses were performed in the positive ion mode, each ionic species also contain 4-5 cations (NH_4^+). Therefore, shaded boxes are used in Figure 4 and 5 to indicate the mass ranges for heparinoid species with different extent of sulfation (the overlap is due to the uncertainty in the number of cationizing agents attached to each polyanionic chain). We used Roepstorff-Henriksen nomenclature $(X,Y,Z)^{80}$ to present sequence distribution of dp8/10, in which X represents number of saccharide, Y is the number of sulfate and Z is the number of acetyl groups.

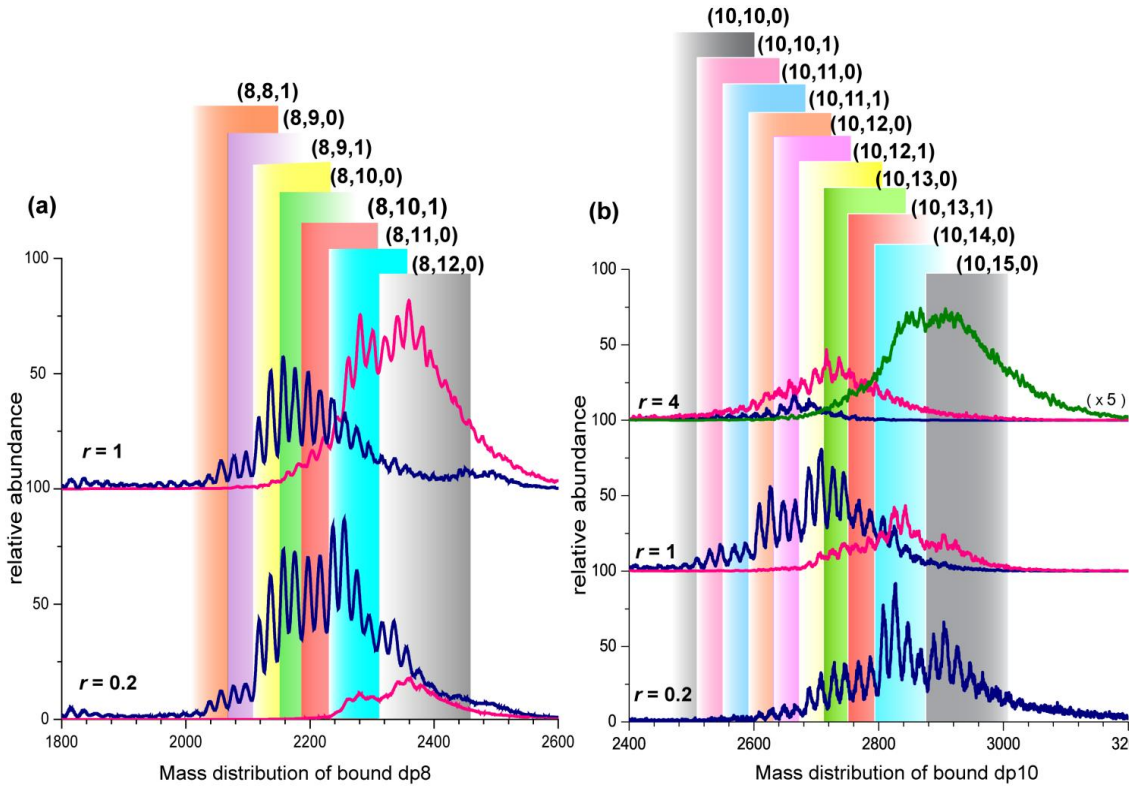

Figure 4.5: The mass distribution of the bound a) dp8 in the *r* = 0.2 and 1, b) dp10 in the *r* = 0.2, 1 and 4 are shown. Blue trace represents the +7 charge states of the 1:1 complexes, pink trace is the +12 charge states of the 2:1 complexes and green trace is the +14 charge states of the 3:1 complexes.

In Figure 4.5 (a), mass distribution of protein bound-dp8 molecules in 1:1 (blue traces) and 2:1 (pink traces) complexes were plotted for r = 1 and r = 0.2. A comparison of these two profiles indicates that protein bound dp8 chains carry 8 to 12 SO_3^- groups. In both cases, the 2:1 complexes were formed only on the highly sulfated chains (11 and 12 SO_3^- groups per chain). Low sulfated chains (with 8, 9 and 10 SO_3^-), retained the binding affinity for FGF-1, but they facilitated formation of only the 1:1 complex. Increasing dp8 concentration (r = 0.2) shifted the complex equilibrium towards 1:1 and the degree of sulfation in the 1:1 complex skewed towards higher sulfation, possibly

reflecting the fact that the lower charge density heparinoids are capable of binding to FGF-1 when their higher charge density counterparts became completely consumed.

Figure 4.5 (b) represents the mass distribution of protein-bound dp10 chains in 1:1 (blue traces) and 2:1(pink traces) complexes at r = 0.2, r = 1 and r = 4. In addition to 1:1 and 2:1 complexes, 3:1 complexes (green trace) are also observed at r = 4, and 3:1 complexes are formed on the chains containing 14 and 15 SO_3^- groups. The 2:1 complexes are formed in the intermediate range of sulfation (11 to 13 SO_3^-) and finally the 1:1 complex contains low sulfated chains. Higher dp10 concentration (r = 1) raises the number of available binding sites for FGF-1, as a result the ionic signal for the 3:1 complex is quite low, and the degree of sulfation in 2:1 and 1:1 complexes is skewed towards higher sulfation, 12-15 and 10-14 SO_3^- groups, respectively. When dp10 concentration is in 5-fold excess over FGF-1 (r = 0.2), only the 1:1 complex formed, in which low sulfated chains are replaced by the high sulfated dp10 chains (the number of sulfation is varied from 11 to 15). These results could indicate that: (1) highly sulfated chains are occupied first; (2) high sulfated chains have multiple binding sites (up to 3) with various degrees of affinity for FGF-1; (3) low sulfated chains are capable of binding to FGF-1; however the affinity is lower than highly sulfated ones.

4.4.3 When bulk stoichiometry leads to a significant amount of bound heparin, the charge density of the free heparin is low relative to the initial heparin

In this work, we utilized mass spectrometric approach to evaluate importance of heparin sulfation for FGF1-dp10 binding. While binding preferences of proteins towards Hp have been generally determined by analyzing protein/Hp complexes,[149,150] an alternative approach to this question utilized monitoring differential depletion of small

molecule ligand from the entire ensemble of heparinoid molecules upon addition of binding partner.[88] Figure 4.6 (a) and 4.6 (b) demonstrates bound and unbound dp10 mass distribution for r = 1, r = 0.5 and r = 0.2, respectively. The calculation described for Figure 4.5 was applied to obtain mass distribution of protein-bound dp10 species (Figure 4.6 (a)). Unbound (free) dp10 species appears at 1200 < m/z <1600 at +2 charge states and m/z values were transformed to the mass distribution.

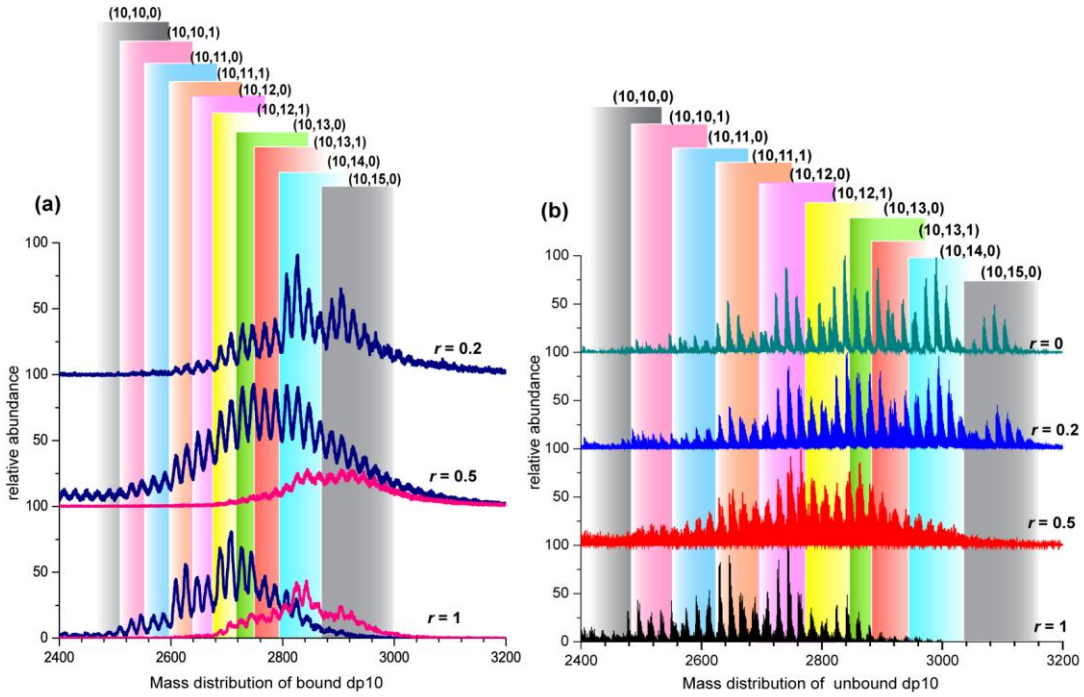

Figure 4.6: The mass distribution of the a) bound and b) unbound dp10 species at *r* = 1, 0.5 and 0.2

Mass distribution of unbound dp10 extends beyond that of the protein-bound dp10, because dp10 contains 11- 14 NH_4^+ adducts when they are free in solution, as opposed to 4-5 NH_4^+ in the protein-bound form. The depletion of dp10 species was more

pronounced at r =1, where the 2:1 ionic signal was more abundant and highly sulfated chains (14 and 15 SO_3^-groups) facilitated the complex formation. Moderate to low number of sulfated groups were engaged in the formation of 1:1 complex (10 to 13 SO_3^-), in which the majority of the binders carry 12 and 13 SO_3^- groups. This observation is clearly consistent with the Figure 4.6 (b): dp10 chains incorporating 13-15 sulfate groups are almost completely depleted; therefore ionic signal from 10 to 12 sulfated species becomes more abundant on a relative scale. The r = 0.5 presents a transition stage in that the 2:1 complex ionic abundance decreased and sulfation distribution is skewed to higher sulfation for the 1:1 complex. Similarly, depletion of the highly sulfated species is quite evident at r = 0.5, as seen in Figure 4.6(b). Since dp10 concentration was quite high relative to the protein at r =0.2, the depletion of the dp10 chains was minimal, and protein-free dp10 spectra (r = 0) and r = 0.2 free regions are almost identical.

These results support the previous identification of highly sulfated species as primary agents triggering formation of in the FGF-1 multimers. The heparin chains may exhibit not only intra-chain heterogeneity, but also inter-chain diversity so that the chains having same number of sulfates may not have the same distribution of sulfate groups. The arrangement of the sulfate groups within these chains can occur in numerous ways considering the possible locations in a disaccharide as represented in Figure 4.4. There are 20 sites available for sulfation within dp10, and if these sites are assumed to have equal probability of carrying a sulfate group; the possible ways to distribute sulfate groups can be calculated by:

$$C_n^k = \frac{n!}{k!(n-k)!} \qquad \textbf{Eq. 4.2}$$

where n is the total sites and k is the number of sulfate groups.

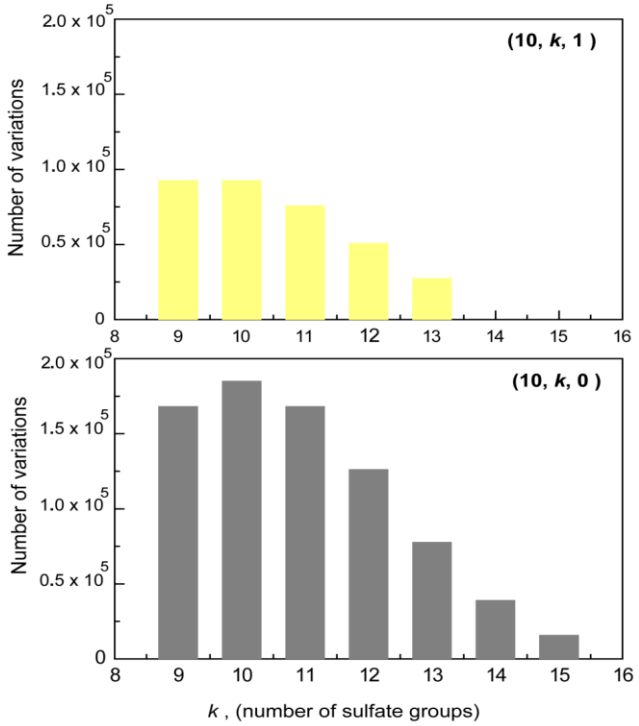

Figure 4.7: The number of possible structural arrangements depending on the number of sulfate groups within dp10.

The results obtained by using Eq. 4.2 are presented in Figure 4.7. The number of variations to distribute sulfate groups is lower in the highly sulfated chains; therefore, the possibility of having equally distributed charges, i.e. "charge segments", along the chain is higher. As seen in Figure 4.6 (b), highly sulfated dp10 chains (carrying 14 and 15 sulfate groups) were completely depleted at r = 1, on the contrary dp10 chains carrying 10- 12 sulfate groups are more abundant on a relative scale. Structural variations are higher for these chains; therefore the probability of having a "charge segment" is much

lower. These observations could explain (1) the preferential binding between FGF-1 molecules and the highly sulfated chains, in which highly sulfated chains can provide properly arranged charged domains for FGF-1; (2) the incapability of the low sulfate chains to induce multimeric complexes of FGF-1 due to the decreased amount of "charge segments".

4.5 Conclusions

ESI-MS results suggested that the nature of the FGF- heparinoid interaction was "promiscuous" in that both high and low sulfated chains could be involved in binding events. Highly sulfated dp8 and dp10 chains are involved in multimer formation than lower sulfated chains. When dp8/dp10 is excess, low sulfated binders are replaced with highly sulfated ones in the 1:1 complex, which is a clear representation of the competition between low and high sulfation in protein recognition. The formation of 3:1 complexes on highly sulfated dp10 chains also indicates a packed structure, in which proteins could be bound with close proximity. Heparin induced multimerization of FGF on the varying degree of sulfation could be an evidence that heparin oligomers "concentrate" FGF molecules along the heparin chain; therefore the probability of the receptor interaction could be increased. Furthermore, these studies emphasize the power of ESI-MS to characterize protein interactions with the highly heterogeneous targets.

ACKNOWLEDGMENTS

This work was supported by grants from the National Science Foundation CHE-0750389 (to I.K.), CHE-0619039 (to P.D.). We would like to thank Daniel Seeman

(UMass, Amherst), Prof. David Pink and Bonnie Quinn (St. Francis Xavier University, Nova Scotia) for Monte Carlo Simulations.

CHAPTER 5

ELECTROSPRAY IONIZATION MASS SPECTROMETRY STUDY TO REVEAL THE EFFECT OF HEPARIN CHAIN LENGTH ON ANTITHROMBIN AND FACTOR XA COMPLEX FORMATION

Minsky, B. B.; Abzalimov, R; Dubin, P. L.; Kaltashov, I. A.

5.1 Introduction

Full-length heparin, low molecular weight heparins and small molecule heparin analogs have been administered as anticoagulant drugs for decades; however, their efficacies are reduced by the high risk of bleeding[151] and the requirements of patient-dependent dose administrations.[152] Safer and more effective therapies can be achieved through greater understanding of the way that heparin mediates antithrombin and protease binding, which is a central inhibitory process in coagulation. However, the accuracy of models for the binding of antithrombin and coagulation proteases is a matter of controversy. In this study, we monitor complexation of antithrombin (AT) and coagulation protease Factor Xa (FXa) in the presence of defined-length heparin (Hp) oligomers using electrospray ionization mass spectrometry (ESI MS) in order to compare the capabilities of various length heparin oligomers to induce binary (AT·FXa) and ternary (AT·FXa·Hp) complexes.

Antithrombin, a natural anticoagulant in the blood, inhibits coagulation proteases, predominantly thrombin and Factor Xa, by forming equimolar and stable complexes.[153-

[155] Although this process occurs naturally in the blood, the binding process is extremely slow. Heparin and heparan sulfate enhance the rate of antithrombin-thrombin/Factor Xa complex formation by up to several orders of magnitude.[156] In both cases, heparin acts as a catalyst, and therefore it is not necessarily a part of the final complex.[33] The mechanism of AT-protease binding has been suggested to follow two sequential events: (1) diffusion-controlled formation of an encounter complex; (2) formation of a reaction-controlled stable covalent complex.[33,157] If heparin promotes the encounter complex, its role would be basically confining two proteins on the same chain, so they have more time to interact. This "approximation effect" is suggested for AT-thrombin binding.[158] If heparin modulates the reaction part, it would do so by inducing the conformational change on AT: this mechanism is proposed for AT-FXa interaction (allosteric effect).[159]

The minimal heparin length required to promote the approximation effect is 18 monosaccharide units;[158] whereas a specific pentasaccharide has been proposed to be capable of activating AT towards Factor Xa[160] as a result of an induced conformational changes on AT (allosteric activation). This model has been challenged by recent studies showing that binding to heparin chains of various length does not significantly change secondary structure, but in fact enhances the conformational stability of AT, a stronger effect observed with shorter heparin oligomers.[161] The formation of encounter complexes and an approximation effect have also been experimentally observed for AT-FXa in the presence of longer chain heparins.[162] Calcium ions have been shown to improve anti-FXa activity with increasing Hp chain length.[163] Consistent with the approximation effect model recent findings indicate that long chain heparins enhance AT-FXa binding, even in the absence of calcium ions.[164] In the crystal structure of Factor IXa, a crystal contact was

observed with heparin pentasaccharide, which was interpreted as a possibility for longer chain to form encounter complex.[165]

The anticoagulant activity of heparin was famously ascribed to a unique pentamer carrying a rare 3-*O*-sulfate substitution,[18] but many observations run counter to this yet influential paradigm. Recent studies indicate that 3-*O*-sulfate substitution may not be needed to promote allosteric activation of AT.[166] Less complex polyanions, such as, sulfated dextran[167] and sulfated lignins,[168] can imitate Hp function in AT-FXa binding. The putative interaction between AT and the high-affinity binding specific pentasaccharide embodied directionally specific short-range interactions (H-bonds and salt bridges).[17-19] This concept of specificity essentially incorporates a frozen state of AT-bound heparin despite the intrinsic flexibility of oligoheparins.[9] Furthermore, non-monotonic salt dependence, difficult to rationalize on the basis of short-range attraction alone, has been observed for AT and low molecular weight and full-length heparin interactions,[28] as for other protein-polyelectrolyte systems.[51] These observations highlight the significance of the combinations of short-range attractions and long-range repulsions between the negatively charged heparin and the highly anisotropic protein surface charges,[28,44,51] and introduce a nuanced view of specificity that takes into account the charge complementarity between the protein surface and the polyanion.[31]

The stoichiometry and the mechanistic interpretations of AT-FXa binding have primarily evolved from crystallography studies,[23,169] involving short heparin analogs. In this way, the effects of the intrinsic heterogeneity of biologically relevant heparin chains could be overlooked. Therefore, in order to investigate the AT-FXa complex stoichiometries, we use a set of well-defined heparin oligomers, whose chain lengths

range from hexa- to icosasaccharide. Electrospray ionization mass spectrometry (ESI MS) serves this purpose exceptionally well by providing remarkable structural details and revealing complex stoichiometries.

5.2 Experimental

Human α-AT (MW = 57.8 kDa), was purified from human plasma using heparin affinity chromatography, generously donated by CSL Behring (Marburg, Germany),. Heparin oligomers (dp6, dp8, dp10 and dp20) and native heparin were provided by John T. Gallagher (Iduron, Manchester, UK). Human Factor Xa, which is a mixture of α (45.3 kDa) and β (43.3 kDa) subforms, was purchased from Haematologic Technologies, Inc (Vermont, USA). Factor Xa(β) is formed as a result of autoproteolysis of Factor Xa(α), and both subforms have equal roles in coagulation.[170] Protein and heparin oligomer solutions for ESI MS analysis were prepared in 150 mM ammonium acetate at pH 7.0 to final concentrations of 1.8 μM for AT and 1.8 μM for FXa, and 7.5 to 15 μM for heparin oligomers. All binding experiments, both in the absence and in the presence of heparin oligomers, were completed within an hour after mixing of the components. ESI MS experiments were performed with a QStar-XL hybrid quadrupole-time-of-flight MS with a nano-ESI-source (AB Sciex, Toronto, Canada) and the measurements were performed using closed (2 μm id) glass nanospray capillaries (New Objective, Woburn, MA).

5.3 Results

5.3.1 Short heparin oligomers induced formation of AT·FXa binary complex

Figure 5.1A shows the ESI mass spectra of AT-FXa in the presence of dp10 with concentrations varying from 0 to 15 μM. In the absence of dp10, the ionic signal representing AT·FXa complexes is in very low abundance, whereas free AT and free FXa species contribute to the ionic signal significantly.

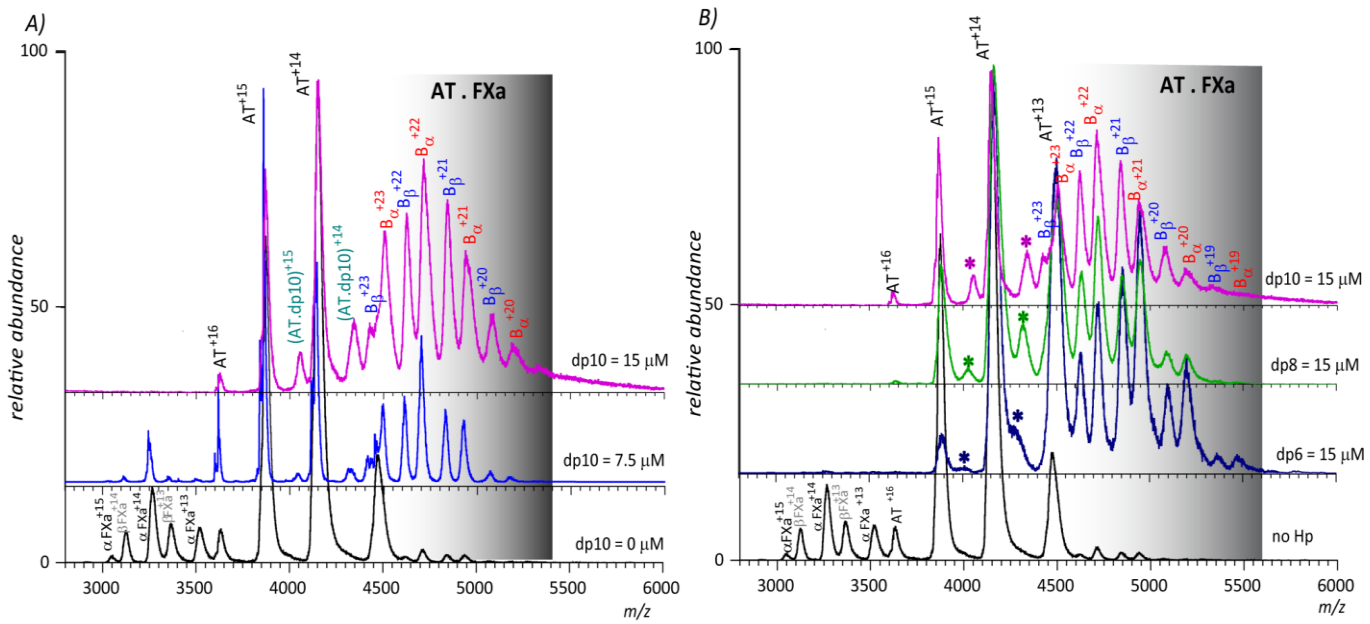

Figure 5.1: ESI mass spectra of AT (1.8 µM) and FXa (1.5 µM) in the absence and presence of Hp oligomers at 150 mM ammonium acetate, pH 7.0. A) The dependence of AT and FXa binary complex formation to dp10 concentration. B) AT and FXa complex formation with various lengths heparin oligomers (dp6, dp8 and dp10) using 15 µM of oligomers. The notations represent: Bα = AT + FXa (α) = 103.3 kDa and Bβ = AT + FXa (β) = 101.3 kDa

In the presence of dp10, ESI MS spectra provide clear evidence for the formation of 1:1 AT·FXa complexes. Raising dp10 concentration from 0 to 15 µM leads to a progressive increase in AT·FXa complexes and a decrease in free FXa ionic species. In the presence of dp10, the resultant complex was assigned to a mass distribution with a 1:1 AT·FXa stoichiometry and dp10 was not detected as a part of the complex, at least with the standard deconvolution methods. Using 15 µM dp10 concentration results in optimal ratio of AT·FXa to free AT and FXa ratio; thus this concentration was used to determine complex stoichiometries with even shorter heparin oligomer chains. As seen in Figure

1B, similar binding patterns were observed between AT an FXa in the presence of 15 μM dp6, dp8 and dp10, and there was no evidence for the ternary AT·FXa·dp6 and AT·FXa·dp8 complexes.

In order to provide further evidence for the absence of ternary complexes, dp10 free and dp10 present spectra are overlaid in the AT·FXa complex region ($4600 < m/z < 5200$), and peak widening was observed in the dp10 present spectrum (Figure 5.2A). The wider peaks could be an indication of the presence of AT·FXa·dp10 complexes; therefore these peaks were deconvoluted using Gaussian fittings to investigate any possible contributions from AT·FXa(α)·dp10 and AT·FXa(β)·dp10 complexes. The widths of these complexes were estimated relative to the AT·dp10 complex, which is already present in the spectra. As seen from the Figure 5.2B, there is a small contribution from AT·FXa·dp10 complexes, and this contribution does not exceed 20% of the total binary complex.

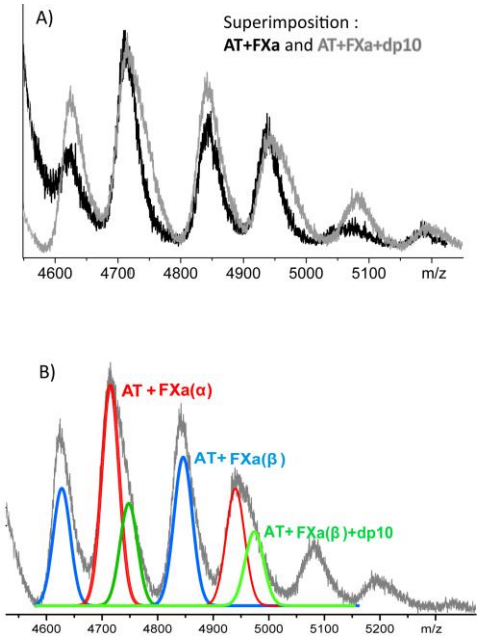

Figure 5.2: A) Superimposition of AT-FXa and AT-FXa-dp10 spectra in the binary complex region. B) Gaussian fittings to investigate the contributions of ternary AT-FXa-dp10 complexes to the binary complex

5.3.2 Longer chains induce formation of higher order AT-FXa complexes (dp20 and native heparin chains

Short heparin chains (dp ≤ 10) facilitated AT-FXa interaction, and intriguingly these chains were dissociated from the resultant complex in the course of the experimental time scale. However, longer heparin chains (dp 20) were capable of inducing AT·FXa(α)·dp20 and AT·FXa(β)·dp20 complexes, corresponding to 107.3 kDa and 109.3 kDa complexes, respectively (Figure 5.3A). Gaussian fittings were generated using the peak shapes of the AT·dp20 complex and the resultant peaks matched with the AT·FXa(α)·dp20 and AT·FXa(β)·dp20 complex peaks. This analysis distinctly demonstrates that AT·FXa complexes are absent from the spectra (Figure 5.3B).

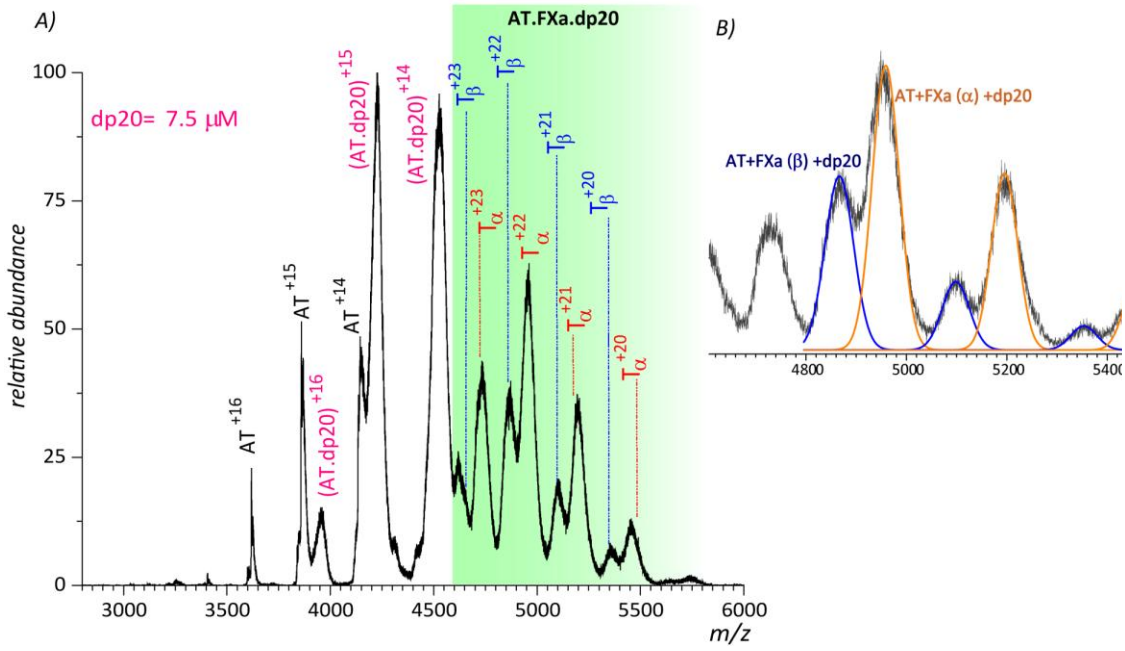

Figure 5.3: A) ESI mass spectra of AT (1.8 µM) and FXa (1.5 µM) in the presence of heparin dp20 (7.5 µM) at 150 mM ammonium acetate, pH 7.0 representing ternary AT-FXa(α)-dp20 (109.3 kDa) and AT -FXa (β)-dp20 (107.3 kDa) complexes. B) Gaussian fittings to validate ternary AT-FXa(α)-dp20 and AT -FXa (β)-dp20 complexes.

The concentration of dp 20 used in this experiment was 7.5 µM, and this amount was sufficient to induce the formation of AT·FXa·dp20 complexes and deplete the free FXa components notably. Similar complex formation and depletion patterns were obtained using a 15 µM concentration of shorter heparin oligomers (dp ≤ 10). In addition, the relative abundance of free AT as a function of heparin oligomer chain length is significantly lower with dp20 compared to the shorter heparinoids (dp ≤ 10).

AT and FXa binding, in the presence of native (un-fractionated) heparin represents the most challenging case. Figure 5.4 shows the addition of ~2.4 µM native heparin at the same conditions used for shorter heparinoids in AT and FXa binding

experiments. Even though the relative abundances of free AT and FXa components have been substantially decreased, the immense structural heterogeneity of native heparin limits any meaningful interpretations for the probable AT-FXa complexes in the *m/z* region beyond 4500. Nonetheless, this highly complex spectrum suggests promising future studies to distinguish higher order AT-FXa complexes on native heparin chains with more sophisticated ESI MS methods, such as limited charge reduction on FTICR MS.[171]

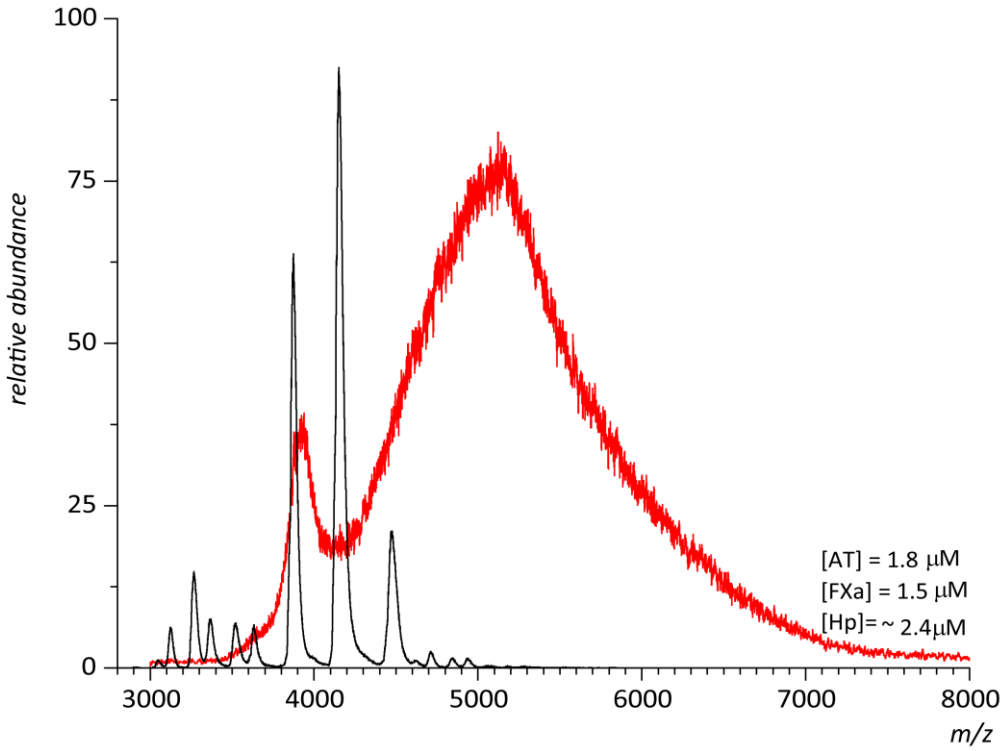

Figure 5.4: Superimposition of ESI mass spectra of AT (1.8 µM) and FXa (1.5 µM) in the absence (black trace) and presence of native heparin (~2.4 µM) (red trace) at 150 mM ammonium acetate, pH 7.0.

5.4 Discussion

ESI MS has advantages over other biophysical techniques to determine the stoichiometry of the multi-protein complexes, which exist in solution under equilibrium.[172] In this study, we have investigated the effect of heparin chain length on mediation of complex formation between AT and FXa, which is an inhibitory event in coagulation. In this diffusion-controlled macromolecular reaction, an AT·FXa·Hp encounter complex forms prior to reaction.[173] At the final step of the reaction, an AT·FXa covalent binary complex forms[174,175] and heparin dissociates from the complex. Our ESI MS results demonstrated that the formation of the AT·FXa binary complexes is greatly enhanced in the presence of short heparin oligomers (dp $\leq$ 10). The AT·FXa binary complex signal was correlated with the concentration of heparin oligomer, as also suggested by the previous findings.[176] In our studies, Hp oligomers were not detected as a part of the final complex, especially with dp6 and dp8, which could indicate that short heparin oligomers catalyzed the encounter and reaction completed faster. This observation could be in accordance with recent studies, in which short heparin oligomers were proven to be more efficient in catalyzing AT-FXa binding by improving the conformational stability of AT.[161]

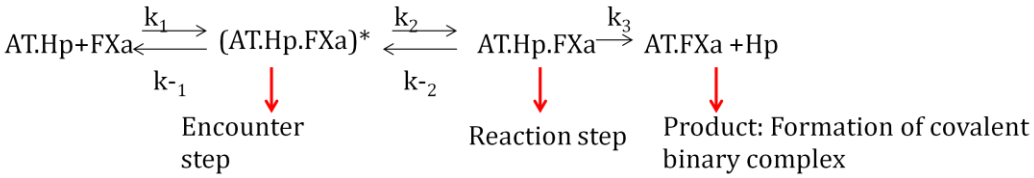

Figure 5.5: Proposed the reaction steps in diffusion-controlled AT, Hp and FXa interactions.

In the presence of dp20, ESI MS clearly demonstrates that dp20 facilitates the formation of stable ternary AT·FXa·dp20 complexes. AT·FXa binary complexes were certainly absent from the spectra, as confirmed by the deconvolution analysis. One possible reason is that dp20 binds simultaneously to AT and FXa. This "reduction in dimensionality effect"[33] is consistent with the previous observations for AT and thrombin interactions.[158,162] While proteins are bound on the same chain, they might spend more time interacting and this might delay the formation of final binary covalent AT·FXa complex.

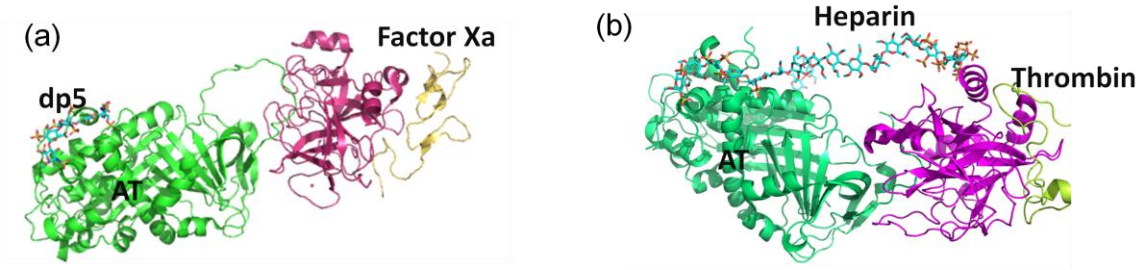

Figure 5.6: Crystal structures for (a) AT-FXa-pentasaccharide and (b) AT-Thrombin-heparin (18 monosaccharide length)

The other possibility is that dp20 exhibits higher affinity towards AT; therefore it does not dissociate from AT even after the reaction stage is completed. The higher affinity of dp20 compared to shorter heparin oligomers can be qualitatively assessed from the ESI MS spectra by the comparison of the relative abundance of free AT or AT-heparinoid complex as a function of heparin oligomer chain length. The most dramatic difference can be seen in the case of dp20 binding, in which the AT·dp20 complex exhibits higher relative abundance compared to the shorter chains, even though the concentration of dp20 is half that of the shorter heparinoids. Specific Hp chains that facilitate the AT-FXa interactions are the main interest in pharmaceutical applications; however, the structural heterogeneity is such that the resolution of our experiments was not sufficient to determine the specific heparin oligomer species.

5.5 Conclusions

Short Hp chains (dp $\leq$ 10) promoted binary AT·FXa complexes and they most likely have improved the conformational stability of AT towards FXa to facilitate the reaction. On the contrary, dp 20 induced ternary AT·FXa·dp20 complexes, possibly by binding simultaneously to AT and FXa. Furthermore, higher affinity between AT and long heparin chains could be the reason that dp20 stays in the ternary complex longer. Native heparin chain could promote formation of higher order AT-FXa complexes, (possible 4:1) and this observation could be further supported by the future studies using limited charge reduction method in FTICR MS. This study also demonstrated (for the first time) the capability of ESI MS to resolve the complex stoichimetries between AT and FXa in the absence and in the presence of heparin oligomers.

CHAPTER 6

ANTITHROMBIN AND FULL-LENGTH HEPARIN COMPLEXES DETECTED ON FTICR MS BY LIMITED CHARGE REDUCTION

Abzalimov, R.; Minsky, B. B.; Kaltashov, I. A.

6.1 Introduction

The preeminent challenge in the characterization of protein-heparin interactions is the immensely polydisperse heparin structure, which limits the application of various analytical techniques. Thus, the most common approach is to use heparin oligomers with a reduced-heterogeneity in protein interactions. Even though heparin oligomers have provided insights on the protein binding, the structural properties of these oligomers deviate from the biologically relevant full-length, "native" heparin (Hp). Electrospray ionization mass spectrometry (ESI MS) has emerged as a fundamental technique to study heparin oligomers and detect their non-covalent complexes; however correct mass and charge assignment is a major obstacle for the highly heterogeneous systems, especially for full-length heparin-protein complexes. We approached this problem using a recently evolved technique, limited charge reduction, in order to determine the complex stoichiometries between antithrombin (AT) and full-length heparin.

Characterization of native heparin-protein complexes have been achieved using various analytical tools, such as light scattering,[134] analytical ultracentrifuge,[125] size exclusion chromatography.[177] Even though these techniques provide size distributions of macromolecular complexes, deducing complex stoichiometry can be challenging due to the coexistence of multi-protein complexes in solution. In addition, these techniques provide average solution properties and do not provide detailed structural information.

ESI MS appears as a significant tool for the detailed structural information of the protein-heparin complexes; however native ESI MS has not been fully implemented in this field so far. The applications have been limited to relatively homogeneous and shorter length heparinoids and their complexes with proteins.[88,178-181]

The enhanced applicability of the short heparin analogs has generated concerted efforts to define the specific heparinoid structure in protein binding.[18] However, this reductionist approach not only deviates from biological relevance, but also ignores the polyelectrolyte properties of heparin. In heparin-protein binding, long-range electrostatic forces and chain dynamics contribute significantly to the protein recognition and selectivity process.[139] Therefore, there is a need for improved analytical tools to characterize native heparin-protein complexes in more detail and obtain structural information. ESI MS can be utilized for this purpose, but the challenges associated with the immense heterogeneity need to be addressed.

A recently developed technique, limited charge reduction, mass-selects a narrow subpopulation of the ionic species in the highly heterogeneous spectra, which are then subjected to electron capture reactions to induce formation of well-defined charge ladders. The resulting charge state "ladder" can be used to calculate the mass of isolated complex ions. This method was successfully implemented to analyze highly heterogeneous systems, such as glycosylated proteins[182] , protein aggregates[183] and protein multimers.[184] AT-Hp interactions possess a great deal of interest due to the clinical usage of heparin in anticoagulation, but the studies so far have been greatly focused on the synthetic and short heparin mimetics to modulate AT binding.[168,185,186] The challenges associated with the heterogeneous native Hp can be overcome using

limited charge reduction to determine the AT-Hp complex stoichiometries in near physiological conditions.

6.2 Experimental

Human α-AT (MW = 57.8 kDa) was generously donated by CSL Behring (Marburg, Germany) and was purified from human plasma using heparin affinity chromatography. Full-length "native" heparin (Hp) was provided by John T. Gallagher (Iduron, Manchester, UK). AT and Hp solutions for ESI MS and FTICR MS analysis were prepared in 150 mM ammonium acetate to final concentrations of 1.8 μM for AT and 0.044 g/L, ca. 2.4 μM for Hp. Both nano-ESI Qstar-MS and FTICR MS show that the concentration of AT should not exceed 1.5 μM to prevent formation of AT multimers prior to Hp addition. ESI MS experiments were performed with a QStar-XL hybrid quadrupole-time-of-flight MS with a nano-ESI-source (AB Sciex, Toronto, Canada) and the measurements were performed using closed (2 μm id) glass nanospray capillaries (New Objective, Woburn, MA). Protein ion charge reduction was carried out with a SolariX 70 (Bruker Daltonics, Billerica,MA) Fourier transform ion cyclotron resonance (FTICR) MS. Ion isolation was done in the collision cell (up to 2 seconds of accumulation time) and electron capture was applied is in the ICR cell. Molecular weight distribution of full-length heparin was determined by SEC-MALLS (Wyatt) using TOSOH SW3000xl column to elute 1 g/L heparin sample with 0.1M NaCl. AT-Hp complexes were also determined by SEC using TOSOH SW3000xl column (mobile phase: 150mM ammonium acetate, pH 7.0).

6.3 Results and Discussion

6.3.1 AT-native Hp complexes were obtained using native ESI MS and SEC

AT is a highly glycosylated protein (58 kDa) with an approximately 15% carbohydrate content by weight.[187] ESI mass spectrum of AT and native Hp indicates free AT monomer and AT-Hp complexes which appear in the range of $4500 < m/z < 6500$ (Figure 6.1a). There are two distinct regions representing AT-Hp ionic species; however both AT glycosylation and immense Hp structural heterogeneity give rise to a highly complex and unresolved mass spectrum. In this case, it is not possible to determine the exact mass and charge state distributions of these species due to overlapping ionic peaks representing different charge states.

More evidence for the formation of AT-Hp complexes comes from SEC profiles as shown in the inset of Figure 6.1b. SEC results shows that approximately 50 % of AT monomer are depleted in the presence of Hp, and AT-Hp complexes form as shown by the appearance of the early eluting peak. The complex peak has a broad width, which can designate unresolved and various size AT-Hp complexes. Furthermore, the elution profile of the native heparin on SEC-MALLS demonstrated that the native heparin chains have an average mass of 18 kD with a 1.1 polydispersity index (Figure 6.1c). Both SEC and native ESI MS evidently show the formation of multiprotein complexes of AT and Hp, with a better resolution in ESI MS; however the limited charge reduction method is certainly needed to resolve the exact complex stoichiometries.

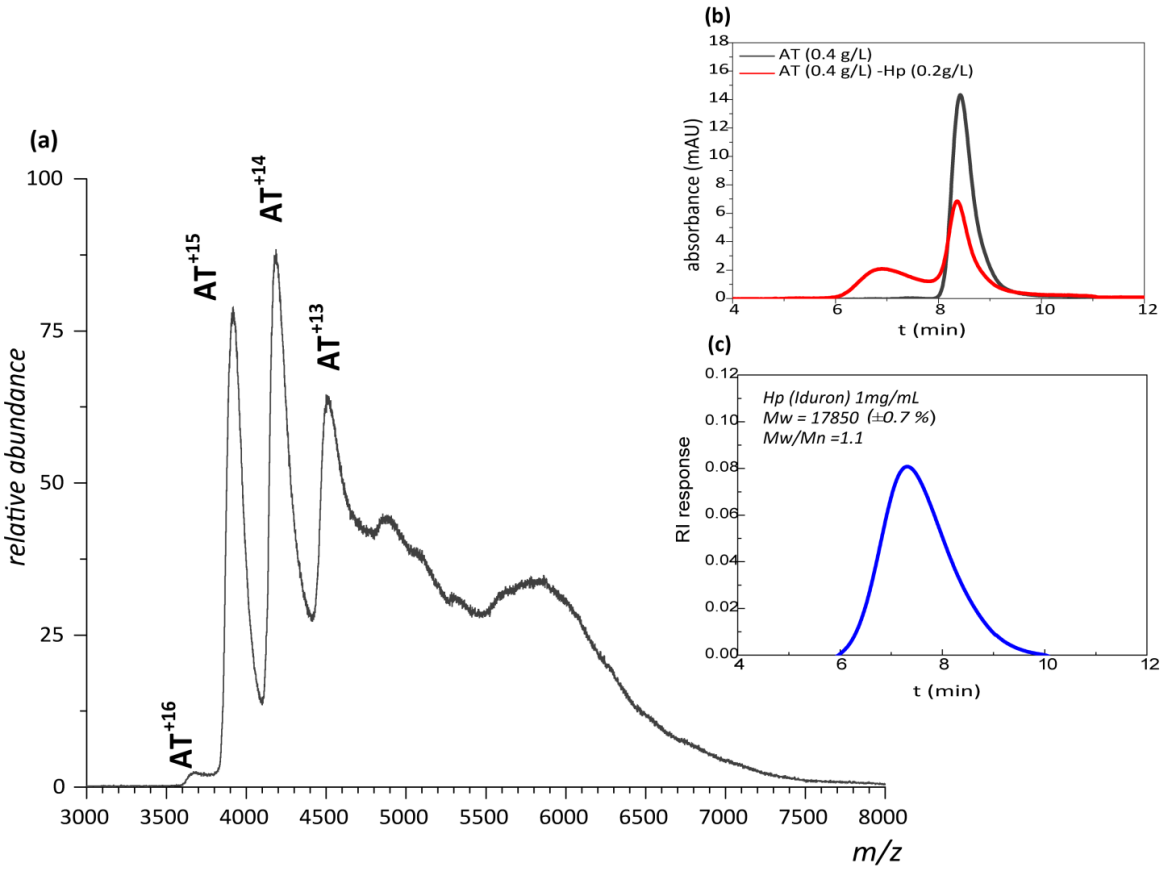

Figure 6.1: (a) ESI mass spectrum of AT (1.8 µM) and native Hp (0.044 g/L, ca. 2.4 µM) acquired using nano-ESI Qstar-MS (at 150 mM Ammonium acetate, pH 7.0). (b) AT (0.4 g/L) and native Hp (0.2 g/L) complexes detected on SEC (c) Elution of native heparin on SEC-MALLS.

6.3.2 Correct mass assignment of the AT-Hp complexes was achieved by limited charge reduction

AT alone and AT-Hp mixture were also acquired on FTICR MS; however transfer optics of FT-ICR MS was optimally tuned to detect ions at higher *m/z* range (>4000). Therefore, the intensity of the ionic species that represents AT-Hp complexes was more abundant in FTICR MS than nanospray ESI MS. Protein self association was not observed in the absence of Hp and the complex peaks were still unresolved due to the Hp polydispersity and overlapping charge states.

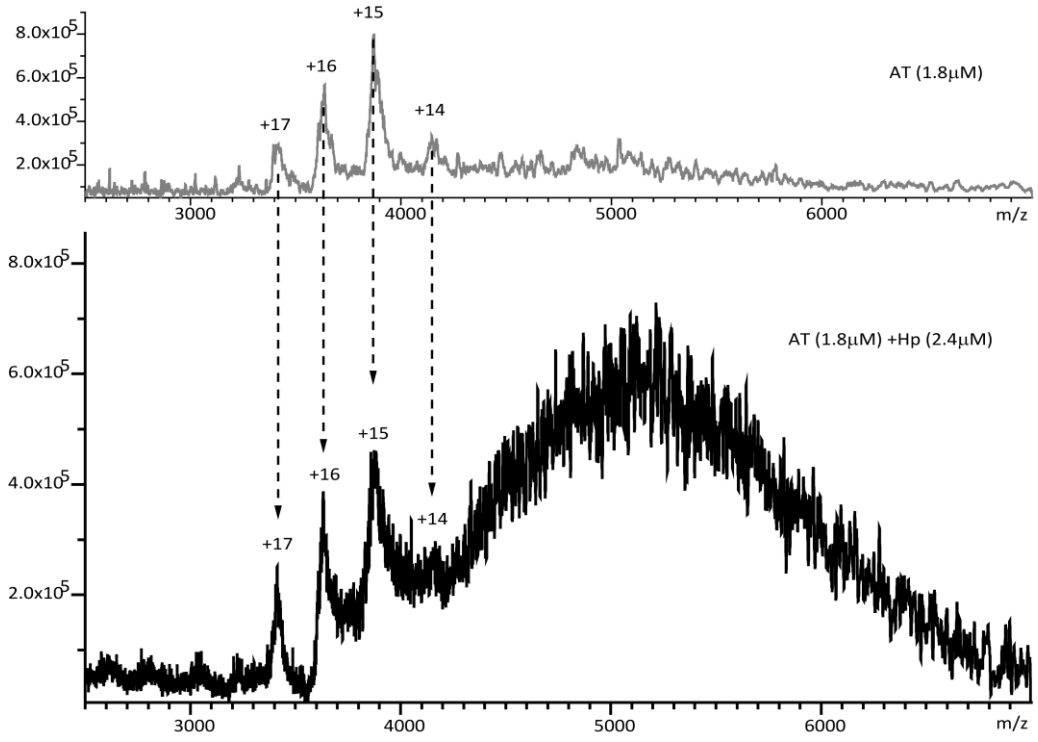

Figure 6.2: ESI mass spectrum of AT (1.8 μM) and native Hp (0.044 g/L, ca. 2.4 μM) acquired using FTICR MS (at 150 mM Ammonium acetate, pH 7.0).

In the process of partial charge reduction, an isolated fraction of the Z^+ charge state ions is mass selected in the collision cell width w_0. When these selected ions are exposed to electron irradiation, they should produce charge reduced peaks and the widths can be assigned to $w=w_0*(Z/Z-K)$ on the m/z scale, where K represents the number of captured electrons. This approach was tested with the selection of m/z = 4580 (Figure 6.3a) and m/z = 4740 (Figure 6.3b) and they both showed that the equation accurately estimates the widths of the charge reduced peaks (fitted with Gaussians in blue) based on the defined widths of isolated peaks (fitted with Gaussians in black). Deconvolution analysis reveals the mass distributions, which are ~73,180 Da in (a); ~75,820 Da in (b), corresponding to AT·Hp (1:1) complexes. Therefore, it is quite reasonable to consider this method for reliable identification of charge reduced peaks in more challenging cases, which is shown in Figure 6.3c. The selection of m/z = 5200 yield two distinct

distributions: (1) 88, 489 Da (green trace), which correspond to AT·Hp_2 (1:2) species, (2) 135,510 Da (pink trace) which is assigned to AT_2·Hp (2:1) complexes.

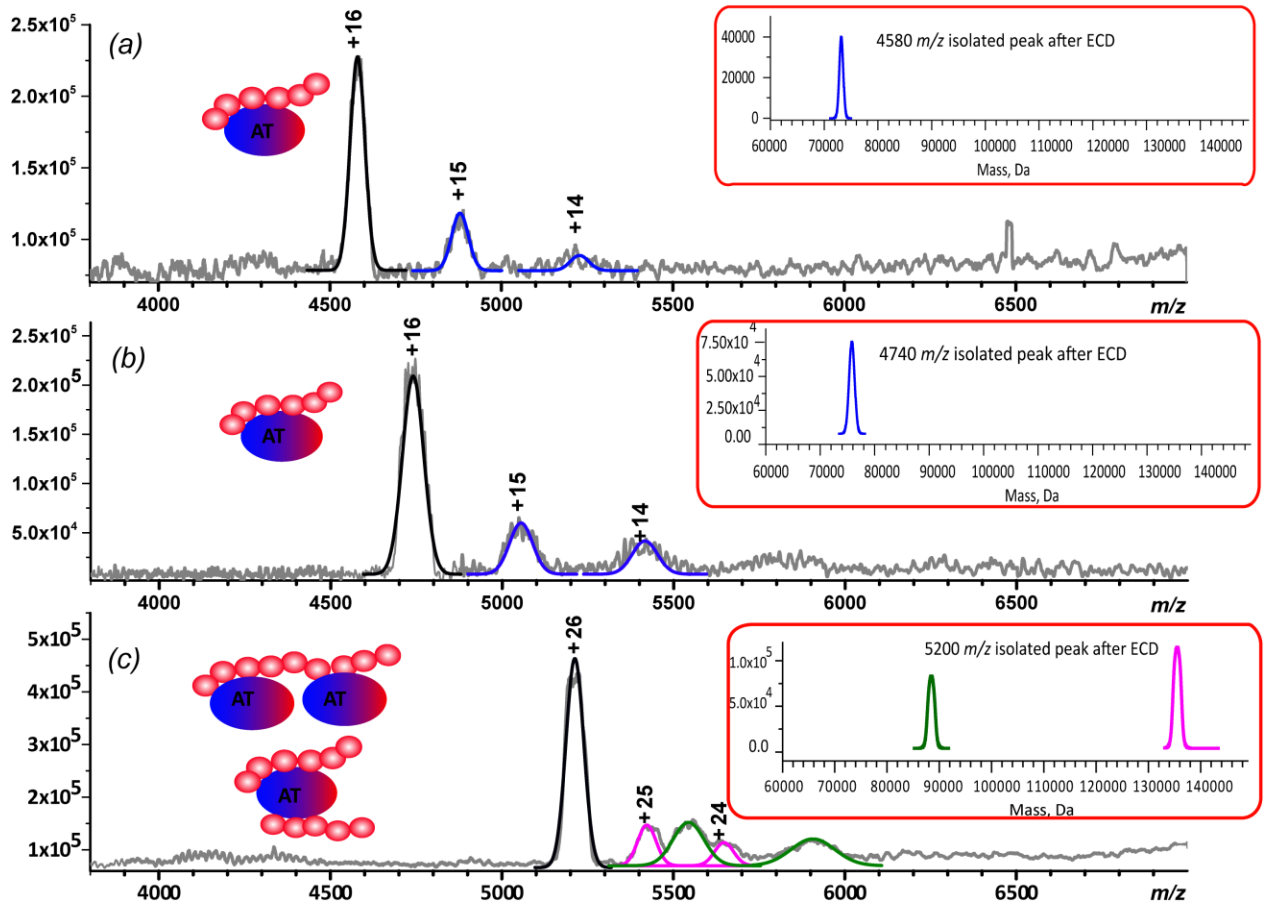

Figure 6.3: The results of partial charge reduction of mass-selected AT-Hp complex populations. Insets represent the convoluted mass distributions of the detected complexes.

The mass distribution of Hp molecules in the AT·Hp complexes with 1:1 stoichiometry are detected as 15 and 17 kDa (Figure 6.3a and 6.3b). On the contrary, Hp mass is 19 kDa in the AT_2 ·Hp complex (2:1) indicating that two AT molecules are able

to bind to long Hp chains, which are approximately 33-mer (as the average mass of a disaccharide is assigned to 571 Da[10]). Intriguingly, $AT{\cdot}Hp_2$ (1:2) complexes were observed (Figure 6.3c), in which the total mass of bound two Hp chains are in the range of 25 to 30 kDa.

Multiple heparin oligomer binding to AT has also been observed with shorter chains. Figure 6.4 shows ESI mass spectra of AT-dp10 complexes with increasing dp10 concentration from (a) to (c), in which a progressive increase in the dp10 to AT bulk ratio leads to the formation of $AT{\cdot}(dp10)_2$ and $AT{\cdot}(dp10)_3$ complexes. Multiple dp10 bindings were achieved by using more than 25-fold higher concentration of dp10 over AT. On the contrary, $AT{\cdot}(Hp)_2$ complexes were observed when native Hp molar ratio was 1.6-fold excess over AT. This may indicate that the probability of finding the selective AT binding domain is higher with the native Hp chains.

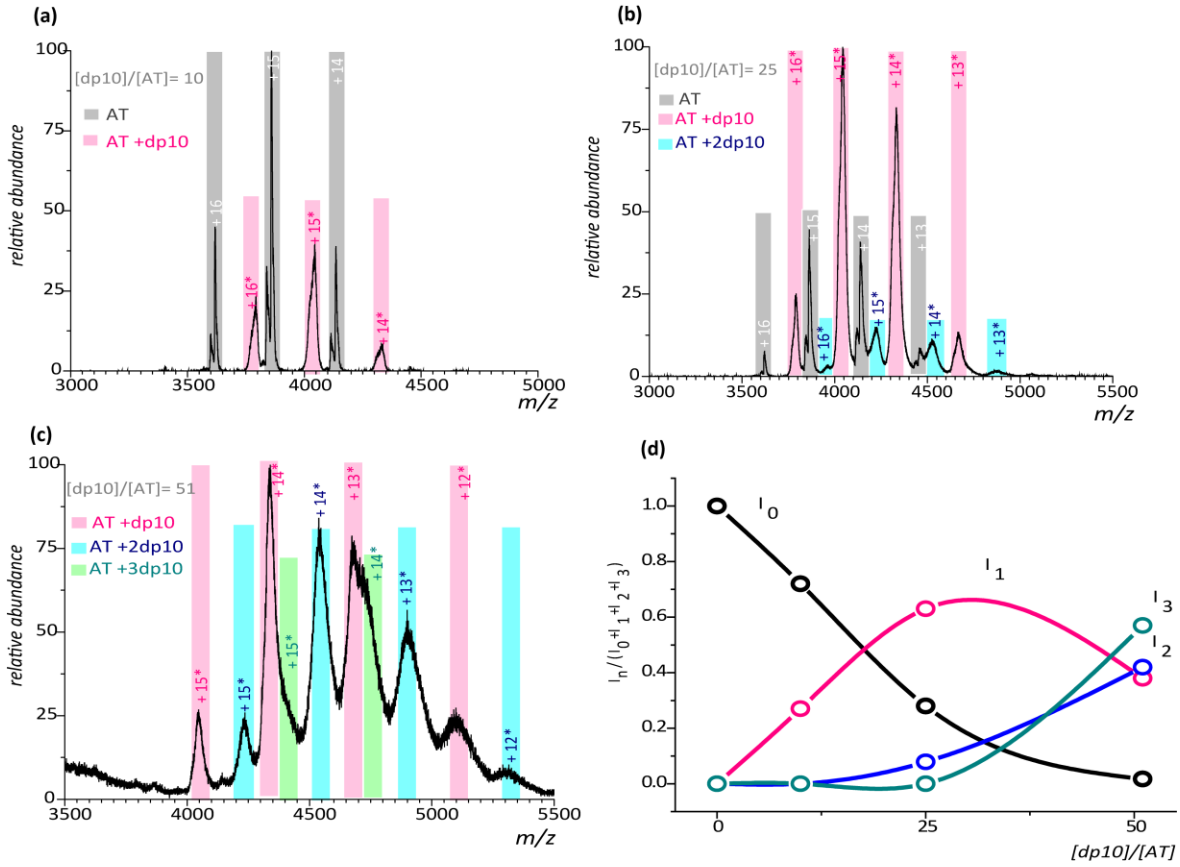

Figure 6.4: ESI mass spectra of AT (~1 µM) and dp10 with dp10/AT mixing ratio (a) 10, (b) 25 and (c) 50 at 150mM ammonium acetate, pH 6.8. Panel (d) shows the relative abundances of AT· $(dp10)_0$, AT· (dp10), AT· $(dp10)_2$ and AT· $(dp10)_3$ complexes with respect to bulk mixing ratio.

6.4 Conclusions

Unresolved ESI mass spectra of extremely heterogeneous AT and native Hp complexes were successfully analyzed by mass-selecting narrow ionic subpopulations followed by limited charge reduction in the gas phase. The resulting charge state "ladders" were used to calculate the mass of isolated protein ions; thus AT·Hp (1:1),

$AT{\cdot}Hp_2$ (1:2) and $AT_2{\cdot}Hp$ (2:1) stoichiometric complexes were detected. Relatively shorter heparin chains were involved in 1:1 and 1:2 complexes, whereas longer Hp chains were able to induce 2:1 complex formation. This study indicated that the limited charge reduction method, complementary to native ESI MS, can be effectively used to obtain structural information from highly heterogeneous complexes of biopolymers.

CHAPTER 7

INHIBITION OF ANTITHROMBIN AND BOVINE SERUM ALBUMIN NATIVE STATE AGGREGATION BY HEPARIN

Minsky, B. B.; Zheng, B.; Dubin, L. P., Inhibition of antithrombin and bovine serum albumin native state aggregation by heparin. *Langmuir* **2013**

7.1 Abstract

Protein native state aggregation, a major problem in pharmaceutical and biological processes, has been addressed pharmacologically by the addition of protein-binding excipients. Heparin (Hp), a highly sulfated polysaccharide, interacts with numerous proteins with moderate to high affinity, but reports about its effect on protein aggregation are contradictory. We studied the pH dependence of the aggregation of antithrombin (AT) and bovine serum albumin (BSA) in the presence and absence of heparin. High-precision turbidimetry showed strong aggregation for both AT and BSA in I = 10 mM NaCl, conditions at which electrostatically-driven Hp binding and aggregation both occur, with more obvious aggregation of heparin-free AT appearing as larger aggregate size. Aggregation of AT was dramatically inhibited at Hp: protein 6:1 (mole ratio); however, the effect at 0.5:1 Hp: protein was greater for BSA. Frontal analysis capillary electrophoresis showed a much larger equilibrium association constant K_{obs} between Hp and AT, in accord with the onset of Hp binding at a higher pH; both effects are explained by the higher charge density of the positive domain for AT as revealed by modeling with DelPhi. The corresponding modeling images showed that these domains persist at high salt only for AT, consistent with the 160-fold drop in K_{obs} at

100 mM salt for BSA-Hp binding. The smaller inhibition effect for AT arises from the tendency of its uncomplexed monomer to form larger aggregates more rapidly, but the stronger binding of Hp to AT does not facilitate Hp-induced aggregate dissolution which occurs more readily for BSA. This can be attributed to the higher density of AT aggregates evidenced by higher fractal dimensions. Differences between inhibition and reversal by Hp arise because the former may depend on the stage at which Hp enters the aggregation process and the latter on aggregate size and morphology.

7.2 Introduction

The effect of heparin (Hp) on protein aggregation would appear from the literature to comprise both promotion and inhibition. These conflicting results could reflect the problem of comparing different proteins with different levels of Hp affinity and different aggregation mechanisms, both dependent on solution pH and ionic strength. Native state aggregation could facilitate the study and interpretation of Hp effects, because protein surface is better conserved and formation of unfolded states minimized**.** Native state protein aggregation is driven by electrostatics, and the protein surface charge anisotropy regulates protein self-association mechanisms. Electrostatics also controls Hp-protein binding to understand its effects on aggregation. There is a need to explain the possible linkage between electrostatically driven native state aggregation and Hp-protein binding. It is of interest to establish whether this relation holds for "heparin-binding" proteins which exhibit different Hp-affinities, such as antithrombin (AT) and bovine serum albumin (BSA). Therefore, we studied the native state aggregation of AT and BSA and the roles of Hp in both aggregation and disaggregation processes, using ionic strength

(*I*) and pH as a probe to investigate protein self-association mechanisms and Hp binding affinities.

The detection of GAGs in deposits of fibrillar aggregates in amyloid diseases initiated a number of conflicting hypotheses about the promotion/inhibition of the aggregation of amyloid forming peptides and proteins in the presence of GAGs. The enhancement of gelosin aggregation by heparin (Hp) was correlated with its sulfate content and MW.[188] Both Hp and CS (chondroitin sulfate) appeared to promote Aβ peptide aggregation.[189] On the other hand, while p25-α aggregated in the presence of stoichiometric amounts of low MW Hp (10-14 monosaccharides), excess Hp diminished its aggregation.[190] Hp induces aggregation/ fibril formation of some proteins under certain conditions, but may have more ambiguous or even benign effects, depending on conditions, as observed for the prion protein.[191,192] Injection of low molecular weight heparin suppresses AA amyloid deposition in mice[193] , and even when fibrils are promoted by Hp are less toxic than the earlier forms of aggregates.[189,194-196] Finally, inhibition of Aβ aggregation is reported for GAG-mimetic sulfated glycopolymers.[197]

These conflicting reports of Hp effects on amyloidogenesis may arise because the point at which Hp enters the aggregation process can vary and is often not well defined. This suggests that effects of Hp could be better understood with systematic studies with folded proteins that include elucidation of self-aggregation mechanisms and identification of the aggregation stage influenced by Hp. The self-aggregation of folded proteins is mostly studied under "accelerated" conditions, such as high temperature[198] and low pH;[199-202] however these conditions generally lead, either intentionally or fortuitously, to formation of intermediate states of the native structure, and the contribution of these

states to the aggregation processes could be difficult to evaluate.[203] The two proteins chosen for study here, AT and BSA, are examples of this; as both of them are commonly studied at elevated temperatures.[204-208] In contrast, the influence of Hp on native state aggregation can be more amenable to modeling;[209] therefore consistent with general rules; because the hydrated protein surface is retained, and formation of intermediate states can be minimized. The charge distribution on this surface, which plays a central role in inter-protein interactions,[124,133] is controlled by protein structure and pH.

Although native state protein aggregation is most readily seen at pH ~ pI ("isolectric precipitation"), its suppression by added salt indicates the primacy of electrostatic attraction.[210] The central role of inter-protein surface interactions makes such aggregation amenable to colloid models, in which the aggregation kinetics could determine the aggregate structure. Aggregation follows formation of clusters from monomers, and growth could follow particle-cluster or cluster-cluster, and formation of these could be limited by diffusion.[211] As shown in previous work, [22,25] protein charge anisotropy dictates the balance of attractive and repulsive electrostatic interactions that leads to one or more of the preceding aggregation mechanisms, which then control aggregate structure. The charge anisotropy of proteins also controls their interactions with Hp,[31] and this suggests an implicit linkage between heparin-suppression and electrostatic aggregation.[209,210] For example, Hp inhibits native state aggregation of BSA and BLG, with the inhibitory effect depending on charge-induced Hp-protein binding affinity.[209] Beyond affinity, the stage at which Hp enters the aggregation process plays an important role: inhibition of the aggregation of native state insulin seems to be enhanced when Hp is added after aggregation has begun.[210] The availability of Hp-binding domains is

evidently subject to alterations in protein conformation.[212] In the present work, we avoid contributions of protein unfolding by selection of conditions and proteins by on two stable proteins, AT and BSA.

Heparin-protein binding affinity arises principally from polyelectrolyte-protein electrostatic interactions,[44,45] for which different models have been widely applied. One model, inspired by theories for the salt dependence of oligolysine-DNA interactions,[46,47] has also been applied to DNA-protein binding. The linear dependence of log K_{obs} (equilibrium association constant) on log I (ionic strength) is consistent with a purely entropic ΔG_{obs} which arises from the release of DNA counterions. However, directly replacing oligolysines with proteins fails to consider the influence of protein charge anisotropy.[48] Nevertheless, extension of this treatment to Hp-protein binding yields a physically realistic value of Hp structural charge density deduced from measured $d\log K_{obs} / d\log I$.[49] On the other hand, many polyelectrolyte-protein systems show clearly different salt dependence, more consistent with Debye-Hückel screening.[44,50] This model takes into account protein charge anisotropy, and effectively explains for the non-monotonic salt dependence seen when polyelectrolytes (e.g., heparin) bind to proteins with net charge of the same (i.e. negative) sign, through a domain of opposite (i.e. positive) charge. This domain is best identified through representation of protein charge calculations.[51] Therefore, it is possible to account for the observed salt dependence of protein-Hp binding by using specific models of heparin binding along with quantitative protein visualization.[28,51]

The way in which Hp inhibits protein aggregation depends on Hp-protein binding affinity, and the stage at which Hp enters the aggregation process. The ability of Hp to

reverse aggregation depends also on aggregate structure. Resolution among these effects has not been achieved because variables such as pH and ionic strength influence both the mechanism and rate of aggregation, and the interaction of Hp with either aggregates or free proteins. Protein charge anisotropy could in fact enhance both inter-protein and Hp-protein interactions. Systematic studies of pH and ionic strength effects on appropriately selected aggregating and heparin-binding proteins are needed to elucidate these primarily electrostatic effects. Also, further insight into the effect of heparin on protein solubility could help guide the extensive but largely empirical use of polyelectrolyte precipitation for protein purification.[213-215]

In order to elucidate the way in which the anti-aggregation effect of Hp is influenced by protein self-association and Hp affinity, we examine two Hp-binding proteins, Hp-cognate AT and non-cognate BSA. The literature clearly indicates larger rates of aggregation for AT than for BSA,[205] although perspectives on their mechanisms of aggregation differ.[205,216] In our work, native states have been preserved; therefore the behavior of the proteins is determined by its (hydrated) surface For this reason, general rules about aggregation (e.g. "isoelectric precipitation") can be put forward, in contrast to unfolding aggregation in which any or all residues may contribute to a wide variety of interactions involving many intermediates. We used high-precision turbidimetry to assess both aggregation rates and Hp-affinity, and dynamic light scattering (DLS) to determine the size and the relative intensity of the aggregates as a function of pH and ionic strength. The fractal dimensions of the respective aggregates were measured by static light scattering. Electrostatic protein modeling was used to visualize domains of positive charge and to rationalize both aggregation and Hp-binding.

7.3 Experimental

7.3.1 Materials

Human recombinant AT (ATyrn, 58 kDa, pI ~ 5.0) was generously donated by GTC Biotherapeutics (Framingham, MA). Bovine Serum Albumin (BSA, 66 kDa, pI ~ 4.9) and Heparin (Hp), with nominal MW 14 kDa, were purchased from Calbiochem and Sigma, respectively.

7.3.2 Methods

7.3.2.1 Turbidimetry

High-precision turbidimetry was performed using a Brinkman PC800 digital display probe colorimeter equipped with a 1cm path length probe (at 420 nm), integrated into a system of our own design which is programmed for (1) automated constant delivery of selected titrant volume via a 2 mL Gilmont microburette at selected rates of addition, (2) selection of the number of percent transmittance (% T) and pH readings to be averaged, and (3) choice of the terminal pH. The data were reported as $\tau = 100 - \%T$, which is unitless and linear with the turbidity over a certain range of transmittance. AT (0.25 g/L, 10 mL total volume) and BSA (1g/L, 10 mL total volume) solutions were prepared at desired NaCl concentrations (10-50 mM), filtered (0.22 μm Millipore), and titrated with either 0.1 N HCl or 0.1 N NaOH. AT-Hp and BSA-Hp mixtures were prepared by 1:1 v/v mixing of AT/BSA and Hp stock solutions (0.5 g/L) at a non-interacting pH 8.5 (± 0.2). All measurements were done at ambient temperature. The precision in the volume of titrant added is typically ±2 ppt (0.2 %). The ability to average

multiple readings leads to transmittance measurement with a precision of 0.1 %T (±1 ppt).

7.3.2.2 Dynamic Light Scattering (DLS)

DLS measurements were made after filtration (Millipore 0.22 μm) using a Malvern Instruments Zetasizer Nanosystem ZS, operating at 173º scattering angle with a 633 nm He−Ne laser, at 25 °C. The measurement duration was 10-12 s. The distributions of the mean apparent translational diffusion coefficients (D_T) were determined by fitting the DLS autocorrelation functions using nonnegative constrained least-squares (NNLS). The distribution of apparent hydrodynamic diameters D_h was obtained from the distribution of mean apparent translational diffusion coefficients (D_T) via

$$D_h = \frac{2kT}{6\pi\eta D_T} \qquad \textbf{Eq. 7.1}$$

where *k* is the Boltzmann constant and η is the solvent viscosity, taken as that of water. Sample transfer and automated optimization steps result in a delay of 2−3 min. between initial pH adjustment and the first measurement.

7.3.2.3 Static Light Scattering (SLS)

SLS experiments were performed using a BI-200 SM goniometer and BIC-2030D photon counting system (Brookhaven Instruments Inc.) with an Omnichrome Ar ion laser (100 mW, λ = 488 nm) at ambient temperature, 25 °C. The scattering intensity was measured as a function of scattering angle between 45 and 130°. Fractal dimensions (D_f)

were extracted from angle dependence in the high-q limit via linearization of the scattering data using the relation:

$$I(q) \propto q^{-Df} \qquad \textbf{Eq. 7.2}$$

where I(q) is the scattering intensity and the scattering vector q = $(4\pi n/\lambda)$ sin $(\theta/2)$, with *n* the refractive index of the fluid, λ the wavelength, and θ the scattering angle. The radius of gyration (R_g) was obtained using Guinier relation at relatively low-q region:

$$\ln(I(q) = \ln(I(0) - \frac{q^2 R_g^2}{3} \qquad \textbf{Eq. 7.3}$$

7.3.2.4 Computational Methods

DelPhi V. 4r1.1[130,131] was used to model the electrostatic potential around the protein as a function of ionic strength. PDB id is 3V03 and 2B4X were taken from protein data bank (http://www.rcsb.org/) for BSA monomer and AT monomer, respectively. The charges of amino acids on the proteins were determined using the spherical-smeared charged model put forward by Tanford.[132]

7.4 Results

7.4.1 Protein aggregation: effects of pH

7.4.1.1 AT shows higher turbidimetric rates of aggregation

Figure 1 shows the increase in 100 - %T in the range 4 < pH < 7 upon addition of acid to 1 g/L BSA in 10 mM NaCl. A reduced concentration of 0.25 g/L was used for the more rapidly aggregating AT in order to maintain 100 - %T < 20. In this range 100 - %T is linear with the true turbidity τ = - log T, and can be most readily identified with the

accumulation of soluble aggregates.[217,218] The pH for the onset of aggregation is qualitatively seen to be about 1 pH unit above pI for AT, in contrast to BSA for which pI-pH = 0.5. Since protein concentrations are not the same, the difference in absolute values of τ is handled by comparing the turbidimetric rates of aggregation $(d\tau/dt)_{pH}$. This is calculated as $(d\tau/dpH)\,(dpH/dt)$, where $(d\tau/dpH)$ is obtained from Figure 1, and dpH/dt is automatically recorded at every pH. In the resultant plot (inset of Figure 1), $(d\tau/dt)_{pH} = 0$ would correspond to a maximum. This indicates equal turbidimetric rates of aggregation and disaggregation.[218,219] The maximum rate of aggregation $(d\tau/dt)_{pH}^{max}$ is seen at pH 6 and 5.5 for AT and BSA, respectively. For BSA, the native state is preserved over a wide range of pH encompassing the experimental conditions here.[220-222] For AT, there are additional suggestions of partial unfolding,[223] but not at pH~6 as used here. Those studies refer to the dynamics of loop expulsion, presumably at a time scale that is not relevant to our measurements of relatively slow aggregation.

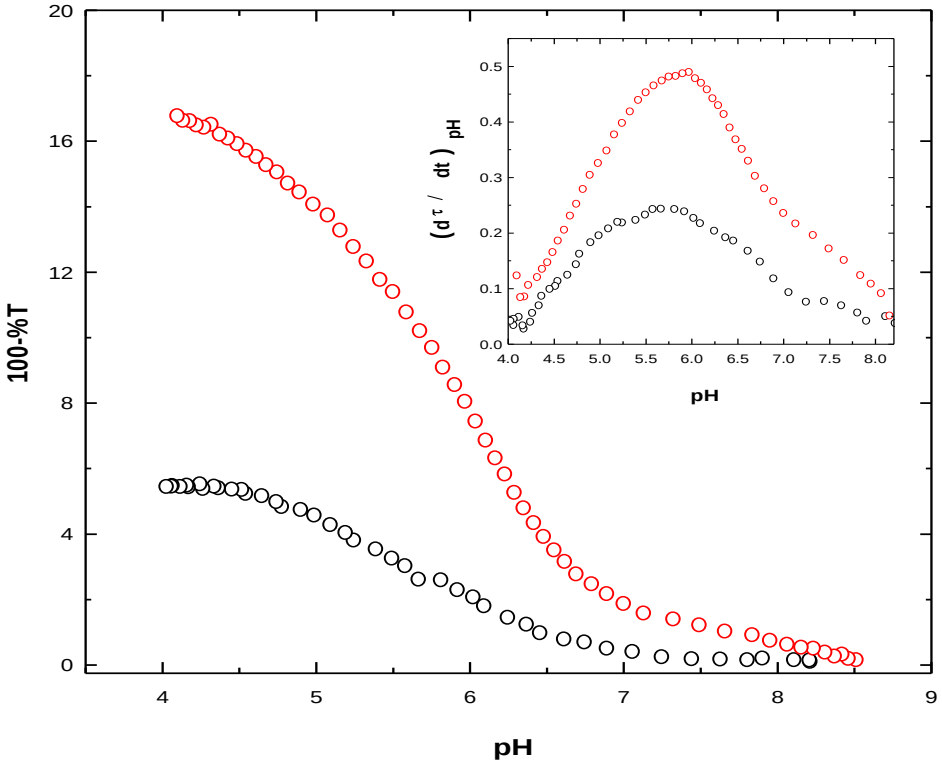

Figure 7.1: Automated turbidimetric titrations of 0.25 g/L AT (red) and 1 g/L BSA (black) in 10 mM NaCl with the addition of 0.1 N HCl. Inset: Aggregation rate (dτ/dt) vs pH obtained from Figure 1 for AT (red) and BSA (black).

7.4.1.2 Time dependence of AT and BSA aggregation can reveal aggregation mechanisms

Figure 7.2 shows time dependent turbidities for AT and BSA under concentration, ionic strength and pH conditions in the vicinity $(d\tau/dt)_{pH}^{max}$ in Figure 7.1. Since c_{AT} / c_{BSA} = 0.25, we focus on mechanistic differences, which are independent of protein concentration. In Figure 7.2, the turbidity reaches a limiting value for AT and BSA at similar times, with a larger limiting value for the former. The turbidity of AT increases rapidly for t < 1.5 min (Figure 7.2 , inset (a)), while the curve for BSA exhibits only a

small decrease in curvature at t = 25 min. Figure 7.2 inset (b) compares the aggregation kinetics of AT and BSA using first-order plots obtained from the data in Figure 7.2. The analysis of turbidity data in this way can be described as:[224,225]

$$\tau = \tau_{\infty}(1 - e^{-kt}) \qquad \textbf{Eq. 7.4}$$

where τ_{∞} is the limiting turbidity value at $t = \infty$ and k is the apparent rate constant.

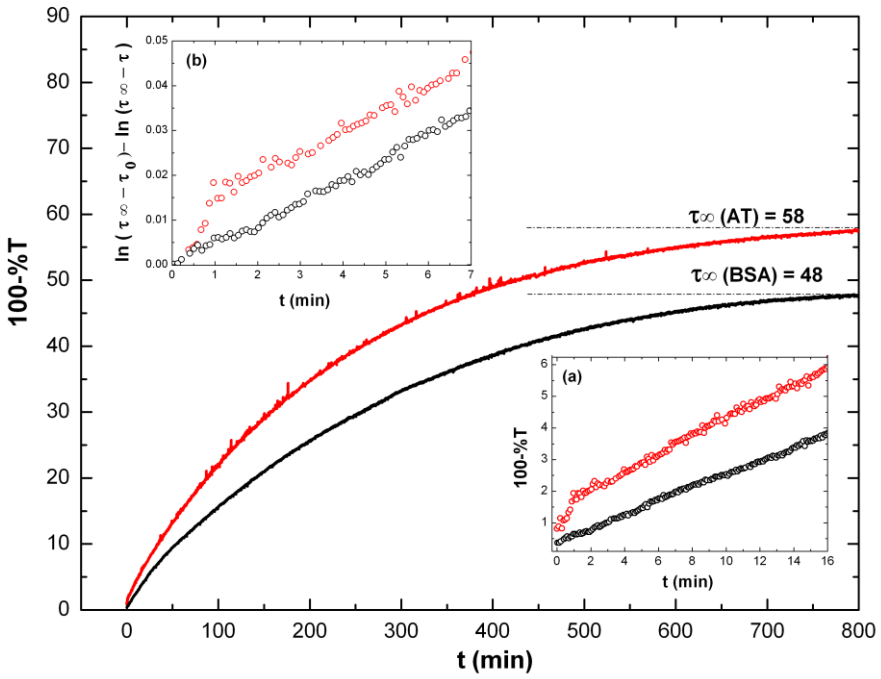

Figure 7.2: Turbidimetric measurements in 10 mM NaCl for the time dependent aggregation of 0.25 g/L AT at pH 6.1 (red) and 1 g/L BSA at pH 5.4 (black). Samples were prepared at high pH (~ 8.5) and then brought to the desired pH within 3 min. using 0.1 N HCl. Inset (a): Expanded time scale for the first 16 min. Inset (b): First order fit for the time vs τ (100-%T) in for AT (red) and BSA (black) in the first 7 min.

The first order appearance of the aggregation kinetics may indicate the mechanisms of aggregation for both proteins (*vide infra*). The evolution of aggregates was also probed with DLS (Figure 7.3) in the absence and presence of Hp (the latter will

be explained below). Contrary to turbidimetry, DLS cannot capture the first 2 min. due to the time lag between the sample pH adjustment and measurement, but provides a better molecular view, as seen in Figure 7.3 (a), in which $c_{AT} = c_{BSA} = 1$ g/L. The experimental lag time, notwithstanding the rapid increase in turbidity for AT can be related to the increase in cluster size, from < 100 nm to 300 nm during the first 15 min. Two differences appear in Figure 7.3 (b) for BSA: the fast mode broadens as opposed to losing intensity; and the slow mode size increases by only a factor of 2.5, from 25 nm to 65 nm. The larger apparent initial rate from turbidity for AT appears to be due to rapid increase in aggregate size (Figure 7.3(a)) at the end of which the fast mode (monomer) no longer dominates the scattering intensity (data not shown).

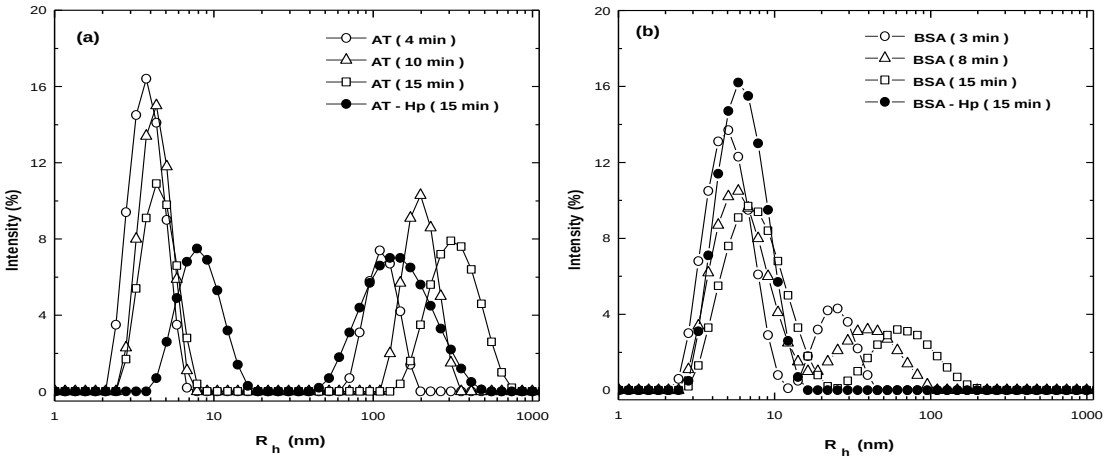

Figure 7.3: Time dependence of particle sizes by DLS in 10 mM NaCl in the absence and presence of Hp: (a) 1 g/L AT and 1 g/L AT with 0.1 g/L Hp (●) at pH 6.2 (b) 1 g/L BSA and 1 g/L BSA with 0.1 g/l Hp (●) at 5.4

7.4.2 Effect of heparin on protein aggregation

7.4.2.1 Heparin suppresses aggregation of both proteins

Figure 7.4 shows inhibition of AT and BSA aggregation in the presence of Hp at various Hp:protein (*r*) ratios. The inhibition of aggregation by Hp can be observed only in the "pH window" bounded by formation of the heparin-protein complexes. At $r = 0.1$, the stoichiometry best suited for comparison of BSA and AT, the suppression of the aggregation is more pronounced for BSA. This is confirmed by DLS results (Figure 7.3), in which data in the absence of Hp are combined with results in the presence of Hp approximately 15 min. after pH adjustment (this time lag leads to a small increase in R_h for the slow mode for AT alone, and to an increase in fast mode R_h for BSA alone). Here, we see that the fast mode intensity of the free monomer (or in the case of BSA, monomer-dimer) never exceeds 50 % for AT, but the fast mode is always the dominant scatterer for BSA. A separate but related effect is the concentration of monomer or monomer/dimer in the presence of Hp, obviously dependent on both the Hp-protein binding affinity, and the Hp:protein ratio *r*. At $r = 0.1$, the doubling of the apparent size corresponding to the fast mode for AT can only be explained by the conversion of AT monomer to its complex with Hp. In contrast, the fast mode for BSA at $r = 0.1$ consistently exhibits an apparent size equal to that of the BSA dimer, regardless of time; BSA-Hp complexes and possibly BSA dimers coexist at that condition.

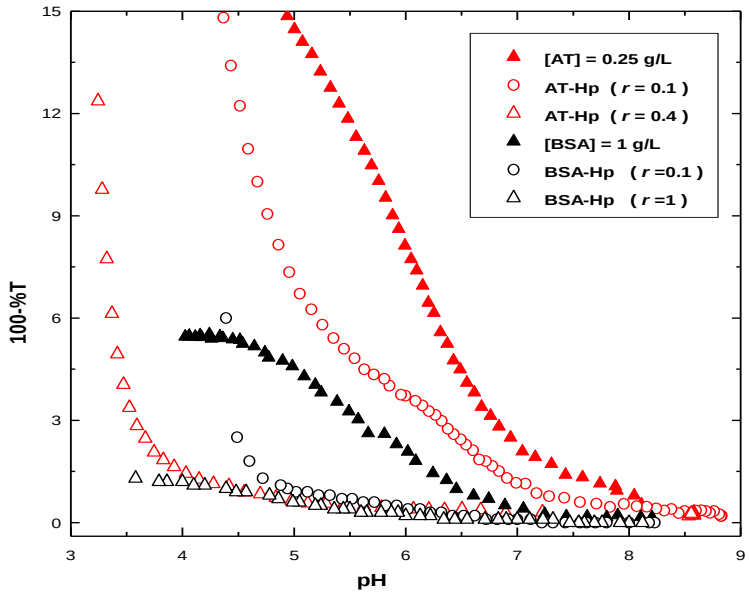

Figure 7.4: Inhibition of 0.25 g/L AT and 1 g/L BSA aggregation by heparin at 10 mM NaCl. Heparin to AT weight ratio is *(r)* is 0.1 and 0.4 and heparin to BSA weight ratio *(r)* is 0.1 and 1.

7.4.2.2 AT-Hp binding less sensitive to salt

In order to evaluate the AT-BSA binding strength, we investigated the effect of salt concentration on the onset of Hp-protein complex formation (Figure 7.5). This event, pH_c experimentally defined by a transition from a region of zero slope, reflects a reversible, equilibrium phenomenon as opposed to the purely or partially kinetic behavior described in all earlier Figures. This critical pH qualitatively represents the condition at which the energy of complex formation just exceeds thermal energy, *kT*. When pH_c appears on the "wrong side of pI" (here when global protein charge is negative), (pH_c – pI) ≡ δpH becomes a qualitative measure of the ability of binding to overcome this global repulsion. Although AT and BSA have similar pI values (4.9 and 5.0), δpH is larger for

AT at all ionic strengths. Addition of salt lowers δ for both AT and BSA, but the effect is more pronounced for BSA.

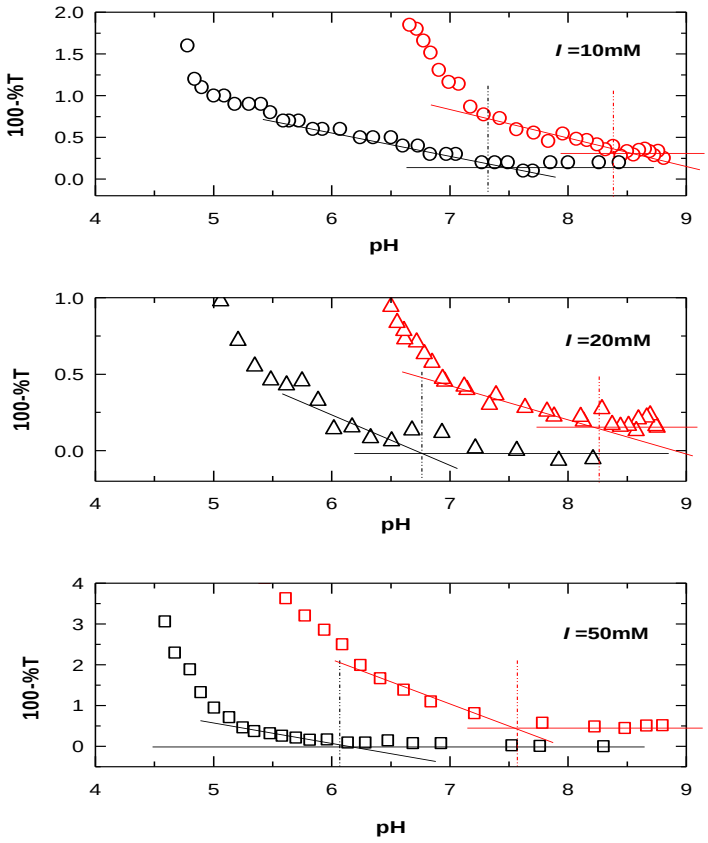

Figure 7.5: Turbidimetric titrations of AT (red), BSA (black) (0.25 g/L) and Hp (0.025 g/L) at 10, 20, 50 mM NaCl, using 0.1 N HCl. Red and black broken lines were used to indicate the pH_c values for AT and BSA, respectively.

7.4.2.3 Hp cannot reverse AT aggregation, but can partially reverse BSA aggregation

The inhibition of AT and BSA aggregation in the presence of Hp is a result of soluble complex formation between protein and Hp. Hp may also interact with the larger aggregates dissolving them into small intra-polymer complexes[209,210] and in some cases

larger inter-polymer soluble species. Figure 7.6 shows the results for AT and BSA upon addition of Hp to a protein:Hp ratio r = 1 (w:w). The addition of Hp partially re-dissolves BSA aggregates (at pH 5.3) but does not reverse the aggregation of AT (at pH ~ 6.1).

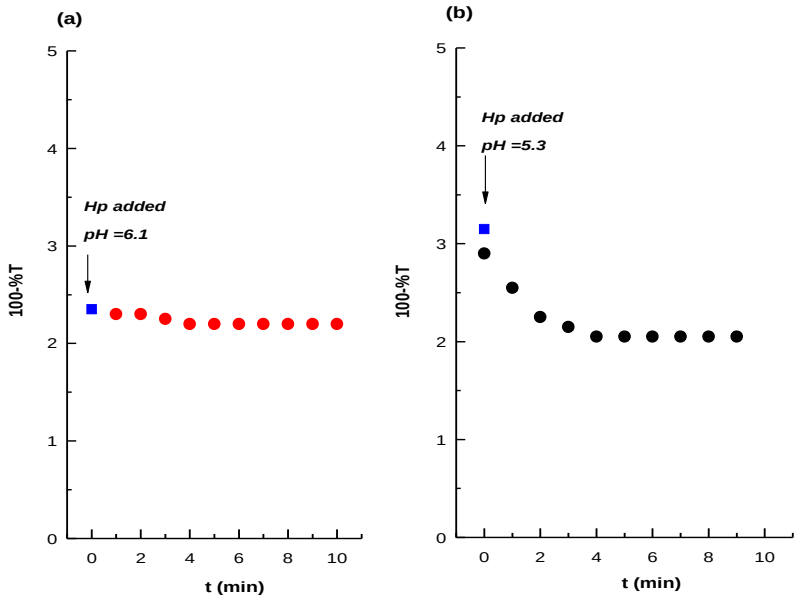

Figure 7.6: Reversal of aggregation in 10 mM NaCl (a) 0.1 g/L AT and (b) 1 g/L BSA by the addition of Hp (r = 1). Both protein solutions were prepared at pH 8.5 and pH was adjusted to 6.1 for AT and 5.3 for BSA within 3 min. using 0.1 N HCl. Solutions were kept for 20 min. at room temperature prior to Hp addition.

7.5 Discussion

7.5.1 AT and BSA aggregation mechanisms are different

The result for AT in the Figure 7.2, inset (b), which shows the first order fit of turbidity vs time, is in agreement with nucleation (rapid initial consumption of monomer to form well-defined clusters) and growth (addition of monomer to these clusters), the

first step difficult to observe for BSA. The initial AT cluster size could not be identified because of the time lag for DLS which can only identify after 4 min. a 100 nm species for AT (Figure 7.3 (a)), and a 25 nm species for BSA (Figure 7.3 (b)). In the first 15 min., the rate of depletion of the AT monomer is slightly faster than that of monomer/dimer (BSA). There are two possible routes for the increase in turbidity over long times: clusters either grow by association ("cluster - cluster"), or by adding monomer/dimer ("growth").[224] The first-order appearance of the curves in Figure 7.2, inset (b) for both proteins suggests that aggregates grow by the latter route. The transition from fast to slow steps, seen after 2 min. for the aggregation of AT, resembles that of BLG at pH near pI and in low salt. This protein also exhibits diffusion limited particle-cluster aggregation as a second step.[219]

A notable difference between AT and BSA aggregation is seen in the evolution of the fast mode in Figure 7.3 (b) for BSA, which in contrast to AT, broadens and shifts to larger R_h with time. While R_h confirms to the AT monomer radius (4 nm) at all times, R_h increases from 5 to 8 nm for BSA in the interval 3-14 min., accompanied by peak broadening. We interpret these results as depletion of BSA monomer from the monomer-dimer pool, with the concentration of monomer then determining the rate of cluster growth, as opposed to cluster-cluster association. For AT, all un-aggregated protein is present as the 4 nm monomer, and cluster growth is more rapid.

The absence of cluster-cluster association for both proteins can be explained by their net charge at pH-pI > 0. However, the interaction of negatively charged AT monomer with negatively charged clusters is ameliorated by the charge anisotropy of the AT monomer as depicted in Figure 7.7. This same charge anisotropy also enhances

monomer-monomer association kinetics and thus the rate of nucleation; this accounts for the nucleation step probably present for both proteins, but more readily detected for AT. Therefore, the greater charge anisotropy (see Figure 7.9) enhances the rate of nucleation.[218] The role of charge anisotropy of the BSA monomer is further complicated by its equilibrium with the dimer, as evidenced by the wide range of R_h values seen for its fast mode in Figure 7.3 (b). The increase from 5 to 7.5 nm during the first 10 min. of aggregation can be best explained as the depletion of monomer through its preferential aggregation. In that sense, dissociation of dimer exerts some control over the rate of aggregation.

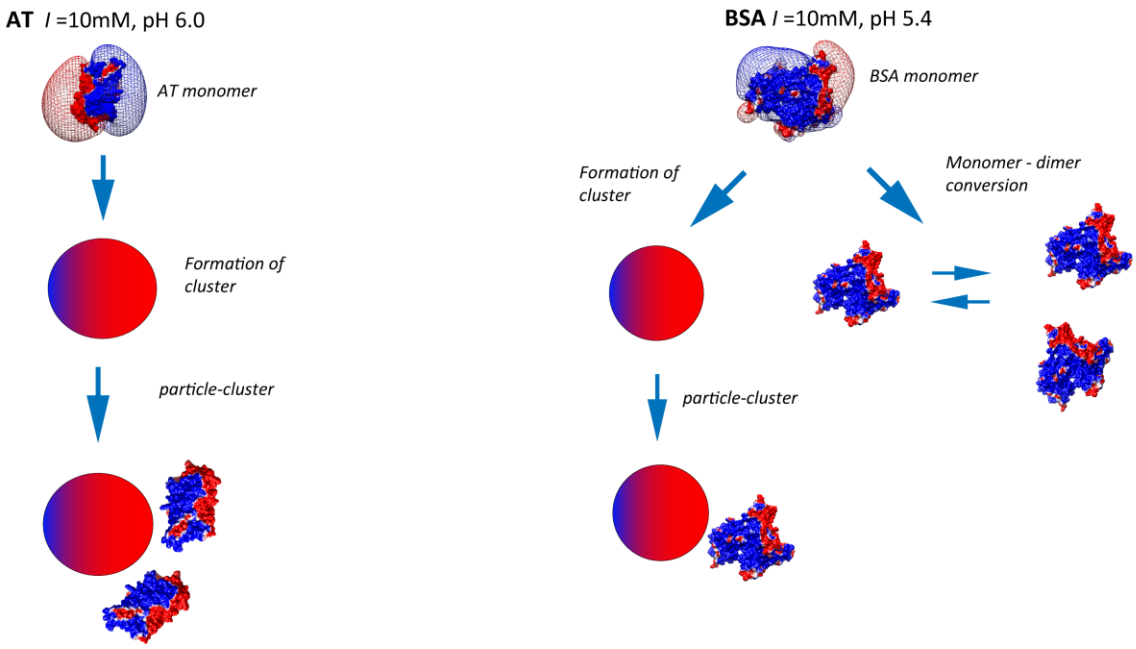

Figure 7.7: Models for the aggregation pathways of AT and BSA.

7.5.2 Inhibition of aggregation is a result of competition between Hp binding and self-aggregation

The magnitude of heparin inhibition is qualitatively assessed by comparison of turbidimetric titrations with and without Hp for the two proteins. As shown in Figure 4, the inhibition effect depends on the heparin concentration (or bulk weight ratio *r*). Together with the protein-Hp binding affinity, this stoichiometry controls the fraction of protein that forms complex, and thereby controls the aggregation rate by modulating the free protein concentration. The assumption is that heparin-protein complexes have no direct influence on aggregation kinetics. At equal $r = 0.1$, the concentration of total protein is 4-fold smaller for AT than for BSA, but the intrinsically rapid aggregation of free AT results in larger turbidity.

Evidence of the depletion of protein monomer upon addition of Hp should emerge from DLS. In Figure 7.3 (a), AT monomer ($R_h = 4$ nm) is well resolved from complex at $R_h = 8.5$ nm, and is seen to be fully converted to a mixture of small and large complexes in the presence of Hp. BSA aggregate clusters vanish in the presence of Hp (Figure 7.3 (b)) but the ca. 8 nm complexes cannot be well resolved from BSA monomer/dimer. BSA monomer/dimer persists in the presence of Hp because of its relatively low Hp affinity; but BSA aggregates fail to form. The effect of Hp on BSA aggregation relative to its weaker effect on AT aggregation, may be related to the differences in aggregate or aggregation mechanism, most notably the presence of an obvious nucleation step for AT. The amount of Hp required for suppression is $r = 0.1$ for BSA and $r = 0.4$ for AT. The larger requirement for AT suppression despite its stronger binding is a reflection of the strong tendency of its monomer to aggregate even at lower concentration. The second

effect of r is the shift of pH_φ to lower pH.[209] This phase separation occurs when complexes achieve charge neutrality. When the ratio of Hp to protein is large, each Hp binds few proteins, and the positive charge per protein needed to overcome Hp charge is large, which corresponds to low pH_φ.

7.5.3 Stronger binding of Hp to AT, notably at high salt, manifested as high values of pHc

We proceed to interpret the results of Figure 5 in terms of binding constants for Hp-BSA and Hp-AT measured elsewhere. The ionic strength dependence of pH_c shown in Figure 7.8 (a) provides a qualitative comparison of Hp affinity for AT vs BSA: the expanded domain of complexation seen for AT indicates its stronger heparin binding. Corresponding measurements by FACCE[28,51] verifies this more quantitatively, and both measurements show that the difference in Hp affinity between AT and BSA strongly increases with added salt (Figure 7.8 (b)). Interestingly, the frequently noted linear log-log dependence of Hp-protein binding[17] is seen to apply only at $I > 10$ mM for BSA and 25 mM for AT.

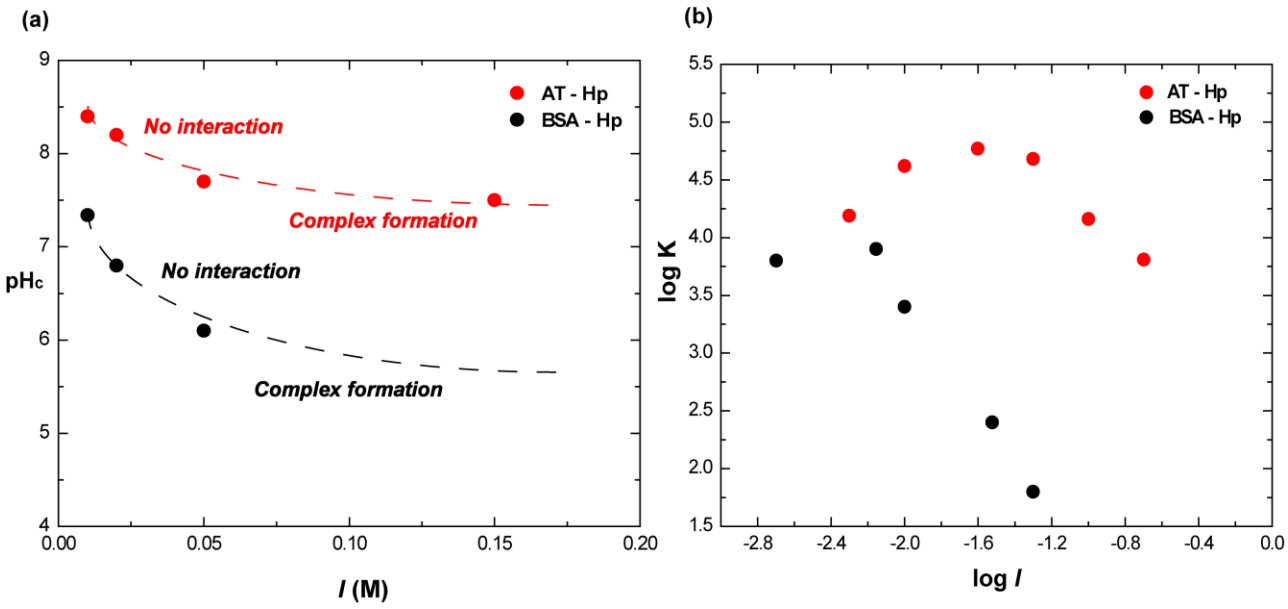

Figure 7.8: (a) Ionic strength dependence of pH_c obtained from turbidimetry (from Figure 7.5). The dashed lines are drawn to guide the eye. (b) Ionic strength dependence of the binding constant obtained by FACCE. The data for BSA and AT from ref. 51 and ref. 28.

The differences between BSA and AT in Figure 7.8 can now be explained by the charge distributions of the two proteins as represented by DelPhi images (Figure 7.9). The maximum in the plot for AT has been interpreted in terms of combined attractive and repulsive forces,[28] which should be more important for AT because of its charge anisotropy. The more pronounced positive domain for AT leads to the formation of an AT-Hp complex that is more salt resistant than the BSA-Hp complex. This is also reflected in the persistence at high salt of the positive (Hp-binding) electrostatic domain of AT, and the virtual disappearance of this domain for BSA at 100 mM salt, entirely consistent with the drop in log K at log I = -1 for BSA in Figure 7.8 (b).

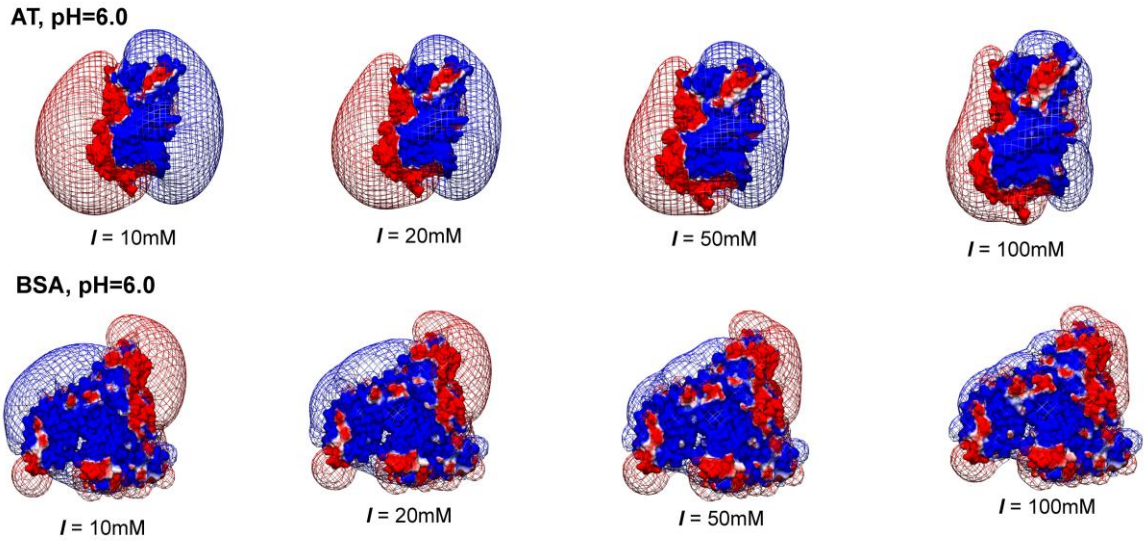

Figure 7.9: Ionic strength dependence of the electrostatic potential contours at - 0.5 kT/e (red) and 0.5 kT/e (blue) for AT and BSA at pH 6.0.

7.5.4 Aggregate fractal dimensions larger for AT than for BSA

The greater charge anisotropy for AT vs. BSA is not only consistent with its stronger Hp binding, but may also explain the inability of Hp to reverse AT aggregation as shown in Figure 7.6. This apparently contradictory relation, the resistance to Hp-induced dissolution is greater for the protein with higher Hp affinity, can be understood in terms of aggregate formation and density. Recent Monte Carlo simulations have contrasted the aggregation behavior of uniformly and non-uniformly charged colloids, in which the latter interact more strongly and form larger clusters.[226] While both proteins here exhibit charge anisotropy, AT more nearly resembles the extreme case of non-uniform charge with correspondingly strong short-range attraction. This is expected to lead to a densely packed aggregate, resistant to dissolution. The binding of Hp as an inhibitor of aggregation can be considered energetically in terms of the equilibrium

between complex and free protein, reducing its concentration and thus lowering the rate of aggregation. The stabilization of the former might be considered to arise from multiple interactions of the flexible Hp chain with the protein. Similar considerations have been referred to as "multivalency", but this does not reflect the role of polyelectrolyte chain dynamics. Aggregate *dissolution* follows a different path involving Hp diffusion onto and into aggregates, and a variety of subsequent kinetically controlled steps which cannot be readily identified by the current methods. The structure of the aggregate may play a role at least as significant as the intrinsic protein-Hp molecular affinity discussed above.

To support this latter hypothesis, fractal dimensions of AT aggregates were determined by static light scattering (Figure 7.10) and compared to published results for BSA. The difference between D_f (AT) = 2.3 ± 0.1 (Figure 7.10 (c)) and 1.7 (BSA)[227] supports the argument that the greater density for AT aggregates makes them impervious to dissolution by Hp. However, when Hp is initially present with AT at pH 8 and r = 0.1 (prior to adjustment to pH 6.1) similar SLS measurements lead to D_f (AT-Hp) = 0.8 ± 0.1, consistent with a highly extended rod-like chain. Since AT is net-negative at this pH, both steric and electrostatic effects lead to intra-polymer repulsion in the Hp-AT complex and consequent chain stiffness. To our knowledge, this is the first reported measurement of the fractal dimension of an Hp-protein complex. Nominally, the values of R_g / R_h are 0.8 and 0.9 for aggregated AT and AT-Hp complex, respectively from the Guinier plot shown in Figure 7.10 (b). The former, very close to the limiting value for spheres, is consistent with the large value of D_f, but the latter is not consistent with the extended conformation deduced from D_f = 0.8. These ratios must be considered in the light of the averaging of signals from large and small scatterers for both systems, unavoidable for

SANS and arbitrary for DLS. These averages tend to be weighted more toward the smaller species in Malvern due to backscattering. More accurate results will require angle dependence of diffusion coefficients complementary to Figure 7.10 (a).

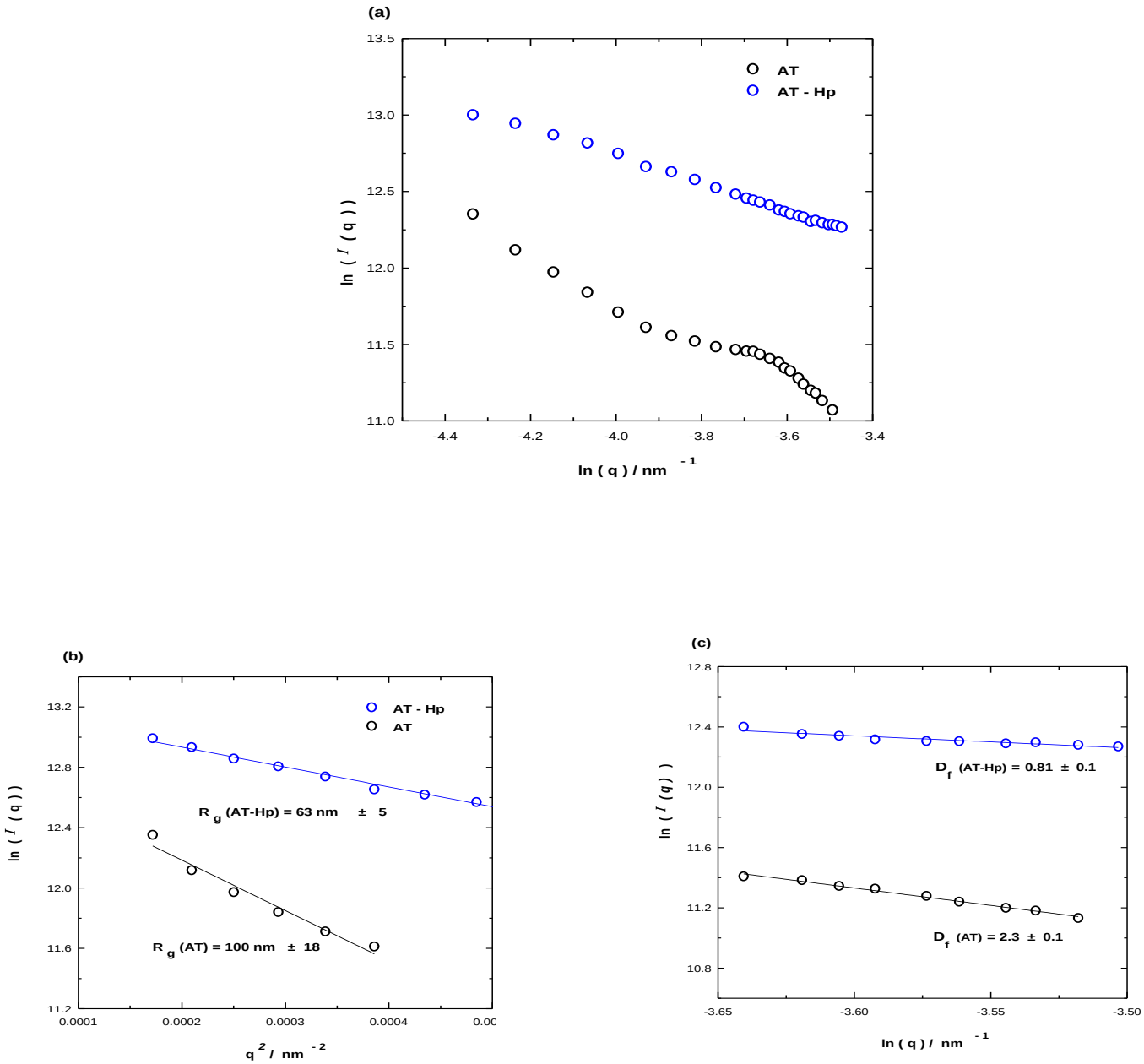

Figure 7.10: SLS of 1 g/L AT and 1 g/L AT and 0.1 g/L Hp (*r* = 0.1) in 10 mM NaCl, pH = 6.2 (a) Scattering intensity (*I*) as a function of scattering vector (q), (b) Guinier plot to determine Rg in the low-q region and (c) High-q region to determine fractal dimensions of AT aggregates and AT-Hp complex.

7.6 Conclusions

Heparin (Hp) inhibits and reverses aggregation more completely for BSA than for antithrombin (AT). Since heparin binds more strongly to AT, this difference is not due to the conversion of protein monomer/dimer to non-aggregating complex, which would be greater for Hp. The reduced effects of heparin for AT occur because the relatively low concentration of uncomplexed AT monomer aggregates far more extensively than the more abundant BSA monomer/dimer. The values of pH at which complexes are first observed at different ionic strengths, relative to pI a measure of the ability of binding to overcome repulsion between heparin and global protein charge -- is in good qualitative agreement with measurements of binding constants by FACCE. These two measures of protein-heparin affinity are shown to be consistent with protein charge anisotropy as revealed by electrostatic modeling. In contrast to inhibition, the reversal of protein aggregation by heparin is also influenced by aggregate structure: the low fractal dimensions of BSA aggregates make them more susceptible to dissolution mediated by heparin binding.

ACKNOWLEDGEMENTS

This work was supported by the National Science Foundation (CHE-0619039). B.Z. acknowledges a Bradspies Research Fellowship. We thank Erin Sutherland for the early method development in turbidimetric detection of time dependent aggregation, and GTC Biotherapeutics for providing ATyrn.

CHAPTER 8

CONCLUSIONS AND FUTURE STUDIES

We have investigated the effects of heparin charge density and chain length in protein binding taking into account both polyelectrolyte properties of heparin and electrostatic interactions between heparin and protein. Charge complementarities between the protein surface and heparin were found to play significant roles in the protein recognition process. In addition, conservation of heparin chain dynamics in the bound state lead us to consider a more nuanced "specificity" and "selectivity" of heparin in protein binding, as opposed to the classical "lock" and "key" type interaction, in which heparin is thought to have specific conformation in order to bind to a well defined epitope on the protein surface.

Our studies showed that heparin is subjected to counterion condensation, and the degree of condensation exhibits an inverse relation with chain length, which is due to the diminished condensation at the chain ends. The remarkable success of the simplified model (as presented in Figure 2.6) to establish effective charge calculations for heparin oligomers, in which each sulfate group is treated as the same, could indicate the significance of overall sulfation, rather than precise sulfate locations to define heparin chain properties. Contrary to Hp, HS structure is comprised of well-defined low (NA) and high sulfation (NS) domains; therefore, the junctions could lead to preservation of the high effective charge density of NS domains by inhibiting counterion condensation. This hypothesis could be tested by measuring the elecrophoretic mobility distributions of HS oligomers and compare them with the heparin oligomer mobilities. The preservation of

the HS high effective charge density could be significant in mediating growth factor binding on the cell surface.

The contribution of counterion condensation in heparin/HS-protein interactions, i.e. the significance of effective charges as opposed to structural charges in protein binding, is not well understood. It has been proposed that heparin-protein binding is analogous to DNA-oligolysine interactions, in the sense of being driven by the entropy of expelled counterions. In this case, an increase in the effective charge of the protein-binding domain on HS could amplify the binding constant in comparison to heparin. This hypothesis could be tested by measuring the apparent association constants between FGF (or AT) –HS and Hp oligomers using frontal analysis capillary electrophoresis (FACCE). If the effective charges are the major determinants for protein binding, we will observe higher association constants with HS compared to Hp.

Highly sulfated heparin oligomer chains were able to induce the formation of multimeric complexes of FGF. This observation could demonstrate that these highly sulfated chains might have the optimal binding sites, i.e. properly arranged charged segments, compared to the lower sulfated chains. The sulfation pattern could be determined by isolating bound Hp/HS oligomers using size exclusion chromatography or capillary electrophoresis, and the isolated Hp/HS fractions could be further sub-fractionated using strong anion exchange chromatography. Then, these sub-fractions could be sequenced using ESI MS fragmentation methods such as collision-induced dissociation (CID) or electron detachment dissociation (EDD). Complementary to ESI MS, Monte Carlo simulations can be applied in FGF and heparin oligomer interactions in order to elucidate the structural selectivity of Hp/HS. Monte Carlo simulations could

enable identifying the Hp/HS configurational flexibility at the protein-bound state, and also calculate the binding energies for the high and low affinity Hp/HS oligomers which were identified from the prior ESI MS studies. These concerted efforts of elucidating affinity, structural charge distribution, and the chain dynamics of HS/Hp could provide a better understanding of the selectivity and the plasticity of protein-HS/Hp interactions. The convergence of ESI MS and simulation studies in order to determine HS/Hp binding motif could build confidence to employ longer HS/Hp oligosaccharides in growth factor interactions. The complementarities between protein surface charge and detected HS/Hp binding motifs could be used to predict the relative affinities of various protein-Hp/HS pairs, which could explain how Hp/HS provide binding sites for a multitude of proteins.

The incorporation of well-defined heparin oligomers into biomedical scaffolds is a new approach in tissue engineering. In our model system, heparin decamer (dp10) could bind both tetralysine (K_4) and a growth factor (FGF1). Tetralysine is bound in regions rich in condensed counterions, as opposed to chain ends, and the binding of a single tetralysine, which still leaves "space" for FGF to bind, is significantly weaker than the binding of FGF. An alternative approach, more relevant to tissue engineering applications, would be an examination of longer Hp chains where the ratio of condensed counterions to structural charges would be larger, so that binding of oligopeptide and FGF on the heparin oligomer chain could be more competitive. Cationic biopolymer chitosan is an alternative for oligopeptide as a scaffold material because chitosan has a high degree of biocompatibility andbiodegradability, its chemical structure can be easily modified, and it form complexes with heparin. Heparin-chitosan complexes can be used as a platform for growth factor delivery, and using oligoheparins and oligochitosans, as

opposed to native heparin and high molecular weight chitosan, could provide a better control for growth factor capture and release due to the reduced heterogeneity. The binding of oligoheparin to low-charge density chitosan could be weaker than growth factor-heparin oligomer binding; however the extent to which oligochitosan interferes with growth factor binding should be elucidated. Therefore, the ternary complex formation between heparin oligomers, oligochitosans and growth factors can be investigated using ESI MS at varying ionic strength and pH values.

Monte Carlo simulations could also be used to propose interaction mechanisms for FGF-Hp and AT-FXa - Hp interactions taking into account our ESI MS results. Monte Carlo simulations showed that a small portion of the Hp mimetic interacted with FGF at any time. This result could be used to assess the mechanism of three FGF molecules binding to Hp decamer chain, in which three FGF molecules may be bridged by heparin oligomer with transient interactions. This observation may raise a possibility for their catalytical roles in growth factor binding, which has also suggested in AT interactions with coagulation proteases. Our ESI MS studies indicated that short Hp chains ($dp \leq 10$) promote binary AT·FXa complexes. Shorter Hp chains may transiently bridge the positive domains of AT and FXa, but that the most favorable orientation of AT and FXa may no longer need that bridge. Thus, Monte Carlo simulation could be employed in AT, FXa, and short heparin chain ($dp \leq 10$) binding to probe the dynamics of the polymer and its ability to stabilize AT-FXa complex. This could provide a better understanding of how short heparin chains catalyze the formation of binary complex and at what stage heparin oligomer dissociates from the complex.

The resultant AT-FXa complex has been suggested as covalent, and this covalent nature of can be further investigated either with MS/MS fragmentation methods or by inducing dissociation in solution via acid-induced denaturation. In addition, ESI MS spectrum of AT and FXa in the presence of native heparin showed evidence of higher order complexes; however the complex peaks were not resolved due to extensive heterogeneity. This experiment can be repeated using FTICR MS, and limited charge reduction method can be applied to isolate the complex peaks, and then determine the exact stoichiometry of the AT-FXa complexes.

The complex formation between native heparin and AT was studied using limited charge reduction method on FTICR MS, and 1:1, 2:1 and 1:2 (AT:Hp) complexes were detected. This could show that there are multiple Hp binding sites on one AT, as well as multiple AT binding sites on one Hp. The formation higher order complexes on the heparin chain can be studied by varying the solution mixing ratio between AT and Hp. Complementary to mass spectrometry, small-angle scattering techniques, such as small-angle neutron scattering (SANS) or small angle X-ray scattering (SAXS) can be employed to determine size, shape and structure of the complexes. By this way, the proximity of the bound proteins on the Hp/HS chains can be detected.

AT aggregation has been studied in the absence and in the presence of heparin and the morphology of the AT aggregates and AT-Hp complexes have shown different structural features, as revealed by the measured fractal dimensions in static light scattering (SLS). Small-angle scattering techniques, which accesses wider range of q-values than SLS, could be used to probe the structural arrangements, correlation length and the dynamics of AT aggregates and higher order AT-Hp complexes.

BIBLIOGRAPHY

1. Bernfield, M.; Gotte, M.; Park, P. W.; Reizes, O.; Fitzgerald, M. L.; Lincecum, J.; Zako, M. Functions of cell surface heparan sulfate proteoglycans. Annu. Rev. Biochem. 1999, 68, 729-777.

2. Turnbull, J.; Powell, A.; Guimond, S. Heparan sulfate: decoding a dynamic multifunctional cell regulator. *Trends Cell Biol.* **2001**, *11*, 75-82.

3. Lindahl, U.; Kjellen, L. Pathophysiology of heparan sulphate: many diseases, few drugs. *J. Intern. Med.* **2013**, *273*, 555-571.

4. Sasisekharan, R.; Raman, R.; Prabhakar, V. Glycomics approach to structure-function relationships of glycosaminoglycans. *Annu. Rev. Biomed. Eng.* **2006**, *8*, 181-231.

5. Lindahl, U.; Kusche-Gullberg, M.; Kjellén, L. Regulated Diversity of Heparan Sulfate. *J. Biol. Chem.* **1998**, *273*, 24979-24982.

6. Kreuger, J.; Spillmann, D.; Li, J. P.; Lindahl, U. Interactions between heparan sulfate and proteins: the concept of specificity. *J. Cell Biol.* **2006**, *174*, 323-327.

7. Bishop, J. R.; Schuksz, M.; Esko, J. D. Heparan sulphate proteoglycans fine-tune mammalian physiology. *Nature* **2007**, *446*, 1030-1037.

8. Stringer, S. E.; Gallagher, J. T. Heparan sulphate. *Int. J. Biochem. Cell Biol.* **1997**, *29*, 709-714.

9. Seyrek, E.; Dubin, P. Glycosaminoglycans as polyelectrolytes. *Adv. Colloid Interface Sci.* **2010**, *158*, 119-129.

10. Pavlov, G.; Finet, S.; Tatarenko, K.; Korneeva, E.; Ebel, C. Conformation of heparin studied with macromolecular hydrodynamic methods and X-ray scattering. *Eur. Biophys. J.* **2003**, *32*, 437-449.

11. Jacques, L. B. Heparin: an old drug with a new paradigm. *Science* **1979**, *206*, 528-533.

12. Bertini, S.; Bisio, A.; Torri, G.; Bensi, D.; Terbojevich, M. Molecular weight determination of heparin and dermatan sulfate by size exclusion chromatography with a triple detector array. *Biomacromolecules* **2005**, *6*, 168-173.

13. Guo, X.; Condra, M.; Kimura, K.; Berth, G.; Dautzenberg, H.; Dubin, P. L. Determination of molecular weight of heparin by size exclusion chromatography with universal calibration. *Anal. Biochem.* **2003**, *312*, 33-39.

14. Turnbull, J. E.; Fernig, D. G.; Ke, Y.; Wilkinson, M. C.; Gallagher, J. T. Identification of the basic fibroblast growth factor binding sequence in fibroblast heparan sulfate. *J. Biol. Chem.* **1992**, *267*, 10337-10341.

15. Habuchi, H.; Suzuki, S.; Saito, T.; Tamura, T.; Harada, T.; Yoshida, K.; Kimata, K. Structure of a heparan sulphate oligosaccharide that binds to basic fibroblast growth factor. *Biochem. J.* **1992**, *285 (Pt 3)*, 805-813.

16. Jemth, P.; Kreuger, J.; Kusche-Gullberg, M.; Sturiale, L.; Gimenez-Gallego, G.; Lindahl, U. Biosynthetic oligosaccharide libraries for identification of protein-binding heparan sulfate motifs. Exploring the structural diversity by screening for fibroblast growth factor (FGF)1 and FGF2 binding. *J. Biol. Chem.* **2002**, *277*, 30567-30573.

17. Olson, S. T.; Bjork, I.; Sheffer, R.; Craig, P. A.; Shore, J. D.; Choay, J. Role of the antithrombin-binding pentasaccharide in heparin acceleration of antithrombin-proteinase reactions. Resolution of the antithrombin conformational change contribution to heparin rate enhancement. *J. Biol. Chem.* **1992**, *267*, 12528-12538.

18. Petitou, M.; Barzu, T.; Herault, J. P.; Herbert, J. M. A unique trisaccharide sequence in heparin mediates the early step of antithrombin III activation. *Glycobiology* **1997**, *7*, 323-327.

19. Olson, S. T.; Srinivasan, K. R.; Bjork, I.; Shore, J. D. Binding of high affinity heparin to antithrombin III. Stopped flow kinetic studies of the binding interaction. *J. Biol. Chem.* **1981**, *256*, 11073-11079.

20. Jastrebova, N.; Vanwildemeersch, M.; Lindahl, U.; Spillmann, D. Heparan Sulfate Domain Organization and Sulfation Modulate FGF-induced Cell Signaling. *J. Biol. Chem.* **2010**, *285*, 26842-26851.

21. Kreuger, J.; Jemth, P.; Sanders-Lindberg, E.; Eliahu, L.; Ron, D.; Basilico, C.; Salmivirta, M.; Lindahl, U. Fibroblast growth factors share binding sites in heparan sulphate. *Biochem. J.* **2005**, *389*, 145-150.

22. Kreuger, J.; Spillmann, D.; Li, J.-p.; Lindahl, U. Interactions between heparan sulfate and proteins: the concept of specificity. J. Cell Biol. 2006, 174, 323-327.

23. Johnson, D. J.; Li, W.; Adams, T. E.; Huntington, J. A. Antithrombin-S195A factor Xa-heparin structure reveals the allosteric mechanism of antithrombin activation. *EMBO J.* **2006**, *25*, 2029-2037.

24. Pellegrini, L.; Burke, D. F.; von Delft, F.; Mulloy, B.; Blundell, T. L. Crystal structure of fibroblast growth factor receptor ectodomain bound to ligand and heparin. *Nature* **2000**, *407*, 1029-1034.

25. Schlessinger, J.; Plotnikov, A. N.; Ibrahimi, O. A.; Eliseenkova, A. V.; Yeh, B. K.; Yayon, A.; Linhardt, R. J.; Mohammadi, M. Crystal structure of a ternary FGF-FGFR-heparin complex reveals a dual role for heparin in FGFR binding and dimerization. *Mol. Cell* **2000**, *6*, 743-750.

26. Verli, H.; Guimaraes, J. A. Insights into the induced fit mechanism in antithrombin-heparin interaction using molecular dynamics simulations. *J Mol Graph Model* **2005**, *24*, 203-212.

27. Jin, L.; Abrahams, J. P.; Skinner, R.; Petitou, M.; Pike, R. N.; Carrell, R. W. The anticoagulant activation of antithrombin by heparin. *Proc Natl Acad Sci U S A* **1997**, *94*, 14683-14688.

28. Seyrek, E.; Dubin, P. L.; Henriksen, J. Nonspecific electrostatic binding characteristics of the heparin-antithrombin interaction. *Biopolymers* **2007**, *86*, 249-259.

29. Henry, B. L.; Connell, J.; Liang, A.; Krishnasamy, C.; Desai, U. R. Interaction of antithrombin with sulfated, low molecular weight lignins: opportunities for potent, selective modulation of antithrombin function. *J Biol Chem* **2009**, *284*, 20897-20908.

30. Powell, A. K.; Yates, E. A.; Fernig, D. G.; Turnbull, J. E. Interactions of heparin/heparan sulfate with proteins: appraisal of structural factors and experimental approaches. *Glycobiology* **2004**, *14*, 17R-30R.

31. Kayitmazer, A. B.; Quinn, B.; Kimura, K.; Ryan, G. L.; Tate, A. J.; Pink, D. A.; Dubin, P. L. Protein specificity of charged sequences in polyanions and heparins. *Biomacromolecules* **2010**, *11*, 3325-3331.

32. Kreuger, J.; Spillmann, D.; Li, J.-p.; Lindahl, U. Interactions between heparan sulfate and proteins: the concept of specificity. *Journal of Cell Biology* **2006**, *174*, 323-327.

33. Lander, A. D. Proteoglycans: Master regulators of molecular encounter? *Matrix Biol.* **1998**, *17*, 465-472.

34. Catlow, K. R.; Deakin, J. A.; Wei, Z.; Delehedde, M.; Fernig, D. G.; Gherardi, E.; Gallagher, J. T.; Pavao, M. S.; Lyon, M. Interactions of hepatocyte growth factor/scatter factor with various glycosaminoglycans reveal an important interplay between the presence of iduronate and sulfate density. *J. Biol. Chem.* **2008**, *283*, 5235-5248.

35. Jastrebova, N.; Vanwildemeersch, M.; Rapraeger, A. C.; Gimenez-Gallego, G.; Lindahl, U.; Spillmann, D. Heparan sulfate-related oligosaccharides in ternary complex formation with fibroblast growth factors 1 and 2 and their receptors. *J. Biol. Chem.* **2006**, *281*, 26884-26892.

36. Zhang, F.; Liang, X.; Pu, D.; George, K. I.; Holland, P. J.; Walsh, S. T.; Linhardt, R. J. Biophysical characterization of glycosaminoglycan-IL-7 interactions using SPR. *Biochimie* **2012**, *94*, 242-249.

37. Jones, L. S.; Yazzie, B.; Middaugh, C. R. Polyanions and the proteome. *Mol Cell Proteomics* **2004**, *3*, 746-769.

38. Imberty, A.; Lortat-Jacob, H.; Pérez, S. Structural view of glycosaminoglycan–protein interactions. *Carbohydr. Res.* **2007**, *342*, 430-439.

39. Lortat-Jacob, H.; Turnbull, J. E.; Grimaud, J. A. Molecular organization of the interferon gamma-binding domain in heparan sulphate. *Biochemical Journal* **1995**, *310 (Pt 2)*, 497-505.

40. Stringer, S. E.; Gallagher, J. T. Specific binding of the chemokine platelet factor 4 to heparan sulfate. *J. Biol. Chem.* **1997**, *272*, 20508-20514.

41. Spillmann, D.; Witt, D.; Lindahl, U. Defining the interleukin-8-binding domain of heparan sulfate. *Journal of Biological Chemistry* **1998**, *273*, 15487-15493.

42. Vives, R. R.; Sadir, R.; Imberty, A.; Rencurosi, A.; Lortat-Jacob, H. A kinetics and modeling study of RANTES(9-68) binding to heparin reveals a mechanism of cooperative oligomerization. *Biochemistry* **2002**, *41*, 14779-14789.

43. Robinson, C. J.; Mulloy, B.; Gallagher, J. T.; Stringer, S. E. VEGF165-binding sites within heparan sulfate encompass two highly sulfated domains and can be liberated by K5 lyase. *Journal of Biological Chemistry* **2006**, *281*, 1731-1740.

44. Kayitmazer, A. B.; Seeman, D.; Minsky, B. B.; Dubin, P. L.; Xu, Y. Protein-polyelectrolyte interactions. *Soft Matter* **2013**, *9*, 2553-2583.

45. Jones, L. S.; Yazzie, B.; Middaugh, C. R. Polyanions and the Proteome. *Mol. Cell. Proteomics* **2004**, *3*, 746-769.

46. Record, M. T., Jr.; Lohman, M. L.; De Haseth, P. Ion effects on ligand-nucleic acid interactions. *J. Mol. Biol.* **1976**, *107*, 145-158.

47. Mascotti, D. P.; Lohman, T. M. Thermodynamic extent of counterion release upon binding oligolysines to single-stranded nucleic acids. *Proc. Natl. Acad. Sci. U. S. A.* **1990**, *87*, 3142-3146.

48. Fenley, M. O.; Russo, C.; Manning, G. S. Theoretical Assessment of the Oligolysine Model for Ionic Interactions in Protein–DNA Complexes. *J. Phys. Chem. B* **2011**, *115*, 9864-9872.

49. Mascotti, D. P.; Lohman, T. M. Thermodynamics of charged oligopeptide-heparin interactions. *Biochemistry* **1995**, *34*, 2908-2915.

50. Grymonpre, K. R.; Staggemeier, B. A.; Dubin, P. L.; Mattison, K. W. Identification by integrated computer modeling and light scattering studies of an electrostatic serum albumin-hyaluronic acid binding site. *Biomacromolecules* **2001**, *2*, 422-429.

51. Seyrek, E.; Dubin, P. L.; Tribet, C.; Gamble, E. A. Ionic strength dependence of protein-polyelectrolyte interactions. *Biomacromolecules* **2003**, *4*, 273-282.

52. Hirsh, J.; Levine, M. N. Low molecular weight heparin. *Blood* **1992**, *79*, 1-17.

53. Ma, C.; Bloomfield, V. A. Gel electrophoresis measurement of counterion condensation on DNA. *Biopolymers* **1995**, *35*, 211-216.

54. Manning, G. S. Limiting Laws and Counterion Condensation in Polyelectrolyte Solutions I. Colligative Properties. *J. Chem. Phys.* **1969**, *51*, 924-933.

55. Manning, G. S. Limiting laws and counterion condensation in polyelectrolyte solutions: V. Further development of the chemical model. *Biophys. Chem.* **1978**, *9*, 65-70.

56. Manning, G. S.; Ray, J. Counterion condensation revisited. *J. Biomol. Struct. Dyn.* **1998**, *16*, 461-476.

57. Zimm, B. H.; Bret, M. L. Counter-Ion Condensation and System Dimensionality. *J. Biomol. Struct. Dyn.* **1983**, *1*, 461-471.

58. Hoagland, D. A.; Arvanitidou, E.; Welch, C. Capillary Electrophoresis Measurements of the Free Solution Mobility for Several Model Polyelectrolyte Systems. *Macromolecules* **1999**, *32*, 6180-6190.

59. Hoagland, D. A.; Smisek, D. L.; Chen, D. Y. Gel and free solution electrophoresis of variably charged polymers. *Electrophoresis* **1996**, *17*, 1151-1160.

60. Popov, A.; Hoagland, D. A. Electrophoretic evidence for a new type of counterion condensation. *J. Polym. Sci., Part B: Polym. Phys.* **2004**, *42*, 3616-3627.

61. Anik, N.; Airiau, M.; Labeau, M. P.; Vuong, C. T.; Reboul, J.; Lacroix-Desmazes, P.; Gerardin, C.; Cottet, H. Determination of Polymer Effective Charge by Indirect UV Detection in Capillary Electrophoresis: Toward the Characterization of Macromolecular Architectures. *Macromolecules* **2009**, *42*, 2767-2774.

62. Ibrahim, A.; Ohshima, H.; Allison, S. A.; Cottet, H. Determination of effective charge of small ions, polyelectrolytes and nanoparticles by capillary electrophoresis. *J. Chromatogr. A* **2012**, *1247*, 154-164.

63. Kim, M. Y.; Varenne, A.; Daniel, R.; Gareil, P. Capillary electrophoresis profiles of fucoidan and heparin fractions: significance of mobility dispersity for their characterization. *J. Sep. Sci.* **2003**, *26*, 1154-1162.

64. Lindahl, U. Heparan sulfate-protein interactions--a concept for drug design? *Thromb. Haemost.* **2007**, *98*, 109-115.

65. Capila, I.; Linhardt, R. J. Heparin-protein interactions. *Angew. Chem. Int. Ed. Engl.* **2002**, *41*, 391-412.

66. Park, P. W.; Reizes, O.; Bernfield, M. Cell surface heparan sulfate proteoglycans: selective regulators of ligand-receptor encounters. *J. Biol. Chem.* **2000**, *275*, 29923-29926.

67. Whitelock, J. M.; Iozzo, R. V. Heparan sulfate: a complex polymer charged with biological activity. *Chem. Rev.* **2005**, *105*, 2745-2764.

68. Esko, J. D.; Selleck, S. B. Order out of chaos: assembly of ligand binding sites in heparan sulfate. *Annu. Rev. Biochem.* **2002**, *71*, 435-471.

69. Record, M. T.; Anderson, C. F.; Lohman, T. M. Thermodynamic analysis of ion effects on the binding and conformational equilibria of proteins and nucleic acids: the roles of ion association or release, screening, and ion effects on water activity. *Q. Rev. Biophys.* **1978**, *11*, 103-178.

70. Lohman, T. M.; deHaseth, P. L.; Record, M. T., Jr. Pentalysine-deoxyribonucleic acid interactions: a model for the general effects of ion concentrations on the interactions of proteins with nucleic acids. *Biochemistry* **1980**, *19*, 3522-3530.

71. Dais, P.; Peng, Q. J.; Perlin, A. S. A relationship between 13C-chemical-shift displacements and counterion-condensation theory, in the binding of calcium ion by heparin. *Carbohydr. Res.* **1987**, *168*, 163-179.

72. Comper, W. D.; Preston, B. N. Model connective-tissue systems. A study of polyion-mobile ion and of excluded-volume interactions of proteoglycans. *Biochem. J.* **1974**, *143*, 1-9.

73. Winzor, D. J.; Carrington, L. E.; Deszczynski, M.; Harding, S. E. Extent of charge screening in aqueous polysaccharide solutions. *Biomacromolecules* **2004**, *5*, 2456-2460.

74. Dong, Q.; Stellwagen, E.; Dagle, J. M.; Stellwagen, N. C. Free solution mobility of small single-stranded oligonucleotides with variable charge densities. *Electrophoresis* **2003**, *24*, 3323-3329.

75. Gunay, N. S.; Linhardt, R. J. Capillary electrophoretic separation of heparin oligosaccharides under conditions amenable to mass spectrometric detection. *J. Chromatogr. A* **2003**, *1014*, 225-233.

76. Karamanos, N. K.; Hjerpe, A. Strategies for analysis and structure characterization of glycans/proteoglycans by capillary electrophoresis. Their diagnostic and biopharmaceutical importance. *Biomed. Chromatogr.* **1999**, *13*, 507-512.

77. Mao, W.; Thanawiroon, C.; Linhardt, R. J. Capillary electrophoresis for the analysis of glycosaminoglycans and glycosaminoglycan-derived oligosaccharides. *Biomed. Chromatogr.* **2002**, *16*, 77-94.

78. Volpi, N.; Maccari, F.; Linhardt, R. J. Capillary electrophoresis of complex natural polysaccharides. *Electrophoresis* **2008**, *29*, 3095-3106.

79. Pervin, A.; Alhakim, A.; Linhardt, R. J. Separation of Glycosaminoglycan-Derived Oligosaccharides by Capillary Electrophoresis Using Reverse Polarity. *Anal. Biochem.* **1994**, *221*, 182-188.

80. Henriksen, J.; Ringborg, L. H.; Roepstorrf, P. On-line size-exclusion chromatography/mass spectrometry of low molecular mass heparin. *J. Mass Spectrom.* **2004**, *39*, 1305-1312.

81. Laremore, T. N.; Leach, F. E., 3rd; Solakyildirim, K.; Amster, I. J.; Linhardt, R. J. Glycosaminoglycan characterization by electrospray ionization mass spectrometry including fourier transform mass spectrometry. *Methods Enzymol.* **2010**, *478*, 79-108.

82. Schenauer, M. R.; Meissen, J. K.; Seo, Y.; Ames, J. B.; Leary, J. A. Heparan sulfate separation, sequencing, and isomeric differentiation: ion mobility spectrometry reveals specific iduronic and glucuronic acid-containing hexasaccharides. *Anal. Chem.* **2009**, *81*, 10179-10185.

83. Zaia, J.; Costello, C. E. Tandem Mass Spectrometry of Sulfated Heparin-Like Glycosaminoglycan Oligosaccharides. *Anal. Chem.* **2003**, *75*, 2445-2455.

84. Cottet, H.; Gareil, P.; Theodoly, O.; Williams, C. E. A semi-empirical approach to the modeling of the electrophoretic mobility in free solution: application to polystyrenesulfonates of various sulfonation rates. *Electrophoresis* **2000**, *21*, 3529-3540.

85. Zhang, B.; Hattori, T.; Dubin, P. L. Observation of Compositional Heterogeneity in Poly(styrene sulfonate) Using Frontal Analysis Continuous Capillary Electrophoresis. *Macromolecules* **2001**, *34*, 6790-6794.

86. Böhme, U.; Scheler, U. Hydrodynamic Size and Electrophoretic Mobility of Poly(styrene sulfonate) versus Molecular Weight. *Macromol. Chem. Phys.* **2007**, *208*, 2254-2257.

87. Manning, G. S. Approximate Solutions to Some Problems in Polyelectrolyte Theory Involving Nonuniform Charge Distributions. *Macromolecules* **2008**, *41*, 6217-6227.

88. Abzalimov, R. R.; Dubin, P. L.; Kaltashov, I. A. Glycosaminoglycans as naturally occurring combinatorial libraries: developing a mass spectrometry-based strategy for characterization of anti-thrombin interaction with low molecular weight heparin and heparin oligomers. *Anal. Chem.* **2007**, *79*, 6055-6063.

89. Grubisic, Z.; Rempp, P.; Benoit, H. A universal calibration for gel permeation chromatography. *J. Polym. Sci., Part B: Polym. Phys.* **1996**, *34*, 1707-1713.

90. Staggemeier, B.; Huang, Q. R.; Dubin, P. L.; Morishima, Y.; Sato, T. Determination of the compositional distribution of copolymers by frontal analysis continuous capillary electrophoresis. *Anal. Chem.* **2000**, *72*, 255-258.

91. Oudhoff, K. A.; Buijtenhuijs, F. A.; Wijnen, P. H.; Schoenmakers, P. J.; Kok, W. T. Determination of the degree of substitution and its distribution of carboxymethylcelluloses by capillary zone electrophoresis. *Carbohydr. Res.* **2004**, *339*, 1917-1924.

92. Castignolles, P.; Gaborieau, M.; Hilder, E. F.; Sprong, E.; Ferguson, C. J.; Gilbert, R. G. High-Resolution Separation of Oligo(acrylic acid) by Capillary Zone Electrophoresis. *Macromol. Rapid Commun.* **2006**, *27*, 42-46.

93. Grass, K.; Böhme, U.; Scheler, U.; Cottet, H.; Holm, C. Importance of hydrodynamic shielding for the dynamic behavior of short polyelectrolyte chains. *Phys. Rev. Lett.* **2008**, *100*, 096104.

94. Zamfir, A.; Seidler, D. G.; Kresse, H.; Peter-Katalinić, J. Structural characterization of chondroitin/dermatan sulfate oligosaccharides from bovine aorta by capillary electrophoresis and electrospray ionization quadrupole time-of-flight tandem mass spectrometry. *Rapid Commun. Mass Spectrom.* **2002**, *16*, 2015-2024.

95. Shendruk, T. N.; Hickey, O. A.; Slater, G. W.; Harden, J. L. Electrophoresis: When hydrodynamics matter. *Curr. Opin. Colloid Interface Sci.* **2012**, *17*, 74-82.

96. Rahmoune, H.; Chen, H.-L.; Gallagher, J. T.; Rudland, P. S.; Fernig, D. G. Interaction of Heparan Sulfate from Mammary Cells with Acidic Fibroblast Growth Factor (FGF) and Basic FGF: Regulation Of The Activity Of Basic FGF By High And Low Affinity Binding Sites In Heparan Sulfate. *J. Biol. Chem.* **1998**, *273*, 7303-7310.

97. Gallagher, J. T. Heparan sulfate: growth control with a restricted sequence menu. *J. Clin. Invest.* **2001**, *108*, 357-361.

98. Lyon, M.; Deakin, J. A.; Lietha, D.; Gherardi, E.; Gallagher, J. T. The Interactions of Hepatocyte Growth Factor/Scatter Factor and Its NK1 and NK2 Variants with Glycosaminoglycans Using a Modified Gel Mobility Shift Assay: Elucidation Of The Minimal Size Of Binding And Activatory Oligosaccharides. *J. Biol. Chem.* **2004**, *279*, 43560-43567.

99. Sarrazin, S.; Lamanna, W. C.; Esko, J. D. Heparan Sulfate Proteoglycans. *Cold Spring Harb. Perspect. Biol.* **2011**, *3*.

100. Lindahl, U. Heparan sulfate-protein interactions - A concept for drug design? *Thromb. Haemost.* **2007**, *98*, 109-115.

101. Habuchi, H.; Miyake, G.; Nogami, K.; Kuroiwa, A.; Matsuda, Y.; Kusche-Gullberg, M.; Habuchi, O.; Tanaka, M.; Kimata, K. Biosynthesis of heparan sulphate with diverse structures and functions: two alternatively spliced forms of human heparan sulphate 6-0-sulphotransferase-2 having different expression patterns and properties. *Biochem. J.* **2003**, *371*, 131-142.

102. Tae, G.; Scatena, M.; Stayton, P. S.; Hoffman, A. S. PEG-cross-linked heparin is an affinity hydrogel for sustained release of vascular endothelial growth factor. *J. Biomater. Sci. Polym. Ed.* **2006**, *17*, 187-197.

103. Benoit, D. S.; Collins, S. D.; Anseth, K. S. Multifunctional hydrogels that promote osteogenic hMSC differentiation through stimulation and sequestering of BMP2. *Adv. Funct. Mater.* **2007**, *17*, 2085-2093.

104. Benoit, D. S. W.; Anseth, K. S. Heparin functionalized PEG gels that modulate protein adsorption for hMSC adhesion and differentiation. *Acta Biomater.* **2005**, *1*, 461-470.

105. Wu, J. M.; Xu, Y. Y.; Li, Z. H.; Yuan, X. Y.; Wang, P. F.; Zhang, X. Z.; Liu, Y. Q.; Guan, J.; Guo, Y.; Li, R. X.; Zhang, H. Heparin-functionalized collagen matrices with controlled release of basic fibroblast growth factor. *J. Mater. Sci.: Mater. Med.* **2010**, *22*, 107-114.

106. Yamaguchi, N.; Zhang, L.; Chae, B.-S.; Palla, C. S.; Furst, E. M.; Kiick, K. L. Growth Factor Mediated Assembly of Cell Receptor-Responsive Hydrogels. *J. Am. Chem. Soc.* **2007**, *129*, 3040-3041.

107. Yoon, J. J.; Chung, H. J.; Park, T. G. Photo-crosslinkable and biodegradable Pluronic/heparin hydrogels for local and sustained delivery of angiogenic growth factor. *J. Biomed. Mater. Res., Part A* **2007**, *83A*, 597-605.

108. Zhang, L.; Furst, E. M.; Kiick, K. L. Manipulation of hydrogel assembly and growth factor delivery via the use of peptide–polysaccharide interactions. *J. Control. Release* **2006**, *114*, 130-142.

109. Jeon, O.; Powell, C.; Solorio, L. D.; Krebs, M. D.; Alsberg, E. Affinity-based growth factor delivery using biodegradable, photocrosslinked heparin-alginate hydrogels. *J. Control. Release* **2011**, *154*, 258-266.

110. Seal, B. L.; Panitch, A. Physical Polymer Matrices Based on Affinity Interactions between Peptides and Polysaccharides. *Biomacromolecules* **2003**, *4*, 1572-1582.

111. Maxwell, D. J.; Hicks, B. C.; Parsons, S.; Sakiyama-Elbert, S. E. Development of rationally designed affinity-based drug delivery systems. *Acta Biomater.* **2005**, *1*, 101-113.

112. Sakiyama-Elbert, S. E.; Hubbell, J. A. Development of fibrin derivatives for controlled release of heparin-binding growth factors. *J. Control. Release* **2000**, *65*, 389-402.

113. Wood, M. D.; Sakiyama-Elbert, S. E. Release rate controls biological activity of nerve growth factor released from fibrin matrices containing affinity-based delivery systems. *J. Biomed. Mater. Res., Part A* **2008**, *84A*, 300-312.

114. Minsky, B. B.; Atmuri, A.; Kaltashov, I. A.; Dubin, P. L. Counterion Condensation on Heparin Oligomers. *Biomacromolecules* **2013**, *14*, 1113-1121.

115. Thompson, L. D.; Pantoliano, M. W.; Springer, B. A. Energetic characterization of the basic fibroblast growth factor-heparin interaction: identification of the heparin binding domain. *Biochemistry* **1994**, *33*, 3831-3840.

116. Friedrich, U.; Blom, A. M.; Dahlbäck, B.; Villoutreix, B. O. Structural and Energetic Characteristics of the Heparin-binding Site in Antithrombotic Protein C. *J. Biol. Chem.* **2001**, *276*, 24122-24128.

117. Ashikari-Hada, S.; Habuchi, H.; Kariya, Y.; Itoh, N.; Reddi, A. H.; Kimata, K. Characterization of growth factor-binding structures in heparin/heparan sulfate using an octasaccharide library. *J. Biol. Chem.* **2004**, *279*, 12346-12354.

118. Ashikari-Hada, S.; Habuchi, H.; Sugaya, N.; Kobayashi, T.; Kimata, K. Specific inhibition of FGF-2 signaling with 2-O-sulfated octasaccharides of heparan sulfate. *Glycobiology* **2009**, *19*, 644-654.

119. Faham, S.; Hileman, R. E.; Fromm, J. R.; Linhardt, R. J.; Rees, D. C. Heparin structure and interactions with basic fibroblast growth factor. *Science* **1996**, *271*, 1116-1120.

120. Zhang, F.; Zhang, Z.; Lin, X.; Beenken, A.; Eliseenkova, A. V.; Mohammadi, M.; Linhardt, R. J. Compositional Analysis of Heparin/Heparan Sulfate Interacting with Fibroblast Growth Factor·Fibroblast Growth Factor Receptor Complexes. *Biochemistry* **2009**, *48*, 8379-8386.

121. Seyrek, E.; Dubin, P. L.; Henriksen, J. Nonspecific electrostatic binding characteristics of the heparin-antithrombin interaction. *Biopolymers* **2007**, *86*, 249-259.

122. Chen, K.; Xu, Y.; Rana, S.; Miranda, O. R.; Dubin, P. L.; Rotello, V. M.; Sun, L.; Guo, X. Electrostatic Selectivity in Protein–Nanoparticle Interactions. *Biomacromolecules* **2011**, *12*, 2552-2561.

123. Xu, Y.; Engel, Y.; Yan, Y.; Chen, K.; Moyano, D. F.; Dubin, P. L.; Rotello, V. M. Enhanced electrostatic discrimination of proteins on nanoparticle-coated surfaces. *Journal of Materials Chemistry B* **2013**, *1*, 5230-5234.

124. Schreiber, G.; Haran, G.; Zhou, H. X. Fundamental Aspects of Protein−Protein Association Kinetics. *Chem. Rev.* **2009**, *109*, 839-860.

125. Perez Sanchez, H.; Tatarenko, K.; Nigen, M.; Pavlov, G.; Imberty, A.; Lortat-Jacob, H.; Garcia de la Torre, J.; Ebel, C. Organization of human interferon gamma-heparin complexes from solution properties and hydrodynamics. *Biochemistry* **2006**, *45*, 13227-13238.

126. Faham, S.; Linhardt, R. J.; Rees, D. C. Diversity does make a difference: fibroblast growth factor-heparin interactions. *Curr. Opin. Struct. Biol.* **1998**, *8*, 578-586.

127. Rosu, F.; Gabelica, V.; Poncelet, H.; De Pauw, E. Tetramolecular G-quadruplex formation pathways studied by electrospray mass spectrometry. *Nucleic Acids Res.* **2010**, *38*, 5217-5225.

128. Park, A. Y.; Robinson, C. V. Protein-nucleic acid complexes and the role of mass spectrometry in their structure determination. *Crit. Rev. Biochem. Mol. Biol.* **2011**, *46*, 152-164.

129. Kim, J.; Blaber, S. I.; Blaber, M. Alternative type I and I' turn conformations in the beta8/beta9 beta-hairpin of human acidic fibroblast growth factor. *Protein Sci.* **2002**, *11*, 459-466.

130. Rocchia, W.; Alexov, E.; Honig, B. Extending the Applicability of the Nonlinear Poisson−Boltzmann Equation: Multiple Dielectric Constants and Multivalent Ions†. *J. Phys. Chem. B* **2001**, *105*, 6507-6514.

131. Rocchia, W.; Sridharan, S.; Nicholls, A.; Alexov, E.; Chiabrera, A.; Honig, B. Rapid grid-based construction of the molecular surface and the use of induced surface charge to calculate reaction field energies: Applications to the molecular systems and geometric objects. *J. Comput. Chem.* **2002**, *23*, 128-137.

132. Tanford, C.; Kirkwood, J. G. Theory of Protein Titration Curves. I. General Equations for Impenetrable Spheres. *J. Am. Chem. Soc.* **1957**, *79*, 5333-5339.

133. Vijayakumar, M.; Wong, K. Y.; Schreiber, G.; Fersht, A. R.; Szabo, A.; Zhou, H. X. Electrostatic enhancement of diffusion-controlled protein-protein association: comparison of theory and experiment on barnase and barstar. *J. Mol. Biol.* **1998**, *278*, 1015-1024.

134. Mach, H.; Volkin, D. B.; Burke, C. J.; Middaugh, C. R.; Linhardt, R. J.; Fromm, J. R.; Loganathan, D.; Mattsson, L. Nature of the interaction of heparin with acidic fibroblast growth factor. *Biochemistry* **1993**, *32*, 5480-5489.

135. Muthukumar, M. Adsorption of a polyelectrolyte chain to a charged surface. *J. Chem. Phys.* **1987**, *86*, 7230-7235.

136. Vongoeler, F.; Muthukumar, M. Adsorption of polyelectrolytes onto curved surfaces. *J. Chem. Phys.* **1994**, *100*, 7796-7803.

137. Cooper, C. L.; Goulding, A.; Kayitmazer, A. B.; Ulrich, S.; Stoll, S.; Turksen, S.; Yusa, S.; Kumar, A.; Dubin, P. L. Effects of polyelectrolyte chain stiffness, charge mobility, and charge sequences on binding to proteins and micelles. *Biomacromolecules* **2006**, *7*, 1025-1035.

138. Henriksen, J.; Ringborg, L. H.; Roepstorrf, P. On-line size-exclusion chromatography/mass spectrometry of low molecular mass heparin. *J. Mass Spectrom.* **2004**, *39*, 1305-1312.

139. Seyrek, E.; Dubin, P. Glycosaminoglycans as polyelectrolytes. *Adv. Colloid Interface Sci.* **2010**, *158*, 119-129.

140. Herr, A. B.; Ornitz, D. M.; Sasisekharan, R.; Venkataraman, G.; Waksman, G. Heparin-induced self-association of fibroblast growth factor-2. Evidence for two oligomerization processes. *J. Biol. Chem.* **1997**, *272*, 16382-16389.

141. Moy, F. J.; Safran, M.; Seddon, A. P.; Kitchen, D.; Bohlen, P.; Aviezer, D.; Yayon, A.; Powers, R. Properly oriented heparin-decasaccharide-induced dimers are the biologically active form of basic fibroblast growth factor. *Biochemistry* **1997**, *36*, 4782-4791.

142. Harada, M.; Murakami, H.; Okawa, A.; Okimoto, N.; Hiraoka, S.; Nakahara, T.; Akasaka, R.; Shiraishi, Y.; Futatsugi, N.; Mizutani-Koseki, Y.; Kuroiwa, A.; Shirouzu, M.; Yokoyama, S.; Taiji, M.; Iseki, S.; Ornitz, D. M.; Koseki, H. FGF9 monomer-dimer equilibrium regulates extracellular matrix affinity and tissue diffusion. *Nat. Genet.* **2009**, *41*, 289-298.

143. Venkataraman, G.; Sasisekharan, V.; Herr, A. B.; Ornitz, D. M.; Waksman, G.; Cooney, C. L.; Langer, R.; Sasisekharan, R. Preferential self-association of basic fibroblast growth factor is stabilized by heparin during receptor dimerization and activation. *Proc. Natl. Acad. Sci. U. S. A.* **1996**, *93*, 845-850.

144. DiGabriele, A. D.; Lax, I.; Chen, D. I.; Svahn, C. M.; Jaye, M.; Schlessinger, J.; Hendrickson, W. A. Structure of a heparin-linked biologically active dimer of fibroblast growth factor. *Nature* **1998**, *393*, 812-817.

145. Ornitz, D. M.; Yayon, A.; Flanagan, J. G.; Svahn, C. M.; Levi, E.; Leder, P. Heparin is required for cell-free binding of basic fibroblast growth factor to a soluble receptor and for mitogenesis in whole cells. *Mol. Cell. Biol.* **1992**, *12*, 240-247.

146. Kaltashov, I. A.; Bobst, C. E.; Abzalimov, R. R. Mass spectrometry-based methods to study protein architecture and dynamics. *Protein Sci.* **2013**, *22*, 530-544.

147. Metropolis, N.; Rosenbluth, A. W.; Rosenbluth, M. N.; Teller, A. H.; Teller, E. Equation of State Calculations by Fast Computing Machines. *J. Chem. Phys.* **1953**, *21*, 1087-1092.

148. Casu, B.; Petitou, M.; Provasoli, M.; Sinay, P. Conformational flexibility: a new concept for explaining binding and biological properties of iduronic acid-containing glycosaminoglycans. *Trends Biochem. Sci.* **1988**, *13*, 221-225.

149. Harmer, N. J.; Robinson, C. J.; Adam, L. E.; Ilag, L. L.; Robinson, C. V.; Gallagher, J. T.; Blundell, T. L. Multimers of the fibroblast growth factor (FGF)-FGF receptor-saccharide complex are formed on long oligomers of heparin. *Biochem. J.* **2006**, *393*, 741-748.

150. Yu, Y.; Sweeney, M. D.; Saad, O. M.; Leary, J. A. Potential inhibitors of chemokine function: analysis of noncovalent complexes of CC chemokine and small polyanionic molecules by ESI FT-ICR mass spectrometry. *J. Am. Soc. Mass Spectrom.* **2006**, *17*, 524-535.

151. Desai, U. R. New antithrombin-based anticoagulants. *Med. Res. Rev.* **2004**, *24*, 151-181.

152. Hirsh, J.; Anand, S. S.; Halperin, J. L.; Fuster, V. Guide to anticoagulant therapy: Heparin : a statement for healthcare professionals from the American Heart Association. *Circulation* **2001**, *103*, 2994-3018.

153. Damus, P. S.; Hicks, M.; Rosenberg, R. D. Anticoagulant action of heparin. *Nature* **1973**, *246*, 355-357.

154. Huntington, J. A.; Carrell, R. W. The serpins: nature's molecular mousetraps. *Sci. Prog.* **2001**, *84*, 125-136.

155. Bourin, M. C.; Lindahl, U. Glycosaminoglycans and the regulation of blood coagulation. *Biochem. J.* **1993**, *289 (Pt 2)*, 313-330.

156. Rosenberg, R. D.; Damus, P. S. The purification and mechanism of action of human antithrombin-heparin cofactor. *J. Biol. Chem.* **1973**, *248*, 6490-6505.

157. Mushunje, A.; Zhou, A.; Carrell, R. W.; Huntington, J. A. Heparin-induced substrate behavior of antithrombin Cambridge II. *Blood* **2003**, *102*, 4028-4034.

158. Olson, S. T.; Bjork, I. Predominant contribution of surface approximation to the mechanism of heparin acceleration of the antithrombin-thrombin reaction. Elucidation from salt concentration effects. *J. Biol. Chem.* **1991**, *266*, 6353-6364.

159. Olson, S. T.; Bjork, I. Role of protein conformational changes, surface approximation and protein cofactors in heparin-accelerated antithrombin-proteinase reactions. *Adv. Exp. Med. Biol.* **1992**, *313*, 155-165.

160. Huntington, J. A.; McCoy, A.; Belzar, K. J.; Pei, X. Y.; Gettins, P. G.; Carrell, R. W. The conformational activation of antithrombin. A 2.85-A structure of a fluorescein derivative reveals an electrostatic link between the hinge and heparin binding regions. *Journal of Biological Chemistry* **2000**, *275*, 15377-15383.

161. Lima, M. A.; Hughes, A. J.; Veraldi, N.; Rudd, T. R.; Hussain, R.; Brito, A. S.; Chavante, S. F.; Tersariol, I. I.; Siligardi, G.; Nader, H. B.; Yates, E. A. Antithrombin stabilisation by sulfated carbohydrates correlates with anticoagulant activity. *MedChemComm* **2013**, *4*, 870-873.

162. Danielsson, A.; Raub, E.; Lindahl, U.; Bjork, I. Role of ternary complexes, in which heparin binds both antithrombin and proteinase, in the acceleration of the reactions between antithrombin and thrombin or factor Xa. *J. Biol. Chem.* **1986**, *261*, 15467-15473.

163. Rezaie, A. R.; Olson, S. T. Calcium Enhances Heparin Catalysis of the Antithrombin−Factor Xa Reaction by Promoting the Assembly of an Intermediate Heparin−Antithrombin−Factor Xa Bridging Complex. Demonstration by Rapid Kinetics Studies†. *Biochemistry* **2000**, *39*, 12083-12090.

164. Wagenvoord, R.; Al Dieri, R.; van Dedem, G.; Beguin, S.; Hemker, H. C. Linear diffusion of thrombin and factor Xa along the heparin molecule explains the effects of extended heparin chain lengths. *Thromb. Res.* **2008**, *122*, 237-245.

165. Johnson, D. J.; Langdown, J.; Huntington, J. A. Molecular basis of factor IXa recognition by heparin-activated antithrombin revealed by a 1.7-A structure of the ternary complex. *Proc. Natl. Acad. Sci. U. S. A.* **2010**, *107*, 645-650.

166. Richard, B.; Swanson, R.; Olson, S. T. The signature 3-O-sulfo group of the anticoagulant heparin sequence is critical for heparin binding to antithrombin but is not required for allosteric activation. *J. Biol. Chem.* **2009**, *284*, 27054-27064.

167. Charef, S.; Petit, E.; Barritault, D.; Courty, J.; Caruelle, J.-P. Effects on coagulation of a synthetic heparan mimetic given intraperitoneally or orally. *Journal of Biomedical Materials Research Part A* **2007**, *83A*, 1024-1031.

168. Henry, B. L.; Connell, J.; Liang, A.; Krishnasamy, C.; Desai, U. R. Interaction of antithrombin with sulfated, low molecular weight lignins: opportunities for potent, selective modulation of antithrombin function. *J. Biol. Chem.* **2009**, *284*, 20897-20908.

169. Gettins, P. G.; Olson, S. T. Activation of antithrombin as a factor IXa and Xa inhibitor involves mitigation of repression rather than positive enhancement. *FEBS Lett.* **2009**, *583*, 3397-3400.

170. Pryzdial, E. L.; Kessler, G. E. Autoproteolysis or plasmin-mediated cleavage of factor Xaalpha exposes a plasminogen binding site and inhibits coagulation. *J. Biol. Chem.* **1996**, *271*, 16614-16620.

171. Abzalimov, R. R.; Kaltashov, I. A. Electrospray ionization mass spectrometry of highly heterogeneous protein systems: protein ion charge state assignment via incomplete charge reduction. *Anal. Chem.* **2010**, *82*, 7523-7526.

172. Kaltashov, I. A.; Bobst, C. E.; Abzalimov, R. R.; Wang, G.; Baykal, B.; Wang, S. Advances and challenges in analytical characterization of biotechnology products: mass spectrometry-based approaches to study properties and behavior of protein therapeutics. *Biotechnol. Adv.* **2012**, *30*, 210-222.

173. Gettins, P. G. Serpin structure, mechanism, and function. *Chem. Rev.* **2002**, *102*, 4751-4804.

174. Huntington, J. A.; Read, R. J.; Carrell, R. W. Structure of a serpin-protease complex shows inhibition by deformation. *Nature* **2000**, *407*, 923-926.

175. Huntington, J. A.; Carrell, R. W. The serpins: nature's molecular mousetraps. *Sci. Prog.* **2001**, *84*, 125-136.

176. Petersen, L. C.; Jorgensen, M. Electrostatic interactions in the heparin-enhanced reaction between human thrombin and antithrombin. *Biochem. J.* **1983**, *211*, 91-97.

177. Robinson, C. J.; Harmer, N. J.; Goodger, S. J.; Blundell, T. L.; Gallagher, J. T. Cooperative dimerization of fibroblast growth factor 1 (FGF1) upon a single heparin saccharide may drive the formation of 2:2:1 FGF1.FGFR2c.heparin ternary complexes. *J. Biol. Chem.* **2005**, *280*, 42274-42282.

178. Przybylski, C.; Gonnet, F.; Hersant, Y.; Bonnaffe, D.; Lortat-Jacob, H.; Daniel, R. Desorption electrospray ionization mass spectrometry of glycosaminoglycans and their protein noncovalent complex. *Anal. Chem.* **2010**, *82*, 9225-9233.

179. Crown, S. E.; Yu, Y.; Sweeney, M. D.; Leary, J. A.; Handel, T. M. Heterodimerization of CCR2 Chemokines and Regulation by Glycosaminoglycan Binding. *J. Biol. Chem.* **2006**, *281*, 25438-25446.

180. Jen, C. H.; Leary, J. A. A competitive binding study of chemokine, sulfated receptor, and glycosaminoglycan interactions by nano-electrospray ionization mass spectrometry. *Anal. Biochem.* **2010**, *407*, 134-140.

181. Yu, Y.; Sweeney, M. D.; Saad, O. M.; Crown, S. E.; Hsu, A. R.; Handel, T. M.; Leary, J. A. Chemokine-glycosaminoglycan binding: specificity for CCR2 ligand binding to highly sulfated oligosaccharides using FTICR mass spectrometry. *J. Biol. Chem.* **2005**, *280*, 32200-32208.

182. Abzalimov, R. R.; Kaltashov, I. A. Electrospray ionization mass spectrometry of highly heterogeneous protein systems: Protein ion charge state assignment via incomplete charge reduction. *Anal. Chem.* **2010**, *82*, 7523-7526.

183. Wang, G.; Johnson, A. J.; Kaltashov, I. A. Evaluation of electrospray ionization mass spectrometry as a tool for characterization of small soluble protein aggregates. *Anal. Chem.* **2012**, *84*, 1718–1724.

184. Abzalimov, R. R.; Bobst, C. E.; Salinas, P. A.; Savickas, P.; Thomas, J. J.; Kaltashov, I. A. Studies of pH-dependent self-association of a recombinant form of arylsulfatase A with electrospray ionization mass spectrometry and size-exclusion chromatography. *Anal. Chem.* **2013**, *85*, 1591-1596.

185. Naimy, H.; Leymarie, N.; Bowman, M. J.; Zaia, J. Characterization of heparin oligosaccharides binding specifically to antithrombin III using mass spectrometry. *Biochemistry* **2008**, *47*, 3155-3161.

186. Guerrini, M.; Elli, S.; Mourier, P.; Rudd, T. R.; Gaudesi, D.; Casu, B.; Boudier, C.; Torri, G.; Viskov, C. An unusual antithrombin-binding heparin octasaccharide with an additional 3-O-sulfated glucosamine in the active pentasaccharide sequence. *Biochem. J.* **2013**, *449*, 343-351.

187. Demelbauer, U. M.; Plematl, A.; Kremser, L.; Allmaier, G.; Josic, D.; Rizzi, A. Characterization of glyco isoforms in plasma-derived human antithrombin by on-line capillary zone electrophoresis-electrospray ionization-quadrupole ion trap-mass spectrometry of the intact glycoproteins. *Electrophoresis* **2004**, *25*, 2026-2032.

188. Suk, J. Y.; Zhang, F.; Balch, W. E.; Linhardt, R. J.; Kelly, J. W. Heparin Accelerates Gelsolin Amyloidogenesis†. *Biochemistry* **2006**, *45*, 2234-2242.

189. Bravo, R.; Arimon, M.; Valle-Delgado, J. J.; García, R.; Durany, N.; Castel, S.; Cruz, M.; Ventura, S.; Fernàndez-Busquets, X. Sulfated Polysaccharides Promote the Assembly of Amyloid β1–42 Peptide into Stable Fibrils of Reduced Cytotoxicity. *J. Biol. Chem.* **2008**, *283*, 32471-32483.

190. Nielsen, S. B.; Yde, P.; Giehm, L.; Sundbye, S.; Christiansen, G.; Mathiesen, J.; Jensen, M. H.; Jensen, P. H.; Otzen, D. E. Multiple Roles of Heparin in the Aggregation of p25α. *J. Mol. Biol.* **2012**, *421*, 601-615.

191. Vieira, T. C.; Reynaldo, D. P.; Gomes, M. P.; Almeida, M. S.; Cordeiro, Y.; Silva, J. L. Heparin binding by murine recombinant prion protein leads to transient aggregation and formation of RNA-resistant species. *J. Am. Chem. Soc.* **2011**, *133*, 334-344.

192. Silva, J. L.; Vieira, T. C.; Gomes, M. P.; Rangel, L. P.; Scapin, S. M.; Cordeiro, Y. Experimental approaches to the interaction of the prion protein with nucleic acids and glycosaminoglycans: Modulators of the pathogenic conversion. *Methods* **2011**, *53*, 306-317.

193. Zhu, H.; Yu, J.; Kindy, M. S. Inhibition of amyloidosis using low-molecular-weight heparins. *Mol. Med.* **2001**, *7*, 517-522.

194. Wilhelmus, M. M.; de Waal, R. M.; Verbeek, M. M. Heat shock proteins and amateur chaperones in amyloid-Beta accumulation and clearance in Alzheimer's disease. *Mol. Neurobiol.* **2007**, *35*, 203-216.

195. Vilasi, S.; Sarcina, R.; Maritato, R.; De Simone, A.; Irace, G.; Sirangelo, I. Heparin Induces Harmless Fibril Formation in Amyloidogenic W7FW14F Apomyoglobin and Amyloid Aggregation in Wild-Type Protein In Vitro. *PLoS ONE* **2011**, *6*.

196. Bergamaschini, L.; Rossi, E.; Vergani, C.; De Simoni, M. G. Alzheimer's disease: another target for heparin therapy. *ScientificWorldJournal* **2009**, *9*, 891-908.

197. Miura, Y.; Yasuda, K.; Yamamoto, K.; Koike, M.; Nishida, Y.; Kobayashi, K. Inhibition of Alzheimer Amyloid Aggregation with Sulfated Glycopolymers. *Biomacromolecules* **2007**, *8*, 2129-2134.

198. Calamai, M.; Chiti, F.; Dobson, C. M. Amyloid Fibril Formation Can Proceed from Different Conformations of a Partially Unfolded Protein. *Biophys. J.* **2005**, *89*, 4201-4210.

199. Carrotta, R.; Manno, M.; Bulone, D.; Martorana, V.; Biagio, P. L. S. Protofibril Formation of Amyloid β-Protein at Low pH via a Non-cooperative Elongation Mechanism. *J. Biol. Chem.* **2005**, *280*, 30001-30008.

200. Jain, S.; Udgaonkar, J. B. Defining the Pathway of Worm-like Amyloid Fibril Formation by the Mouse Prion Protein by Delineation of the Productive and Unproductive Oligomerization Reactions. *Biochemistry* **2011**, *50*, 1153-1161.

201. Park, S.; Saven, J. G. Simulation of pH-dependent edge strand rearrangement in human beta-2 microglobulin. *Protein Sci.* **2006**, *15*, 200-207.

202. Chiti, F.; Bucciantini, M.; Capanni, C.; Taddei, N.; Dobson, C. M.; Stefani, M. Solution conditions can promote formation of either amyloid protofilaments or mature fibrils from the HypF N-terminal domain. *Protein Sci.* **2001**, *10*, 2541-2547.

203. Chiti, F.; Dobson, C. M. Amyloid formation by globular proteins under native conditions. *Nat. Chem. Biol.* **2009**, *5*, 15-22.

204. Wang, G.; Johnson, A. J.; Kaltashov, I. A. Evaluation of Electrospray Ionization Mass Spectrometry as a Tool for Characterization of Small Soluble Protein Aggregates. *Anal. Chem.* **2011**, *84*, 1718-1724.

205. Zhou, A.; Carrell, R. W. Dimers Initiate and Propagate Serine Protease Inhibitor Polymerisation. *J. Mol. Biol.* **2008**, *375*, 36-42.

206. Vetri, V.; Librizzi, F.; Leone, M.; Militello, V. Thermal aggregation of bovine serum albumin at different pH: comparison with human serum albumin. *Eur. Biophys. J.* **2007**, *36*, 717-725.

207. Holm, N. K.; Jespersen, S. K.; Thomassen, L. V.; Wolff, T. Y.; Sehgal, P.; Thomsen, L. A.; Christiansen, G.; Andersen, C. B.; Knudsen, A. D.; Otzen, D. E. Aggregation and fibrillation of bovine serum albumin. *Biochimica et Biophysica Acta (BBA) - Proteins and Proteomics* **2007**, *1774*, 1128-1138.

208. Militello, V.; Casarino, C.; Emanuele, A.; Giostra, A.; Pullara, F.; Leone, M. Aggregation kinetics of bovine serum albumin studied by FTIR spectroscopy and light scattering. *Biophys. Chem.* **2004**, *107*, 175-187.

209. Xu, Y.; Seeman, D.; Yan, Y.; Sun, L.; Post, J.; Dubin, P. L. Effect of Heparin on Protein Aggregation: Inhibition versus Promotion. *Biomacromolecules* **2012**, *13*, 1642-1651.

210. Giger, K.; Vanam, R. P.; Seyrek, E.; Dubin, P. L. Suppression of Insulin Aggregation by Heparin. *Biomacromolecules* **2008**, *9*, 2338-2344.

211. Meakin, P. A Historical Introduction to Computer Models for Fractal Aggregates. *J. Sol-Gel Sci. Technol.* **1999**, *15*, 97-117.

212. Bourgault, S.; Solomon, J. P.; Reixach, N. l.; Kelly, J. W. Sulfated Glycosaminoglycans Accelerate Transthyretin Amyloidogenesis by Quaternary Structural Conversion. *Biochemistry* **2010**, *50*, 1001-1015.

213. Zhang, C.; Lillie, R.; Cotter, J.; Vaughan, D. Lysozyme purification from tobacco extract by polyelectrolyte precipitation. *J. Chromatogr. A* **2005**, *1069*, 107-112.

214. Peram, T.; McDonald, P.; Carter-Franklin, J.; Fahrner, R. Monoclonal antibody purification using cationic polyelectrolytes: an alternative to column chromatography. *Biotechnol. Prog.* **2010**, *26*, 1322-1331.

215. Zhao, J. Y.; Ford, C. F.; Glatz, C. E.; Rougvie, M. A.; Gendel, S. M. Polyelectrolyte precipitation of beta-galactosidase fusions containing poly-aspartic acid tails. *J. Biotechnol.* **1990**, *14*, 273-283.

216. Levi, V.; González Flecha, F. L. Reversible fast-dimerization of bovine serum albumin detected by fluorescence resonance energy transfer. *Biochimica et Biophysica Acta (BBA) - Proteins and Proteomics* **2002**, *1599*, 141-148.

217. Xu, Y.; Yan, Y.; Seeman, D.; Sun, L.; Dubin, P. L. Multimerization and aggregation of native-state insulin: effect of zinc. *Langmuir* **2012**, *28*, 579-586.

218. Yan, Y.; Seeman, D.; Zheng, B.; Kizilay, E.; Xu, Y.; Dubin, P. L. pH-Dependent aggregation and disaggregation of native beta-lactoglobulin in low salt. *Langmuir* **2013**, *29*, 4584-4593.

219. Majhi, P. R.; Ganta, R. R.; Vanam, R. P.; Seyrek, E.; Giger, K.; Dubin, P. L. Electrostatically driven protein aggregation: beta-lactoglobulin at low ionic strength. *Langmuir* **2006**, *22*, 9150-9159.

220. Barbosa, L. R.; Ortore, M. G.; Spinozzi, F.; Mariani, P.; Bernstorff, S.; Itri, R. The importance of protein-protein interactions on the pH-induced conformational changes of bovine serum albumin: a small-angle X-ray scattering study. *Biophys. J.* **2010**, *98*, 147-157.

221. El Kadi, N.; Taulier, N.; Le Huerou, J. Y.; Gindre, M.; Urbach, W.; Nwigwe, I.; Kahn, P. C.; Waks, M. Unfolding and refolding of bovine serum albumin at acid pH: ultrasound and structural studies. *Biophys. J.* **2006**, *91*, 3397-3404.

222. Estey, T.; Kang, J.; Schwendeman, S. P.; Carpenter, J. F. BSA degradation under acidic conditions: a model for protein instability during release from PLGA delivery systems. *J. Pharm. Sci.* **2006**, *95*, 1626-1639.

223. Zhou, A.; Stein, P. E.; Huntington, J. A.; Carrell, R. W. Serpin polymerization is prevented by a hydrogen bond network that is centered on his-334 and stabilized by glycerol. *J. Biol. Chem.* **2003**, *278*, 15116-15122.

224. Wang, K.; Kurganov, B. I. Kinetics of heat- and acidification-induced aggregation of firefly luciferase. *Biophys. Chem.* **2003**, *106*, 97-109.

225. Kurganov, B. I. Kinetics of Protein Aggregation. Quantitative Estimation of the Chaperone-Like Activity in Test-Systems Based on Suppression of Protein Aggregation. *Biochemistry (Moscow)* **2002**, *67*, 409-422.

226. Jho, Y. S.; Safran, S. A.; In, M.; Pincus, P. A. Effect of Charge Inhomogeneity and Mobility on Colloid Aggregation. *Langmuir* **2012**, *28*, 8329-8336.

227. Magazu, S.; Maisano, G.; Mallamace, F.; Micali, N. Growth of fractal aggregates in water solutions of macromolecules by light scattering. *Phys. Rev. A* **1989**, *39*, 4195-4200.